MULTILATERAL WELL MODELING FROM COMPARTMENTALIZED RESERVOIRS

by

Oluwadairo Kayode

A thesis submitted to the School of Graduate Studies

in partial fulfillment of the requirements for the degree of

Master of Engineering

Oil and Gas Engineering

Faculty of Engineering and Applied Science

Memorial University of Newfoundland

St John's, Newfoundland & Labrador

Canada

May 2018

Abstract

The existence of compartmentalization in oil and gas fields have been a major industry challenge for decades. This phenomenon introduces some complexity and uncertainty in the prediction of well productivities and the overall hydrocarbon recovery factor. In the past, multiple vertical wells were drilled to increase recovery. The recent advancement of the multilateral and completions technology made multilateral wells a viable alternative to produce multiple reservoir compartments, most especially offshore. Reservoir compartments may possess a set of unique characteristics, such as average pressures, thicknesses, permeabilities, and porosity distribution. This variation in properties introduced complex dynamics in forecasting the commingled production figures and overall recovery factor from complex reservoir structures using advanced well systems. Existing analytical and semi-analytical productivity models due to the simplifying assumptions in their development are only suitable for first approximations and early estimates in field applications. In this work, a comparison is made between the more widely known finite difference numerical method and the finite volume numerical discretization method in field productivity predictions. The Matlab Reservoir Simulation Toolbox (MRST) which is a collection of open source codes, based on the finite volume discretization methodology is used to develop the reservoir compartment and multilateral well model used in this study. We investigate the pressure drop behavior over time through the lateral for a conventional well completion and compare with the pressure drop behavior for a smart well completion with downhole flow control devices for flow control and optimization. Several cases of compartmentalized reservoirs with faults of varying orientation and sealing capacity is then investigated. The production profile results obtained from the base reservoir case from MRST is compared to those from the IMEX simulator tool in CMG (Computer Modeling Group), a commercial reservoir simulator, based on

the finite difference numerical discretization method. The results we obtain show a more accurate production profile prediction based on the finite volume method over the finite difference method, as expected. The ability of the simulation toolbox as well as the importance of using an improved and more efficient numerical discretization scheme in solving an increasingly complex array of reservoir structures and advanced well geometries, with multiphase fluid flow is demonstrated. Finally, an adjoint gradient – based method of optimization implemented in the toolbox is used to investigate the optimization potential of using the smart well completions versus a conventional well completion with the net present value as the objective function. Results obtained show that an investment in smart completions for the multilateral well ultimately yields a higher net cash flow and net present value over a conventional well of equivalent length designed without smart completions.

`

Acknowledgements

First, I would like to give all glory to God for the journey so far in Grad school. It has been a roller coaster of experiences far away from home.

A whole depth of gratitude and appreciation goes to my supervisor, Dr. Lesley James for her support, corrections, and gentle guidance throughout the period of this thesis work. Her style of mentorship has driven me to self-develop; stretching myself to push the boundaries of learning to acquire knowledge and expertise in new ways of framing a problem and finding solutions to same using a variety of techniques. I also appreciate my ex-co-supervisor, Dr. Thormod Johansen for his assistance in the initial stages of defining the objectives and motivation for this work, before leaving Memorial University.

A special appreciation is extended to my parents and lovely sisters who keep giving me the nudge to keep on going.

I would also like to recognize my friends and team research colleagues who shared the same office space and had a lot of fruitful conversations about diverse topics with.

Finally, the fellowship and financial support of the school of graduate studies, Hibernia Management Development Corporation, Chevron, and other support organizations is greatly appreciated.

Table of Contents

Nomenclature

$q_{\propto,j}$ = flow rate of phase $\propto$ from grid block, j

WI_j = Well Index

$\mu_{\propto}$ = fluid viscosity

$p_{\propto,j}$ = grid block pressure

p_{wf} = bottom hole flowing pressure

k_x, k_y = reservoir permeability in the x- and y-directions

h_j = net thickness of grid block

r_w = wellbore radius

S = skin factor

r_o = equivalent gridblock radius

List of Figures

List of Tables

Chapter One Introduction

A reservoir is said to be compartmentlized when the free flow of fluids is hindered spatially and / or temporally from one part of the reservoir to the other. The separation occurs due to a series of geologic activities during and after the formation of the reservoir zone. The most fundamental mechanisms that cause reservoir compartmentalization include faulting and depositional heterogeneities (Go et al., 2014). There are two basic types of compartmentalization seals: the 'static or isolating seals' which are completely sealing and are capable of withholding oil and gas columns over a long period; and 'dynamic seals' which are basically very low permeability flow barriers that reduce the rate of oil and gas movement through them. When compartmentalization occurs, fluid contacts, saturations, and pressures progressively segregate into separate compartments (Stewart and Whaballa, 1989).

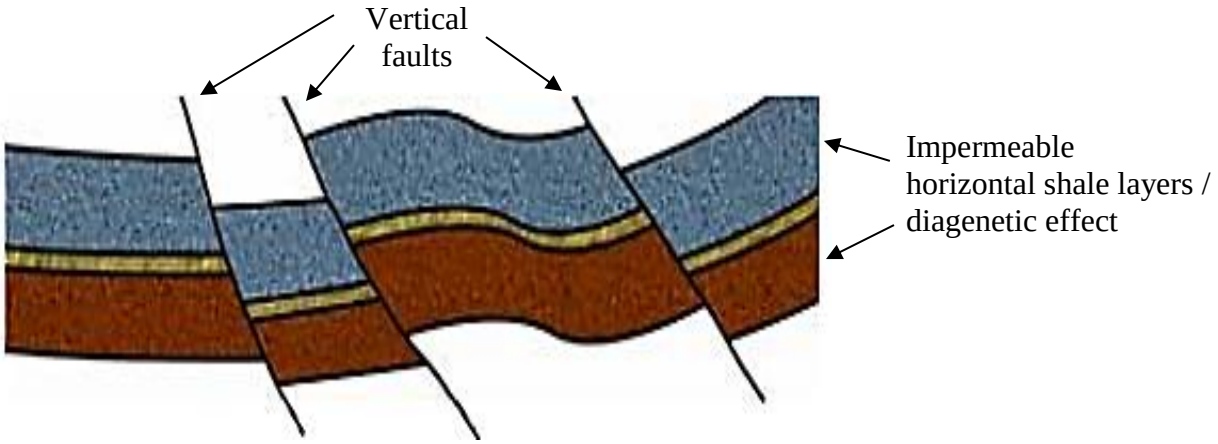

Figure 1 - Conceptual drawing of a compartmentalized reservoir (after Jolley et al., 2003)

Unexpected or undetected compartmentalization can negatively impact the profitability of a field, thereby requiring more data, more study, more delineation / exploratory wells, and more time to produce less oil and gas than may have been originally anticipated. In extreme cases, it may lead

to early field abandonment where a reservoir has only produced a small fraction of the estimated reserves in place, and the production rate starts to decline (Smith, 2008).

Figure 1 above shows a simplified illustration of how fluid distribution in a typical reservoir may be comartmentalized by vertical and horizontal events such as shale layers, faults, and/or diagenetic changes. Compartmentalization is an unwanted phenomenon as it presents a major source of uncertainty during the field development planning process. Oil and gas volume estimation is affected, with the accompanied effect of reduced drainage and sweep efficiency (Jolley et al., 2003). To improve recovery, it was usually recommended to drill several wells to drain each compartment, like the representation in **Figure 2** below where four wells are drilled to increase the drainage efficiency of each of the identified compartments. This implies that the more compartments in a field, the more wells would be required to produce the volumes in place. Drilling costs are a major capital expenditure in oil field exploration, especially offshore.

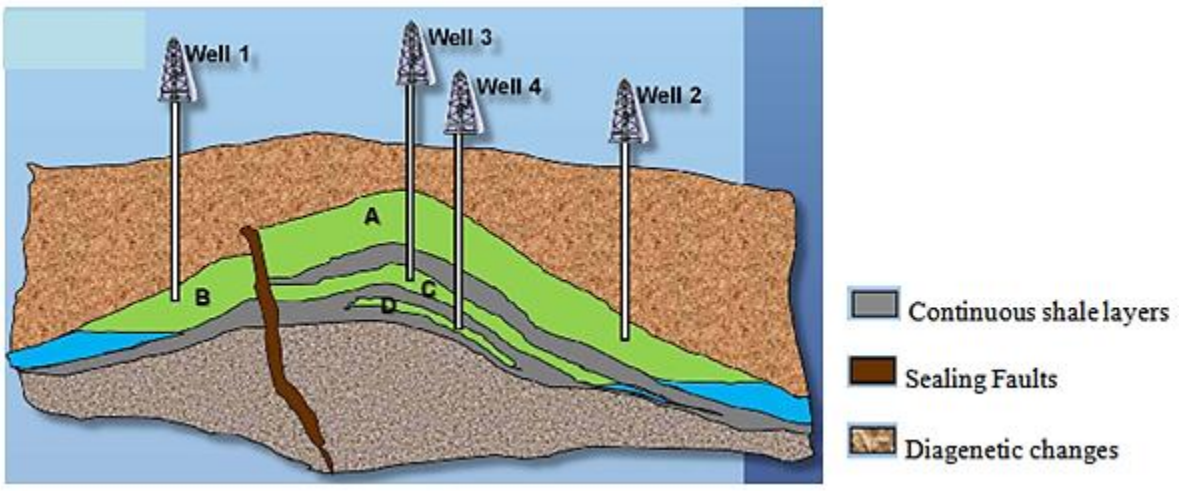

Figure 2 - Simplified reservoir compartments produced by multiple wells (Go et al., 2014)

A feasible strategy being increasingly adopted in the industry to increase project profitability (i. e. productivity) from a set of compartmentalized reservoirs as in **Figure 2** above is the multilateral well technology (**Figure 3** below).

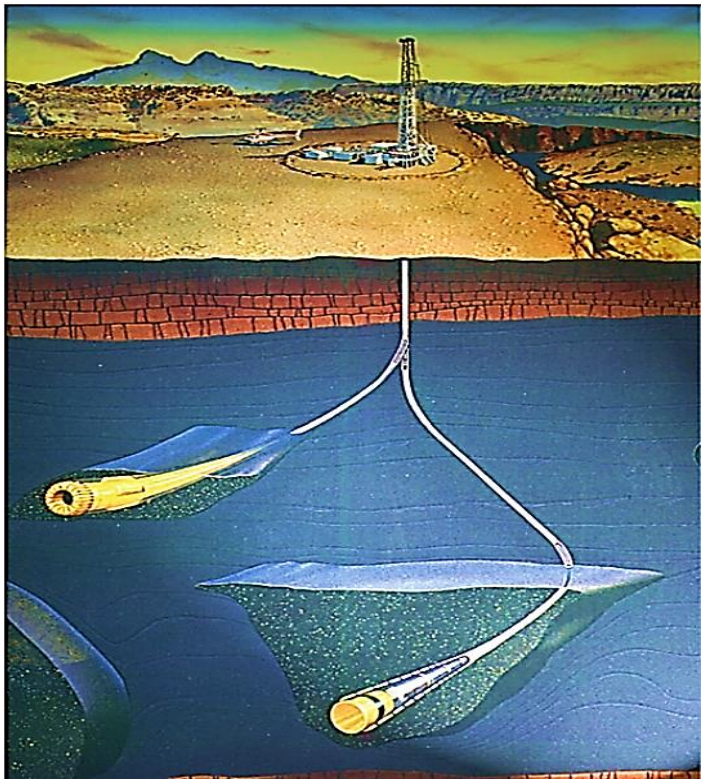

Figure 3 - Multilateral well image (Baker, 2002)

The multilateral well technology is an advanced well technology which evolved from the horizontal well technology. These advanced well technologies (horizontal and multilateral wells) provide an economically feasible alternative to the conventional practice of drilling multiple vertical wells from the surface to produce the reservoir compartments in a field. The surface area required for drilling and production operations, especially for offshore, environmentally harsh and remote locations is reduced. Therefore, the use of multilateral wells in minimizing well count, and maximizing recovery is important (Jalali, 2005).

Multilateral wells require a considerable amount of planning time, and cost on average, at least about 44% more than a conventional vertical well (Jalali, 2005). The complexity of the multilateral well architecture, its increasing use and the economic implication of the technology requires that

we conduct a more accurate modeling of its performance from various reservoir structures where they may be used.

Several models and methods exist for predicting reservoir and well productivity indices: analytical, semi-analytical, and numerical techniques. However, assumptions of single phase flow, reservoir homogeneity, and frictionless wellbore introduced into the analytical and semi-analytical models present a major drawback in their predictive accuracy especially for field applications as they grossly under represent the reality of real life reservoir geometries, geological and petrophysical properties, and wellbore flowing conditions in the ever-growing 'prolific' fields being developed today (Jalali, 2005).

The discretization process entails the transformation of the continuous governing partial differential equations over the reservoir domain into discrete form in numerical reservoir simulation. This process is usually carried out as a first step toward making the equations suitable for numerical evaluation and implementation on a computer (Chen et al., 2006).

The most commonly used numerical discretization methods that we compare in this work are the finite difference and the finite volume methods. The finite difference method is the more commonly used discretization method and is based on the differential approximation of the Taylor series (Aziz, 1979). A point distributed or block centered grid system can be used. However, traditional finite difference methods of numerical modeling describe the pressure everywhere except around the wells. This is because grid-block sizes are usually many orders larger than the well bore. This causes the wells to create near-singularities in pressure which are not well represented by the finite difference equations because of their basis on polynomials. In order to

correct this, finite difference-based reservoir simulators use an empirical productivity index to correct the simulated well cell pressures (Young, 2007).

The finite volume method, however is generally more versatile than the finite difference method due to its greater accuracy in conserving mass over the control domain, greater adaptation to structured and unstructured grid formations, and ease of handling boundary conditions. Also, the clear structure and versatility makes it possible to develop general purpose software for computer applications (Young, 2007).

The increasing adoption and use of the multilateral well technology to produce complex reservoir structures necessitates evaluation of the reservoir and well productivity using more efficient numerical means. This research investigates the versatility of the finite volume numerical discretization methodology implemented in Matlab® Reservoir Simulation Toolbox (MRST) compared to the more commonly used finite difference method implemented in commercialized reservoir simulators like the IMEX simulator in CMG for modeling and simulating the productivity of compartmentalized reservoirs produced by multilateral wells. We present further details on the mathematical basis of both methods in chapter three. Using the multi-segment well option enabled in MRST which allows for easy incorporation of flow-based pressure drop effects and smart completions (flow control devices), we investigate the pressure drop profile in the well and the optimization potential of the multilateral system using the net present value as the objective function.

1.1 History of Multilateral Wells

Multilateral wells in their most simple form have been utilized in oil and gas production activities since the 1950's, although first patented designs were recorded in 1919. These early multilateral

systems were only suitable in their application to a small segment of wells, due to traditional completion techniques at the time. Taylor and Russell (1998) reported that most of the multilateral wells drilled before 1998 were produced with no liners or completion equipment, i. e. open hole. The first multilateral well was drilled in 1953 in the late Soviet Union (USSR) with nine laterals in a carbonate reef formation for increased reservoir contact (Ali et al., 2004). In the 1990s, the development of drilling and completions technology helped engineers to increase the number of laterals and multilateral wells drilled and completed. Prior to December 2006, there were more than 8000 multilateral wells all over the world, with record of remarkable economic benefits (Ali et al., 2004).

1.2 Multilateral Well Configurations

Multilateral wells can have several configurations. They range from having multiple laterals in a single horizontal plane or layer to a stacked type which accesses different vertical layers. There could also be several laterals shooting off a main vertical or horizontal hole into the formation, depending on the geometry of the reservoir to be exploited.

The configurations can be completed using any of the current completion levels one to six as classified by the industry consortium for the advancement of multilaterals. The various completion levels are described next in section 1.3.

A schematic representation of the most common well configurations used in the industry is depicted in **Figure 4** below.

The multi-branched, laterals in a vertical hole, and dual opposing configurations (4a, d, and f) consist of inclined or horizontal laterals shooting off the vertical portion of the well. The laterals

in a horizontal hole and forked configuration (4b and 4c) are characterized by a long main horizontal or inclined lateral with multiple laterals shooting off the main lateral. The stacked configuration (4e) consists of one horizontal lateral drilled on top of the other lateral into the same or different layers in the reservoir.

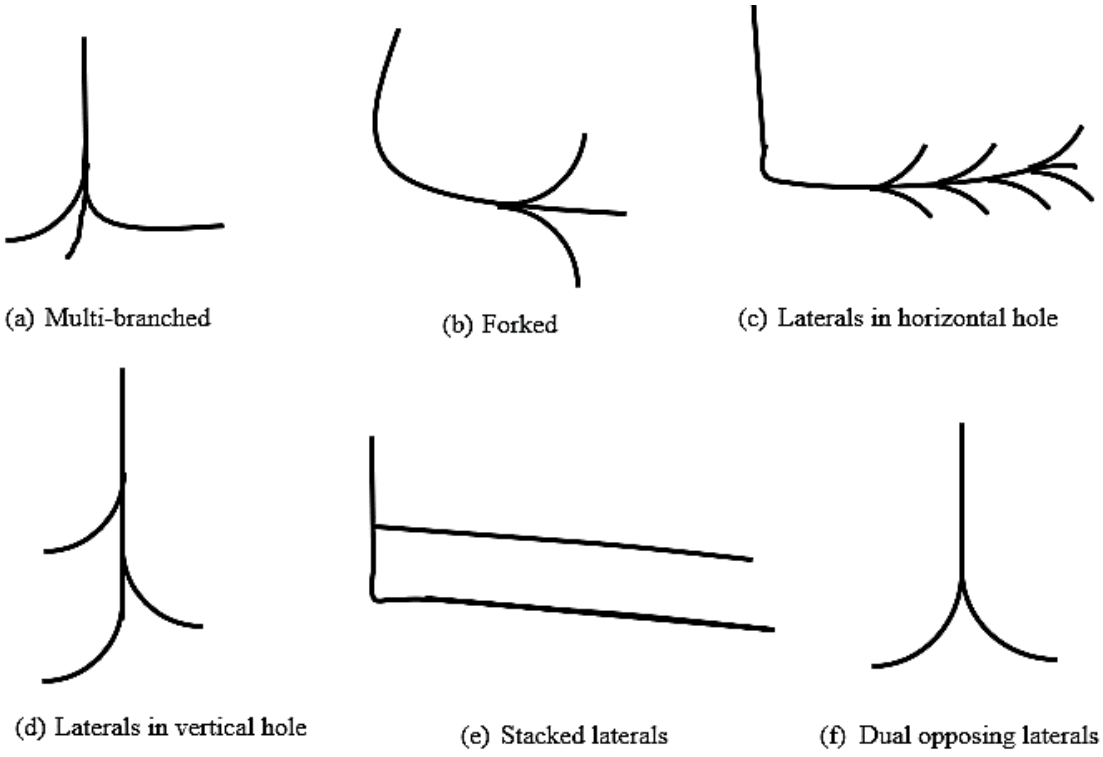

Figure 4 - Multilateral well types / configuration (adapted from Bosworth et al., 2003)

1.3 Multilateral Well Completion Levels

The junction construction is a major distinguishing component between the multilateral well completion and conventional wells (Hill, 2008). The advancement of the completions technology also aided the development and industry adoption of the multilateral well technology.

In 1997, Technology Advancement for Multi-Laterals (TAML), an industry consortium of operators and service companies, categorized multilateral well completions by complexity and functionality based on the extent of mechanical support and pressure integrity provided at the

junction. Six levels defined by TAML is illustrated below in **Figure 5**. The level system made it easier for operators to recognize and compare the functionality and risk-to-reward evaluations of one completion design to another. The associated cost of completion increased with the completion level (Hogg, 1997).

Level 1 — (Open-hole junction)

This is the most fundamental of the multilateral well completion system. The main bore as well as the lateral is uncased. The integrity of the well junction is wholly dependent on hole stability, as there are no completion systems installed for mechanical hole support or hydraulic zone isolation.

Level 2 — (Cased-hole exit)

Here, the laterals are drilled off a cased and cemented main borehole. This completion level provides some measure of stability, support, and zonal isolation but there is no support for the lateral section. If desired, liners can be installed in the lateral section to maintain borehole stability.

Level 3 — (Junction with connection but no seal)

Some similarities exist with the level 2 system, but a slotted liner or screen is installed in the lateral section and anchored to the main cased hole. This configuration offers some level of mechanical support for the junction, but the advantage of zonal isolation is absent, and production is commingled in this system.

Level 4 - (Mechanically sealed junction)

This system offers both a cased and a cemented main bore and lateral giving rise to excellent lateral mechanical support, but the cement itself does not offer pressure integrity at the junction. The possibility of junction failure exists subject to pressure drawdown, as might be experienced in an electrical submersible pump (ESP) application.

Level 5 - (Hydraulically sealed junction with reduced inside diameter)

Pressure integrity is achieved by using tubing strings and packers to isolate the junction in this level. Single-string packers are placed in both the main bore and lateral below the junction and connected by tubing strings to a dual-string isolation packer located above the junction in the main bore. This system offers full access to both the main bore and the lateral. Single zone or commingled production is possible, based on the implemented design.

Level 6 - (Hydraulically and mechanically sealed junction with full inside diameter)

Both mechanical and pressure integrity are achieved by using the casing to seal the junction. The system uses pre-manufactured junction types where the junction is reformed downhole or in the case of two separate wells; the pre-manufactured junction is assembled downhole. (SPE Petro Wiki, 2016)

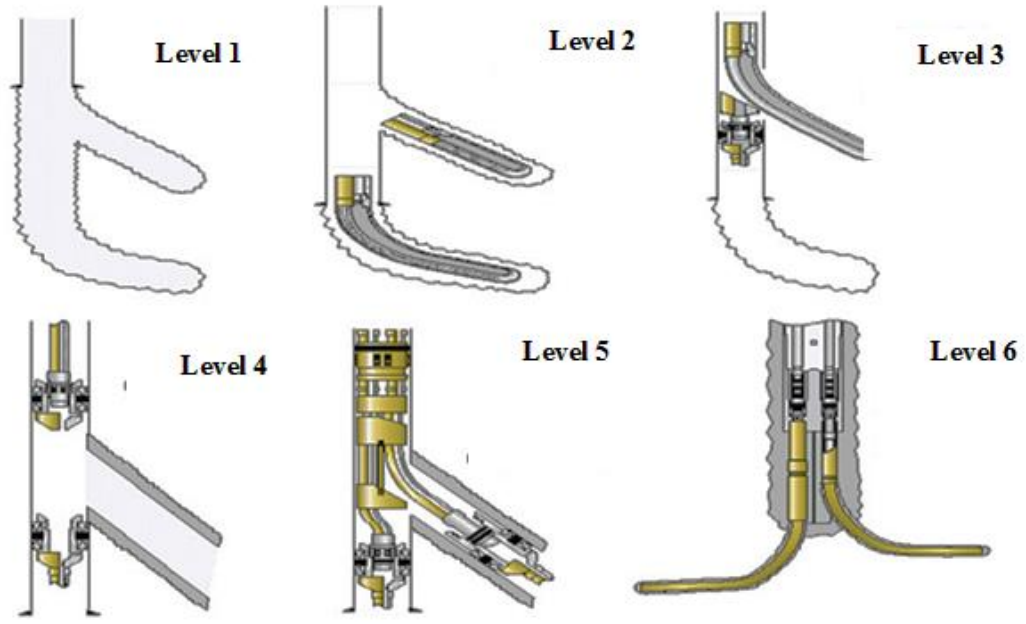

Figure 5 - Multilateral well completion levels (after Guidry et al., 2011)

The world's first level six intelligent multilateral well was drilled and completed in Indonesia in 2002. The two-leg (**Figure 6** below) dual lateral design, drilling, and completion project was completed in the South Java Sea, Indonesia. There was a reported cost saving of approximately one million USD on the project (Fraija et al., 2003).

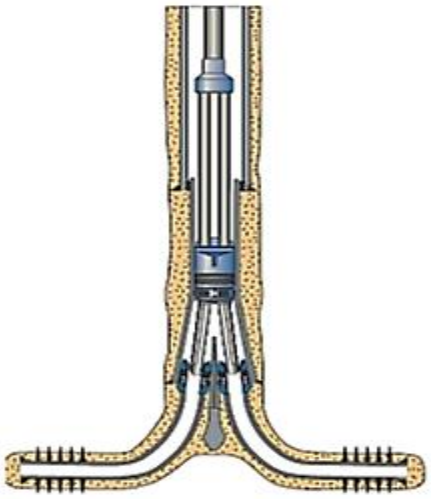

Figure 6 - First level six intelligent dual lateral well completion (Fraija et al, 2003)

1.4 Advantages of the Multilateral (ML) Well Technology

Multilateral wells leverage the existing advantages of horizontal wells with further improvements to produce multilayer pay zones. Rivera et al., (2003) compared the economics of levels 3 and 6 ML junction configurations to a horizontal well (HW) for a natural flow of oil of gravity between 20 – 29^{o} API in a homogeneous reservoir, and permeability ranging from 10 mD to 1250 mD. Results showed that the two-branched MLs produced 13% more oil than the HW in a high permeability reservoir. The MLs also produced 80% more oil than the HW in a low permeability reservoir with low viscosity oil, and 10 to 15% less water than the HW. Horizontal wells have the following benefits over vertical wells: better sweep efficiencies, decreased water, and gas coning tendencies, increased exposure to natural fractures in the formation and increased efficiency of

draining relatively thin formation layers ultimately leading to higher productivity indices from the well.

Multilaterals provide the following advantages:

- Greater contact area to reservoir ratio, and increased exposure to natural fracture systems in formation via multiple laterals.
- Low cost-benefit ratio (reduced capital spends on drilling the well, wellhead installation, platform risers and completion equipment compared to multiple wells). An operator in the Arabian Gulf reported 35% savings per well, despite 44% extra cost compared to a single horizontal (Al-Umair, 2000).
- Access to multiple pay zones including thin layers or older and formerly depleted reservoirs from a single location.
- Improved control over flooding patterns.
- Well slot optimization and minimized environmental impact or footprint in offshore and harsh or remote locations.
- Extend the life of an existing field development by drilling laterals out of the existing wellbores and tapping into reserves that were not recovered during the earlier stage of production.
- Accelerated production- i. e. higher flow rates at lower pressure drops than single-bore wells.
- Minimized frictional pressure losses in the wellbore compared to long single horizontal wells.

1.5 Challenges Encountered

One main challenge in using the ML well technology is that the advancement in well completion technologies lagged the advancement of drilling technologies. (JPT, 2016). Further challenges frequently encountered in employing multilateral wells include: large number of man-hours required for the planning phase alone, higher initial investment, associated drilling risks (unexpected high-pressure zone/formation, hole collapse), completion risks (overburden stability for placement of junction), and difficulty of well re-entry for workover operations (Langley, 2011).

Other challenges include lateral well interference during production (cross flow), production zone allocation; increased formation sensitivity to vertical and horizontal heterogeneities; and managing lateral and overall productivity ratios. Jalali (2005) presented the lessons learnt from a field case study on lateral interference, and the effect of near well bore damage in advanced well scenarios. A more comprehensive review of the analytical, semi analytical, and numerical simulation techniques used to investigate multilateral well productivity is presented in the literature review in chapter two. It can be said that the multilateral well technology is still evolving to address the current challenges, as long as the improvement of the project net present value remains the primary business objective in the industry.

1.6 Compartmentalized Reservoirs

Compartmentalized reservoirs exist in many oil fields around the world: the Raslie and Avondale fields in the Roma Area, North Sea fields and the giant Hibernia oilfield developed in the Jeanne d'Arc Basin on the grand banks of Newfoundland also exhibits compartmentalization to varying degrees (Cervantes, 1996).

Smalley and Muggeridge (2010) in their paper titled: “Reservoir Compartmentalization: get it before it gets you” examined the impact of compartmentalization on oil recovery and submitted that the extent of compartmentalization reduces the recovery by reducing the drainage and sweep efficiencies.

Horizontal well technology presented an advanced alternative technology of producing a set of compartmentalized reservoirs. This was the subject of investigation in the thesis work of Wang (2016). Using a higher order numerical discretization scheme, Wang solved the pressure functions for the set of compartmentalized oil and gas reservoirs separately for communicating and non-communicating reservoir scenarios. Sensitivity studies then investigated varying reservoir and fluid properties such as viscosity, and permeability on recovery indices.

However, industry-based geological and geophysical research continues to propose new techniques, strategies, and technologies for more accurate identification and determination of the extent of compartmentalization in any field to reduce the level of knowledge uncertainty.

With a significant reduction in uncertainty of the reservoir outlay resulting from these studies, new models for reservoir simulation and deliverability studies developed by reservoir engineers will yield accurate results in the description of reservoir flow dynamics and production profile from the reservoir compartments.

1.7 Reservoir Applications of Multilateral Well Technology

The application of multilateral wells can be in the same reservoir layer, where the well penetrates a region within a relatively uniform pressure distribution or in a multi-reservoir scenario where the

laterals penetrate several regions with noticeable pressure variations. The latter is the subject of investigation in this work.

There are two cases for multilateral wells penetrating the same reservoir: A high-drawdown case when the formation pressure exceeds the wellbore pressure. This is believed to be the case in tight formations or formations with viscous crude (heavy oil). The low-drawdown case is the reverse scenario and is generally believed to be the case in unconsolidated formations (Jalali, 2005). Estimating the magnitude of the pressure drop in the horizontal lateral requires knowledge of how the flow profile, lateral undulation, and phase segregation etc. affect the wellbore pressure and flow profile. However, the unavailability of this information seriously hinders analysis and the ability to draw conclusions on the performance of the well using comparative analysis.

Comparative analysis is less relevant to multi-reservoir applications where the critical issue is how formations with contrasting properties and pressure regimes can be commingled to produce an effective drainage of the compartments. While commingling can be achieved with horizontal wells, the drained compartments will usually be of comparable permeability. This was the case in the work of Wang (2016) and the earlier work of Thomas (2012) on dynamic reservoir tank modeling. For applications in zones of contrasting properties, the less productive zone or compartment is usually treated as an auxiliary flow unit. Hence, if the thorough drainage of tight zones is a priority, then multilateral wells are needed. (Jalali, 2005)

One of the advantages of multilateral wells earlier outlined is the ability to produce several payzones using two or more laterals extending from a parent wellbore into the different layers. Field studies conducted by various authors have reported increased productivity, hence profitability because of the use of the multilateral wells: Jalali, (2005), Al-Umair, (2000), Rivera

et al., (2003) among others. Multilateral wells particularly often provide the only existing economical means to produce several isolated reservoir compartments, outlying satellite fields, and small reservoirs containing limited reservoir volumes by connecting vertical and horizontal features, such as natural fractures, laminated formations, and layered reservoirs.

Archives of the Hibernia basin map on the Canada-Newfoundland and Labrador Offshore Petroleum Board (CNLOPB) website depicted the existence of varying levels of compartmentalization. As production continues, the determinate knowledge of the level and type of compartmentalization in the field increases. The level of compartmentalization is generally indicated by disparities in the history matching and future predictions of the field performance in the reservoir simulation models versus the actual volumes produced. The increasing level of knowledge of the reservoir boundaries and active fault regimes necessitated the periodic update of the field geological and reservoir model and production schedule. Even after the cumulative billion-barrel milestone of oil production from the field was achieved in 2016, more hydrocarbon potential remains in place. The use of multilateral wells for increased compartment access and field drainage has been identified and suggested as one the improved oil recovery programs to be implemented within the next 5 years for the next phase of the field development plan.

Previous efforts on the study of compartmentalized reservoirs have focused primarily on the modeling of production performance from compartmentalization systems. Such reservoirs have been commonly modeled using material-balance techniques (Thomas (2012) and Wang (2016)) by modeling the intercompartment barrier with a reduced transmissibility value, while other models considered transient flow within the compartments (Fox et al., 1998). The material-balance approach neglects the internal resistance to fluid flow and possible compartment heterogeneity,

while the transient-flow model which we adopt in this work is more general and consider the internal resistance to fluid flow within the reservoir compartment.

1.8 Thesis Objectives

The objective of this work is to compare the finite volume versus finite difference numerical discretization techniques in predicting the productivity of multilateral wells producing from compartmentalized reservoirs.

A multi-segment approach is adopted for the well model. This enables the easy incorporation of both flow-based (mass velocity) pressure drop effects and pressure drop effects due to smart completions in the lateral. A sensitivity analysis of the pressure drop profile variation with number of valves installed in the lateral is conducted. Further, we compare the productivity of a conventional well to that of a well with smart completions. Using several case studies of the fault orientation and sealing capacity, we investigate the productivity of the compartmentalized reservoir model produced by a trilateral well. The production profile results obtained from MRST (finite volume based) is compared to the production profile results from CMG IMEX Simulator (finite difference based). Finally, the optimization potential of using the multilateral with smart completions versus a conventional completion is investigated using the gradient-based adjoint optimization module in the reservoir simulation toolbox.

Project Flow Chart

Figure 7 below presents an outlay of the project flow chart. We commence by first setting up the base case uncompartmentalized reservoir model and multilateral well model in MRST using the parameters presented in **Tables 1-3** in chapter three. The visualization module (*mrst-gui*) is used to generate the well productivities for the given set of reservoir properties and well constraints. An

overview of this procedure is shown in **Figure 9**. To compare the finite difference method to the finite volume method which is the basis of the numerical implementation in MRST, we use the IMEX simulator in CMG to simulate the reservoir and multilateral well model using the same reservoir and well parameters to generate the well productivity profile in MRST. The comparison of both numerical methods in this work is limited to the base case reservoir model only. This is due to the limited flexibility in individual grid block property manipulation in CMG to effectively represent the compartmentalized reservoir case we intend to investigate in this work. Further advantages of MRST as an open source coding simulator over existing reservoir simulators is also presented in chapter three. Secondly, we conduct a pressure drop and productivity analysis comparison for the case of smart well completions versus conventional completion well of equivalent length. Based on the results obtained, an optimization study to investigate the potential of smart (intelligent) completions technology over conventional completions in MRST using the gradient based adjoint method is done. Finally, the base case reservoir model is modified through introduction of faults (represented by very low porosity grid blocks) to compartmentalize the reservoir. The productivity profiles for the case studies investigated (refer to Section 1.9) is then presented.

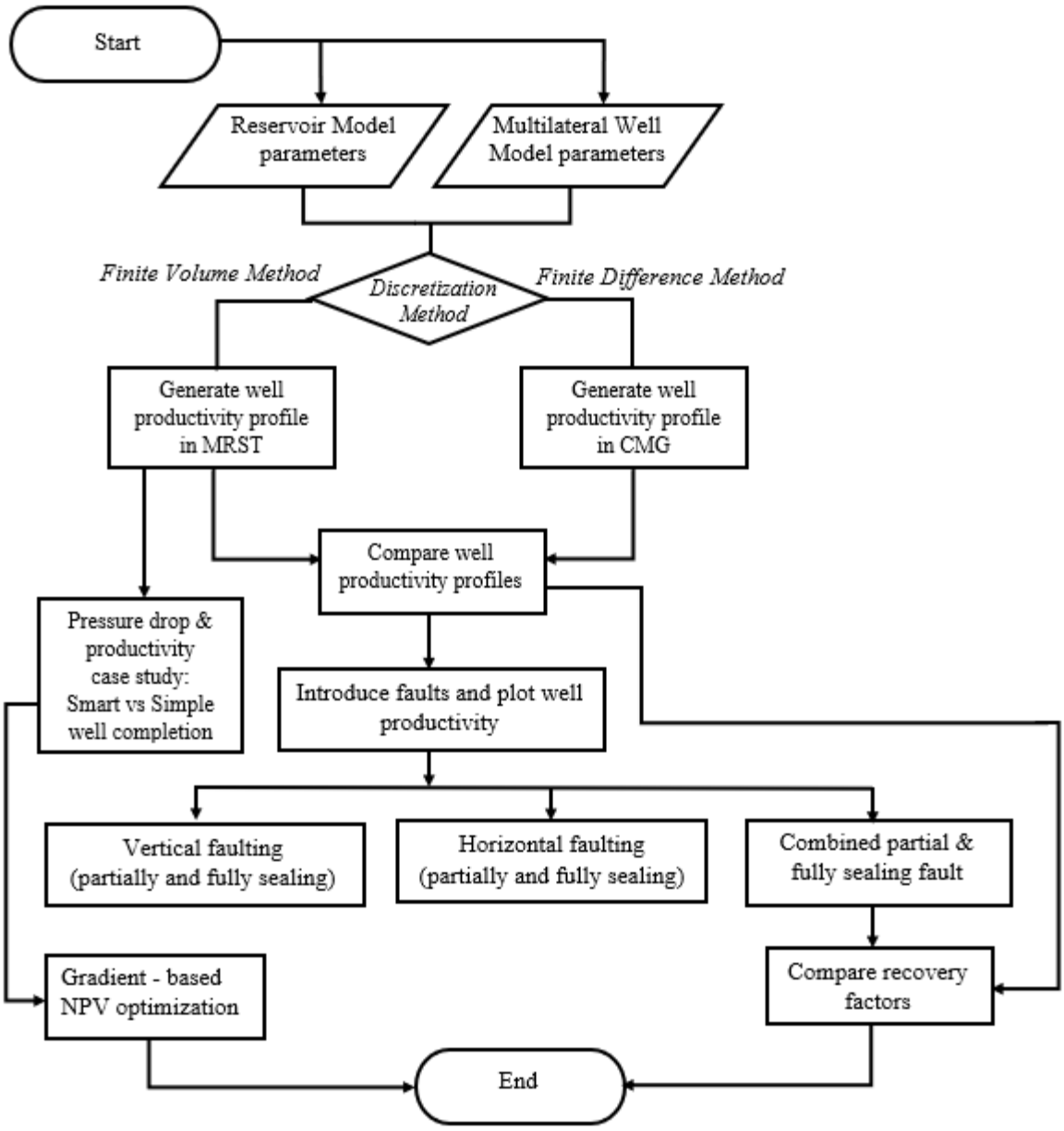

Figure 7 - Project work flow

1.9 Scope of Work

First, a single reservoir compartment with a conventional multilateral well model is set up as the "base case" model. The base case reservoir model is subdivided into three layers with varying macroscopic permeability, thickness, and porosity property distribution throughout the grid model. The well is a trilateral well, with each lateral of equivalent length completed in each of the sub-layers. After complete specification of the reservoir and well parameters, we use the fully implicit solver with automatic differentiation module in MRST to solve the coupled reservoir-well model equation. This method is advantageous because it is unconditionally stable with respect to the time step size, however, in practice the time steps must be set to a small value for the Newton iterations to converge. The robustness of the fully implicit method makes it especially popular for large field simulations. In the well model, each lateral is segmented to ease the incorporation of friction-based pressure drop effects as well as flow control devices (for subsequent optimization study). In order to introduce compartmentalization, the base reservoir model is modified by altering the grid properties representing the fault region in the reservoir with very low porosity values. Further details of the mathematical equations describing the base reservoir and well model setup, the finite volume scheme, and the automatic differentiation method as implemented in MRST is presented in chapter three. The modular design, vectorized framework, finite volume method support for both structured and unstructured grids makes MRST an efficient prototyping and simulation platform for modeling complex reservoir stratigraphies and advanced well models such as the type we explore in this study and represented schematically in **Figure 8** which describes a typical reservoir model compartmentalized by two faults where each compartment may be produced by one or more laterals. The laterals may be of equal or varying lengths depending on the size or

extent of each compartment to be produced. We use horizontal laterals of equal length to produce each of the reservoir compartments in this study.

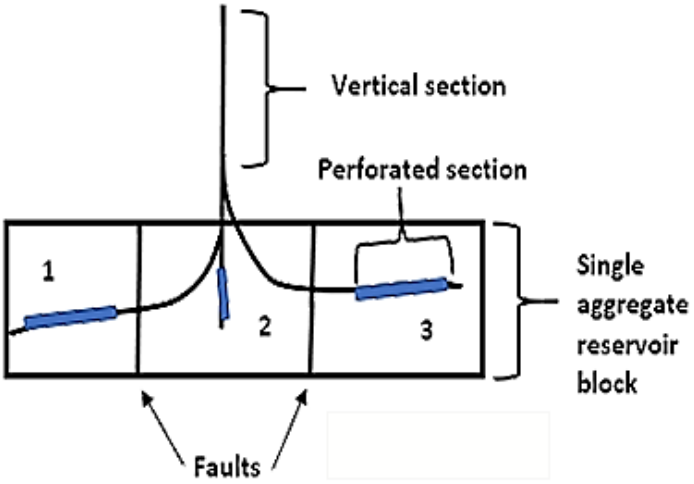

Figure 8 – Compartmentalized reservoir and multilateral well schematic

The following case studies for compartmentalized reservoirs are evaluated:

1. Base case reservoir with no faulting but highly contrasting reservoir sublayer properties
2. Vertical Compartmentalization / Faulting – Noncommunicating (Fully sealing)
3. Vertical Compartmentalization / Faulting – Communicating (Partially sealing)
4. Horizontal Compartmentalization / Shale Layering (Partially sealing)
5. Combined Vertical and Horizontal Compartmentalization (Partially & fully sealing)

1.9.1 Thesis Organization

Chapter two presents a review of literature on compartmentalization, analytical and semi-analytical models for predicting horizontal and multilateral well productivity, numerical reservoir-well coupling and discretization techniques.

Chapter three introduces the Matlab®-based reservoir simulator used in this study, the mathematical model of the reservoir compartment and well model governing equation, the finite

volume numerical discretization scheme and the method of automatic differentiation, the governing equations used in CMG, and description of the case studies investigated.

Results of the base and modified case studies investigated is presented and discussed in chapter four. The conclusions and recommendations for future work is presented in chapter five.

Chapter Two Literature Review

In this chapter, we present findings from literature on early methods of detecting reservoir compartmentalization, the degree of compartmentalization, compartmentalized reservoir pressure transient behavior and the recently developed methods / techniques for detecting compartmentalization in a field. This is followed by a review of current reservoir and well model solution techniques, and brief introduction on the intelligent well technology.

2.1 Compartmentalized field studies

Early researchers in the field of geology and geophysics have posited that the existence of marked differences in fluid and / or rock properties within a field is a crude indication of compartmentalization. Kabir and Izgec (2009) presented a simple diagnostic tool to identify flow behavior from compartmented reservoirs during primary production using a Cartesian pressure – rate graph. They suggested this tool as a precursor to production data analysis and believe that this tool will increase the ease of understanding the reservoir compartmentalization phenomenon and aid the application of appropriate material balance technique to the scenario at hand.

Interestingly, other researchers proposed that the idea of the existence of compartmentalization due to disequilibrium in reservoir and fluid properties (due to geological processes such as uplift, hydrodynamic flow, and biodegradation) may not be accurate simply because there has been insufficient time for the properties to homogenize or equilibrate since the disturbance was introduced to the reservoir. The works of England et al. (1995); Smalley et al., (2004); Muggeridge et al., (2004, 2005); Pfeiffer et al., (2011) showed that different properties reach their equilibrium distribution over significantly different time-scales, even in the absence of compartmentalization. For example, pressure differences tend to equilibrate over years (Muggeridge et al., 2004; 2005)

whereas compositional differences may take millions of years to equilibrate by molecular diffusion over reservoir length scales (Smalley et al., 2004). Thus, observations of spatially varying fluid properties are only likely to provide an accurate indication of compartmentalization if they have existed for longer than the time needed for them to equilibrate. Jolley et al., (2003) emphasized however, that the contrary may also true – highly compartmentalized reservoirs may have very uniform fluid compositions. In other words, fluid data analysis should be used with great care as a tool to assess the level of compartmentalization of a field.

Compartmentalization introduces a significant level of uncertainty during the reservoir appraisal stage, impacting the initial volumetric estimations for recovery from the field. Inaccurate knowledge of the existence and extent of compartmentalization in the reservoir may have a profound, usually adverse effect on oil and gas recovery, most times presenting an otherwise commerical field as uneconomic. It is therefore necessary to characterize compartmentalization early enough in the life of the field, ideally during appraisal, before large investment decisions are made (Jolley et al., 2003).

However, the most indicative data (dynamic prodution data) to identify compartmentalization is not usually available in the early stages of development. Smalley and Hale (1996) using the Ross oilfield in the UK continental shelf as a case study, presented a series of methods to tackle this challenge by integrating various early time field static data: the oil composition geochemistry (molecular maturity parameters, gas chromatography (GC) fingerprinting), oil PVT properties, well test analysis, high resolution stratigraphy, formation water composition (RSA), reservoir heterogeneity modeling, and fault seal analysis to delineate and study the reservoir fluid distribution using various tests such as well test and fault seal analysis, drill stem tests (DST),

density tests, repeat formation testers (RFT). They submit that no single type of static data is definitive when it comes to identifying reservoir compartmentalization, but a combination of several conventional data sources with a few novel ones can greatly enhance the ability to predict compartmentalization. Richards et al., (2010) also illustrated how fluid and pressure distribution in a highly compartmentalized combination trap of the Terra Nova field in the Jeanne D'Arc basin offshore Newfoundland can be understood using a conceptually simple, systematic, three component approach to compartment identification.

Go et al., (2014) then proposed a methodology for determination of the existence of compartments in a reservoir using parameters such as pressure, gravitational overturning and molecular diffusion to propose the time it will take for the fluid property to equilibrate, and submitted that compartmentalization exists if the property variation exists for longer than the time needed for each property to equilibrate.

2.2 Inflow Performance Modeling

Existing solution techniques for well productivity models in literature for horizontal and multilateral wells can be subdivided into three categories:

1. **Simple analytical models** derived on the assumption of infinite wellbore conductivity. These models (Borisov 1964; Giger et al., 1984; Joshi, 1988; Butler, 1994; Helmy and Wattenbarger, 1998; Furui et al., 2003) are widely adopted because they are easy to use. The Joshi model which is one of the most used for calculating the horizontal well productivity is presented as:

$$q_H = \frac{2\pi k_0 h \Delta P/(\mu B_o)}{\ln\left[\frac{a+\sqrt{a^2-(\frac{L}{2})^2}}{L/2}\right] + \frac{h}{L}\ln\left(\frac{h}{2r_w}\right)} \quad (1.0)$$

$for\ L > h\ and\ \left(\frac{L}{2}\right) < 0.9 * r_{eH}$ where r_{eH} is the drainage radius, and *a* is the half major axis of a drainage ellipse in a horizontal plane in which the well is located. *a* is obtained by

$$a = \frac{L}{2}\left[\frac{1}{2} + \sqrt{\frac{1}{4} + \frac{1}{0.5L/r_{eH}}}\right]^{0.5} \quad (1.1)$$

The interested reader can refer to Shadizadeh et al., (2011) for a table listing the correspondence between *L/(2a)* and *L*/ ($2r_{eH}$) values.

However, these analytical models fall short in giving an accurate prediction because they ignore pressure drop in the wellbore. Most horizontal and multilateral wells are frequently thousands of meters. Ignoring pressure drop effects through them can easily lead to an overestimation of the well productivity. These analytical models are hence suitable for first approximations and studying sensitivities of the effect of reservoir and well parameters but are not proper for field applications.

2. The **Semianalytical solution techniques** for calculating inflow productivity can be categorized into two: The method of mathematical physics which uses Laplace Transformation and Green's Functions to derive reservoir inflow, and the use of formation damage skin factor models to calculate specific productivity index, $J_s(x)$ coupled with the drainhole pressure drawdown ($p_r - p_w(x)$) derived from the wellbore flow model. The productivity can be calculated by equation (1.2) below:

$$Q_s = \int_0^L J_s(x)\,[p_r - p_w(x)]dx \tag{1.2}$$

Early work in this area using the semi-analytical models included single horizontal wells (of infinite conductivity) aligned parallel to one side of a box shaped reservoir. Solution methods of successive integral transforms (Goode and Thambynayagam, 1987; Kuchuk et al., 1988) and instantaneous Green's functions (Daviau et al., 1985; Clonts and Ramey, 1986; Ozkan et al., 1989; Babu and Odeh, 1989), resulting in infinite series expressions were employed. More complex well geometries were considered later (Economides et al., 1996; Maizeret, 1996; Ouyang and Aziz, 2001) with the application of numerical integration techniques. Ouyang (1998) and a number of papers cited within included the coupling of wellbore hydraulics (i.e., finite conductivity wells) with reservoir flow.

Aziz et al., (2004) developed a generalized model capable of handling downhole control devices. They also modified the model to incorporate fine scale heterogeneity by introducing an effective skin parameter as a function of location along the wellbore. All the above mentioned authors assume a fully penetrating well, steady state pressure regime and single phase fluid flow. Zhao et al. (2014) most recently presented a novel mathematical model for single-phase fluid flow from unconsolidated formations to a horizontal well with the consideration of stress-sensitive permeability. The model assumes the formation permeability is an exponential function of the pore pressure. Using a perturbation technique, the model is solved for either constant pressure or constant flux or infinite lateral boundary conditions with closed top and bottom boundaries. Through Laplace transformation, finite Fourier transformation, and numerical inversion methods, the solutions were obtained and the pressure response curves are analyzed.

The techniques mentioned above have the advantage of limited data requirements and high degrees of computational efficiency relative to finite difference simulation. This makes them well suited for use as screening tools for approximate simulations of primary production.

However, they are all limited either by the single phase, and/or homogeneous systems or at most strictly layered systems. This represents a substantial limitation because the error in prediction of the production capacity from nonconventional wells, especially for multilaterals which may be producing from several reservoir compartments with varying degrees of deviation from the assumptions incorporated into these models.

3. **Numerical modeling techniques:** While previously presented analytical and semi analytical solution techniques are an attractive method because they require less input, effort, and time, especially for a single bore well, numerical models are more accurate in modeling complex reservoirs and advanced wells. This is because the complex set of governing partial differential equations resulting from the coupled reservoir fluid flow and wellbore flow dynamics are not amenable to manual solution by hand. Hence, numerical approximation techniques are used.

   Classical reservoir simulation methods are based on first-order Finite Difference (FD) schemes applied to regular grids. Although widely used, this method was deficient in resolving sharp material interfaces and oblique faults in realistic models of reservoir geometries. Stone et al. (1989), using the finite difference approach solved the coupled reservoir and the Peaceman well representation for a thermal, three-phase, one dimensional model using the Yale sparse banded matrix package. No mention of the inclusion of friction effect in the well was made. Folefac et al., (1991) incorporated the friction effect into their

own model and examined the effect of well diameter, length and roughness on the magnitude of pressure drop in a horizontal well. The above works are finite difference based and have a measure of inaccuracy in the estimation of pressures near the wellbore.

We present a brief review of the earliest known numerical method and its features:

The Finite Difference Method (FDM):

FDM is the oldest method for numerical solution of Partial Differential Equations and believed to have been introduced by Euler in the 18th century. It is the easiest method for simple geometries. Transformations are needed to map a body-fitted grid into an orthogonal computational grid (Aziz, 1979). Such transformation may not exist for some irregular geometries or may be extremely cumbersome to perform. Hence, the finite difference method utilizes a structured grid to perform calculations (Chen et al., 2006). It uses the differential form of the governing equations (mass, momentum and energy conservation laws) to formulate the mathematical discretization by providing an approximation to the governing partial differential equations using the Taylor series. Methods of forward, backward and central difference can be used either on the point centered or block centered grid systems. Although, the difference equation written for the two grid systems are the same in form. However, when the grids are not uniform; the locations of points and block boundaries do not coincide (Chen et al., 2006). Also, the treatment of boundary conditions with the finite difference grid systems are different. The point centered grid is accurate for Dirichlet conditions (pressure boundary condition), while the block centered grid must be extrapolated to define the pressure on the boundary.

A drawback of the finite difference methods is that the solution of a partial differential problem heavily depends on spatial orientations of the computational grid. This is known as the grid orientation effect (Chen et al., 2006).

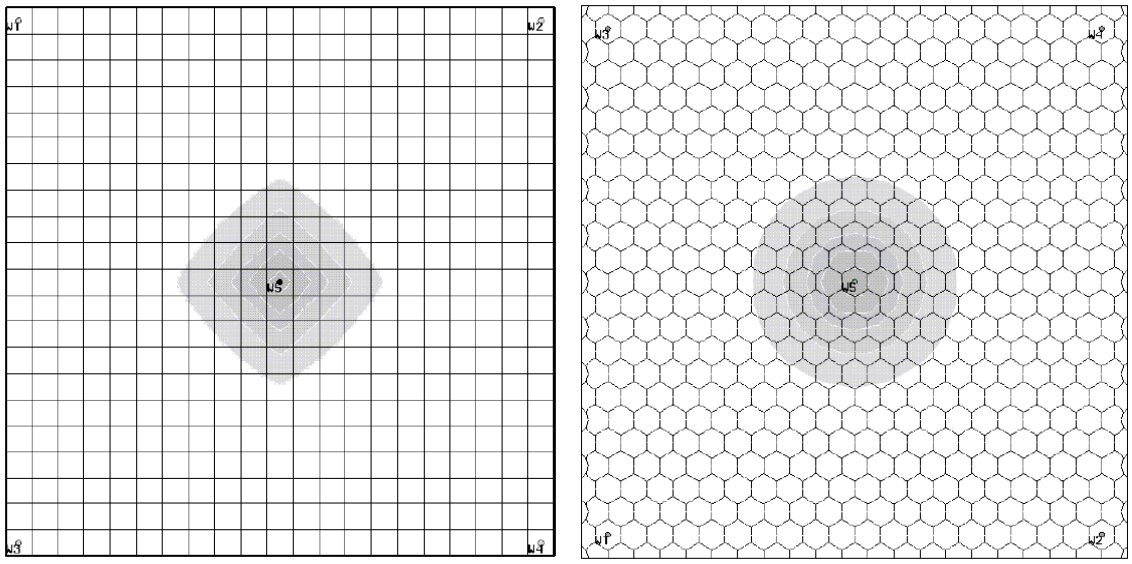

Figure 9 – Dispersion effect in finite difference vs. finite volume methods (Chen et al., 2006).

The above phenomenon implies that predictions with a significant difference can be obtained from simulators using different grid orientations and / or discretization schemes. For instance, the upwind technique used in an explicit finite difference scheme is written as

$$\frac{p_i^{n+1} - p_i^n}{\Delta t} + b\,\frac{p_{i+1}^n - p_i^n}{h} = 0 \tag{1.21}$$

Then for a two-dimensional counterpart, the resulting numerical dispersion is related to the quantity

$$\frac{h_1}{2}\frac{\partial^2 P}{\partial x_1^2} + \frac{h_2}{2}\frac{\partial^2 P}{\partial x_2^2} \tag{1.22}$$

where h_1 and h_2 are coefficients, P is the pressure, $x_1$and x_2 are the coordinate directions.

Equation (1.22) is not rotationally invariant and is thus directionally dependent on the coordinate axes ($x_1$and x_2). Therefore, when we model multiphase flows with a high mobility ratio (mainly due to a large viscosity ratio), once a preferential flow pattern has been established, the greater mobility of the less viscous fluid causes this flow path to dominate the flow pattern. With the five-point (two-space) or seven-point (three -space) finite difference stencil scheme, preferred flow paths are easily established along the coordinate directions. Consequently, the use of an upwind stabilizing technique greatly enhances flow in these preferred directions. This grid orientation effect can be dramatic in cases with very high mobility ratios (Chen et al., 2006).

The Finite Volume Method:

The Finite Volume Discretization Method (FVM) uses the integral form of the governing equations to formulate the mathematical discretization, as compared to finite difference methods (FDM), which uses the differential form. It is suitable for complex geometries, because it can be applied to both structured or unstructured grid types. The mathematical basis for all integral form discretization methods, including the finite volume lies in the ability to find a function, W(x), also known as weight or trial function (Chen et al., 2006). The FVM which is the method of discretization used in MRST has a greater accuracy in yielding the mass, momentum and energy conservation terms despite any discontinuity in the domain (e. g. a domain split by fault line (i. e. compartmentalized reservoirs)). The finite volume discretization scheme also allows for additional flexibility in grid and wellbore geometry modeling (Lie, 2016)

2.3 Multilateral Well Productivity

Predicting the performance of a multilateral well with commingled production is analogous to predicting the interdependent production from multiple wells tied to a common gathering system. The problem consists of predicting the inflow characteristics of each lateral, determining the pressure drop behavior in the build sections between the laterals and the main wellbore, and modeling the flow and pressure drop in the main wellbore from the lowest junction to the surface (Hill et al., 2008). The parts of the multilateral well system are all connected and influence one another, requiring either simultaneous solution of the equations describing the different parts of the system or an iterative solution to solve for the unknowns throughout the system.

Salas et al., (1996) presented one of the earliest analytical models to carry out a rapid assessment of the productivity of several multilateral configurations in homogenous formations, infinite slab, and single-phase fluids. Although their model was not useful for direct application in multiphase well performance, it has been successfully used to validate and develop grid block connection factors for multiphase models. Subsequently, they presented case studies to demonstrate the advantages of multilateral wells over single laterals in reservoirs with certain types of geological heterogeneity where the multilateral well maintained high productivity and at the same time, achieved a high standoff from reservoir faults versus a single lateral.

Chen et al., (2000) then developed a coupled reservoir-wellbore model to predict deliverability for multilayered multilateral wells to examine the effect of varying reservoir pressures and lateral extent on productivity. The drawback of their work was that they considered only single-phase transient and pseudo-steady state flow regimes for non- communicating reservoir compartments.

Yildiz (2002) evaluated the long-term rate decline and cumulative recovery response of multilateral wells connecting non-communicating formations for single phase flow. Cross flow between the layers was investigated. The same author in 2005 developed a three-dimensional multilateral productivity model and then presented a comparative analysis of the results versus experimental study of Salas et al. (1996). Good agreement between both models was observed. Ouyang and Huang (1998) performed a history matching process to validate the oil production from a dual-lateral well by coupling reservoir inflow and wellbore hydraulics in a numerical finite difference simulator. Guo et al., (2007) presented a rigorous composite multilateral well inflow productivity model using the Poettmann and Carpenter correlation. The model yielded more accurate results than earlier models. Pan et al., (2010) presented several scenarios where the application of a generalized semi-analytical segmented model was used in predicting the production performance of multilaterals with an arbitrary number of laterals, *n* and commingled flow from layered reservoirs under constant –rate or constant- pressure well system.

The above proposed models according to the authors have demonstrated reasonable sufficiency in the prediction of the productivity behavior of different multilateral well configurations, they fall short when it comes to predicting the life time production from non-single-phase flows and complex reservoir architecture for all pressure regimes throughout the life of the well.

This work improves on this gap by using an improved discretization technique for productivity prediction and a practical evaluation of the benefits of the multilateral well technology in various complex reservoir scenarios with multiphase flow.

2.4 Smart (Intelligent) Well Completions

A “smart“ or “intelligent” well is considered one of the most advanced types of nonconventional wells. A typical smart well is equipped with a special completion that has packers or sealing elements which allow partitioning of the wellbore, pressure and temperature sensors and downhole inflow control valves (ICV) installed on the production tubing. The sensors allow continuous monitoring of pressure and temperature while the ICVs provide the flexibility of controlling each branch of the multilateral well independently. A smart well can be either a multilateral well where every lateral is controlled by an ICV or a single bore extended length horizontal well where each segment is controlled by an ICV. The advantages of smart wells have been demonstrated in practical applications for both single and multi-reservoir scenarios for commingled and non-commingled production (Jalali, 2005). The ability to control production from each lateral or segment through ICV adjustment and manipulation enable wells with smart completions to mitigate water production by allocating the optimum production rate to the best performing lateral(s), thereby increasing the ultimate hydrocarbon recovery.

Unlike conventional wells where only surface control is used to determine the optimum production rate, optimization of smart wells requires determination of the best combination of ICV settings (or configuration) that yields the highest recovery factor and hence profit. In the case of commingled production, laterals or branches are in contact with each other within the immediate vicinity of the reservoir, this adds another dimension to the optimization process as one lateral might affect the performance of other laterals (in the case of water breakthrough). The production engineer’s goal is to maximize hydrocarbon production from the field assets over the productive life, hence production optimization (maximizing oil production over long term while minimizing

total production costs to achieve the maximum profitability) from the well or field is paramount (Ajayi et al., 2003).

The smart well technology provides the capability to remotely control, monitor and manage production and or injection in a field; especially when commingling from multiple compartmented or layered reservoirs which we investigate in this work. This has the potential to reduce cost of well interventions and accelerating production. Due to increased production, flow control (or stabilization) is critical to maximize the production of desired fluids over the long term. As mentioned previously, flow control of each lateral in the multilateral system is provided by downhole inflow control valves (ICVs). These valves may be binary (on-off behavior) or multi-position, to choke or increase production from any lateral, layer or compartment.

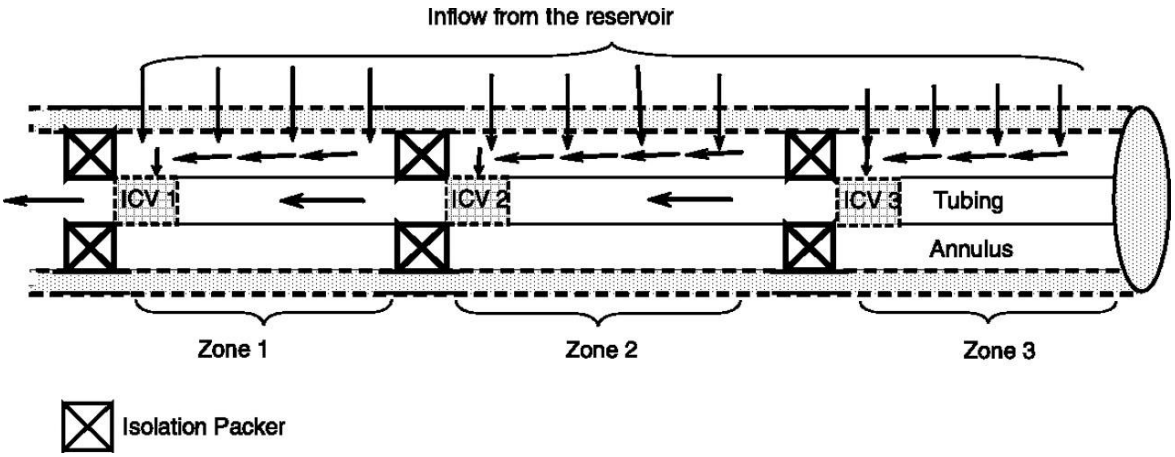

Figure 10 - ICV for downhole lateral control (Ebadi et al., 2008)

The fluid is choked back so fast flowing zones are retarded and uniform low is achieved across the completion. This helps to reduce the localized hydraulic forces that contribute to coning of water or sanding. In a thief zone, or zone of higher permeability, the device exerts a higher back pressure due to higher linear fluid velocity of the fluid. As a result, the thief zones are starved, and the low permeability zones receive more fluid (Ajayi et al., 2003).

Ajayi and Konopczynski (2003) presented an optimization technique which uses a derivative method and iterative process to obtain the optimal valve settings in a bid to simulate the functionality of an intelligent well system in a multi-layer commingled production scenario. It was established that the use of the intelligent well control system resulted in a prolonged plateau for oil production and minimized water production, which ultimately led to a 63% increase in oil recovery from the case studies considered for the intelligent system versus the conventional system.

Mjaavatten et al., (2008) in their work presented a model that introduced an extra pressure drop in the well to reduce the time to gas breakthrough. They submitted that gas inflow into a well will dominate flow after initial gas breakthrough if it is not restricted by gravity or an advanced completion. ICDs introduce an extra pressure drop that is proportional to the square of the volumetric flow rate. The dependence of this pressure drop on fluid viscosity is weak for channel devices and totally absent if nozzle or orifice ICDs are used. Zarea (2010) integrated existing productivity model to predict and optimize the reservoir, well performance and pressure drop profile through an inflow valve model for the case of a single and two-phase flow in the horizontal lateral of the multilateral well. Birchenko et al. (2010) then presented an improved model to describe the effective reduction of inflow imbalance caused by reservoir heterogeneity using ICDs (Inflow Control Devices). Their model addressed a key question relating to the application of the ICD technology: the trade-off between well productivity and inflow equalization. They submitted that the increase in ICD strength causes an effective reduction in the well productivity and an equalized inflow pattern across all segments of the well.

2.5 Mathematical Optimization Scheme

Here, we briefly introduce the concepts, solution algorithms, and applications of major subfields in mathematical programming in the field of optimization related to this study. Applications of optimization techniques to oil production in the industry began in the early 1950s and has continued to receive more attention especially in areas such as enhanced recovery processes, planning and history matching, well placement optimization, and operation, drilling, facility design. Optimization techniques employed in these applications cover almost all subfields in mathematical programming, such as linear programming, integer programming, and nonlinear programming (Wang, 2013).

Optimization problems in the most general form can be formulated as

$$\min\{f(\boldsymbol{x}): \boldsymbol{l_i} \leq c_i(\boldsymbol{x}) \leq u_i, i = 1 \dots m\} \tag{1.3}$$

where the objective function *f* and the constraint functions $\{c_i\}$ are functions of control variable *x*, and l_i and u_i are the lower and upper bounds for the *i*-th constraint, respectively.

An optimization problem can be categorized according to the type of its control variables, and objective and constraint functions.

Linear Programming **(LP)**: When the objective function *f* and constraint functions $\{c_i\}$ are linear functions of control variable $\boldsymbol{x}$, the problem described by Eq. (1.3) is a linear programming (LP) problem. The simplex algorithm, introduced by Dantzig in 1963 finds the optimal solution of an LP problem by moving along the vertices of the feasible region, thus its optimal solution is always a vertex (or an extreme point) of the feasible region. Although the simplex method is efficient, it can take many iterations, an alternative solution methodology called interior point iteration was formulated by Karmakar in 1984 for the LP problem by searching for the optimal solution from the interior of the feasible region. Nowadays, LP problems with thousands or even millions of

variables and constraints can be solved efficiently by both the simplex and interior point algorithm (Bertsimas and Tsitsiklis, 1997).

Integer Programming **(IP)**: When all components of the unknown $\boldsymbol{x}$ are discrete variables, the problem described by Eq. (1.3) becomes an integer programming (IP) problem. When some but not all components of $\boldsymbol{x}$ are discrete, the problem is a mixed integer programming (MIP) problem. Discrete variables are useful to model indivisibility, logical requirements, and on/off decisions (Wang, 2013).

Nonlinear Programming **(NLP)**: Eq. (1.3) becomes a nonlinear programming problem when its objective and/or constraint functions are nonlinear. This form of programming problem is the most encountered in areas related to production optimization. There are several optimization types that fall into this category:

Unconstrained Optimization Method*:* An important class of methods for solving unconstrained optimization problems is the line search method. This method approaches a local minimum using the following iteration scheme:

$$\boldsymbol{x_{k+1}} = \boldsymbol{x_k} + \alpha_k \boldsymbol{p_k} \tag{1.4}$$

where $\boldsymbol{x_k}$ and $\boldsymbol{x_{k+1}}$ are the current and next iterates, $\boldsymbol{p_k}$ is a search direction along which the function decreases, and α_k is a step length that ensures "sufficient" progress toward the solution.

Constrained Optimization Method: The optimum of a constrained optimization problem is characterized by a certain set of conditions which were first established by Kuhn and Tucker (1951). Most used constrained optimization methods include sequential quadratic and linear programming methods, reduced-gradient methods, and methods based on augmented Lagrangians, penalty, and barrier functions (Gill et al., 1981).

Separable Programming is a special class of nonlinearly constrained optimization problems whose objective and constraint functions are sums of functions of one variable. Separable programming problems are usually solved by linear programming techniques (Hillier and Lieberman, 2001).

Direct Optimization methods refer to optimization methods that do not require derivatives. When selecting an optimization method, a general rule is to choose a method utilizing as much derivative information as possible (Gill et al., 1981). However, when problem functions are not smooth, or the derivatives are too expensive to compute, one may choose a direct optimization method. A thorough review of the direct optimization methods is given by Powell (1998).

Genetic Algorithms **(GAs)** are heuristic optimization algorithms introduced by Holland (1975). GAs employ the idea of natural selection and genetics in the process of searching for the global optimum of a problem. In GAs, possible solutions are encoded as chromosomes and modified by means of selection, crossover, and mutation. GAs are versatile in handling both the discrete and continuous variables naturally and require no domain knowledge of the optimization problem.

Sequential Quadratic Programming (SQP) is a derivative-based optimization algorithm. Successful application of SQP requires efficient and accurate evaluations of gradients of objective and constraint functions.

2.6 Dynamic Optimization Scheme

One of the goals of efforts spent on modeling a petroleum field with complex reservoirs and advanced well networks is to devise an optimal strategy to develop, manage, and operate the field. For fields such as these, production optimization can be a major factor in increasing production rates and reducing production costs. While for single wells or other small systems simple nodal

analysis may be adequate, large complex systems demand a much more sophisticated approach to predict the response of a large complicated production system accurately and to examine alternative operational scenarios efficiently (Wang, 2003). The resulting dynamic behavior of these fields is typically simulated with large-scale nonlinear numerical models, containing several orders of state variables and parameters. This poses a level of uncertainty in the parameter values characterizing the properties of the subsurface reservoir. Hence, optimization techniques have developed to proffer solutions, given the current limitations of knowledge about the system parameters which are known only known to varying degrees: the fluid properties can usually be determined from the laboratory, but the reservoir properties are only really known at the wells. The reservoirs are characterized by varying levels of heterogeneity, and the parameters relevant to flow are correlated at different length scales. This leaves a lot of gap in knowledge of the reservoir parameters; hence engineers make simplified assumptions in constructing the reservoir representative models to simulate the fluid flow and recovery process (Jansen et al, 2009).

Two possible ways of implementing control are: Reactive Control and Predictive Control. The reactive control method has been the known method of control which is implemented as an "after effect": after an undesirable situation is in effect. The predictive control however prevents occurrence of the unwanted situation in the first place. This method utilizes a history matched and calibrated reservoir model to forecast future production quotas from the pay zones in the field, to make plans to forestall unwanted expected production (Ajayi et al., 2003).

Generally, production management activity attempts to optimize an entire asset continuously by:

- Using all available information up to that point
- Predict future outcomes with certain confidence
- Make decisions that would produce optimal future outcome

- Implement such decisions until the next decision-making point in time.

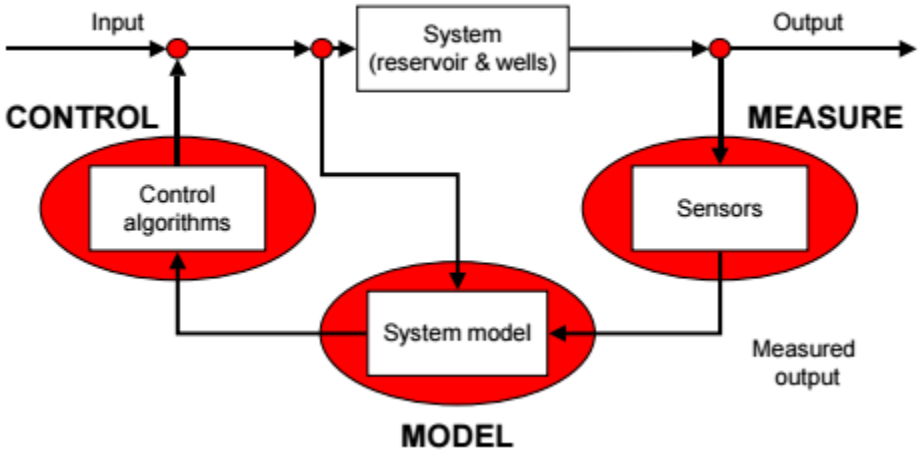

Figure 11 - The field development cycle as an optimization process (Jansen, 2001)

Parameters to determine include number and position of development wells, the optimal water injection and oil production flow rates over the life of the reservoir. Recently, advancement in the technology of measurement and control devices have given us possibilities to control subsurface flow. Now, a suite of downhole tools; sensors, meters, valves are being installed and these devices give near-continuous information about the system pressures and phase rates. In addition, other measurement techniques have emerged that give an impression of the changes in reservoir pressure and fluid saturations in between the wells (Jansen et al, 2008).

Cetkovic et al. (2016) in their paper recently developed a methodology for the optimization of multilateral well productivity with inflow control devices through a multiphase flow simulator. Two factors they investigated are the flow dependent gas-oil ratio rate, and the interference between laterals. Capability to monitor the displacement of oil-water or oil-gas fronts between injection and production wells at regular intervals have increased. By combining the measured response of sensors and the simulated response of the system models it is possible to judge to what extent the models represent reality. With the aid of systematic algorithms for data assimilation it

is then, to some extent, possible to adjust the parameters of the individual grid blocks of the numerical models such that the simulated response better matches with the measured data, and, hopefully, such that the models give better predictions of the future system response (Jansen et al, 2008). Also, Akapo (2016) investigated the effectiveness of using a Proportional-Integral-Derivative controller (PID) to regulate the error and the variations in pressure and saturation during the simulation of a reservoir system. The performance of the PID controller was compared to the basic controller conventionally used in adaptive time-stepping. The results show that PID algorithm used to control the variations in pressure and saturation can be more efficient than the basic controller if the proper PID coefficients are used in the simulation.

For a given reservoir – well configuration, especially in flooding, we can use the well rates or pressures to optimize the flooding process over the life of the reservoir with the objective function expressed as:

$$J\left(\boldsymbol{u}_{1:k}, \boldsymbol{y}_{1:k}(\boldsymbol{u}_{1:k})\right) = \sum_{k=1}^{K} J_k(\boldsymbol{u}_{1:k}, \boldsymbol{y}_{1:k}) \tag{1.5}$$

where K is the total number of time steps, and where J_k represents the contribution to J in each time step. J_k in a typical objective function is written as:

$$J_k = \left\{ \frac{\sum_{i=1}^{N_{inj}} r_{wi}(u_{wi,i})_k + \sum_{j=1}^{N_{prod}} r_{wp}\left(y_{wp,j}\right)_k + r_o(y_{o.j})_k}{(1+b)^{\frac{t_k}{t}}} \right\} \Delta t_k \tag{1.6}$$

where the control variables $u_{wi,i}$, are the water injection rates in wells i =1, … N_{inj}, the output variables $y_{wp,j}$, and $y_{o.j}$, are the water and oil production rates in wells j =1, … N_{prod}, and are the (negative valued) unit costs for water injection and water production, r_o is the unit income for oil production, and t_k and $t_{k+1} - t_k$ are the time and the time interval corresponding to time step k.

The term in the denominator is a discount factor that represents the time-value of money, where *b* is the discount rate (cost of capital) for a reference time, τ. Constraints may be expressed in terms of state variables or the input variables may be equality or inequality constraints, which we represent in a general form as (Jansen et al, 2008)

$$c(\boldsymbol{u}_k, \boldsymbol{x}_k) \leq 0 \tag{1.7}$$

Typical input constraints are limits on the total water injection capacity, and typical state constraints are maximum and minimum pressures in the injection and production wells respectively. The optimization problem can now be formulated as finding the input vector $\boldsymbol{u}_k$ that maximizes J over the time interval $k = 1, \ldots, K$, subject to the system equations, initial conditions, output equations, and constraints. The resulting formulation is nonlinear in the inputs and the constraints, and it is nearly always nonconvex. Usually, a gradient-based optimization technique where the derivative information is obtained using an adjoint equation to iterate to a locally optimal solution is used. (Brouwer and Jansen (2004), Van Essen et al. (2006) and Zandvliet et al. (2007). Implementation of the adjoint formulation in a numerical reservoir simulator is conceptually simple if the simulator is fully implicit, because in that case the Jacobian matrix $\partial g_k / \partial x_k$, which is required in the adjoint formulation, is already available (by automatic differentiation). One disadvantage of gradient-based techniques is their tendency to arrive at a local optimum rather than a global solution. This is particularly the case if we have several well controls and a large number of points in time at which we may change the control setting, resulting in a very large number of possible control trajectories.

Chapter Three Methodology

The first step in this work as outlined presented in the project flow chart in **Figure 7** entails setting up the base reservoir and multilateral well model to be used in MRST and CMG IMEX Simulator. A comprehensive description of the base case reservoir and well model parameters used is outlined later in **section 3.5**. The procedure followed in setting up the reservoir and multilateral well code in MRST is presented below in **Figure 12**. The goal is to compare the well productivity profiles generated by the numerical discretization method underlying the simulators; the finite difference method in CMG and the finite volume method implemented in MRST. After obtaining the results from both methods, a grid refinement operation is then carried out in CMG to determine the optimal grid resolution which will produce a similar productivity (fluid cut fraction vs. time) result between the two methods. After obtaining a close comparison between the two methods in this stage, we then proceeded to conduct further simulations using MRST to investigate the pressure drop behavior and associated productivity of a smart completion (lateral with downhole low control valves) versus simple or conventional well (without downhole flow control valves) using the in-built simulation toolbox coding algorithm. A nozzle valve model (refer to Section 3.6.2 for valve description) is implemented at the node centrally located between the reservoir grid block and the well block in the lateral. Based on the results from this case, we conduct an optimization study to investigate the cash flow potential and net present value of using smart well completions over conventional completions (without downhole flow control device). After investigating the pressure drop profile, we then alter the base case reservoir model by introducing fault bodies (represented by grid blocks of very low porosity) to compartmentalize the reservoir. Finally, the production profile resulting from these cases is presented and discussed. The Matlab codes for

setting up the reservoir and well model as well as the compartmentalized case studies is outlined in **Appendix B3**.

3.1 Reservoir and Well Model Setup

As stated in the preceding section above, the reservoir and multilateral well is modeled using the collection of recently developed open source code data structures, functions, and workflows for reservoir simulation based in Matlab® called the Matlab Reservoir Simulation Toolbox (MRST Version 2017a, released April 2017).

An overview of the procedure for building the reservoir compartment and well model in MRST is outlined in **Figure 12** below. The coding scripts used to set up the base case and subsequent case study runs are provided in **Appendix B3.**

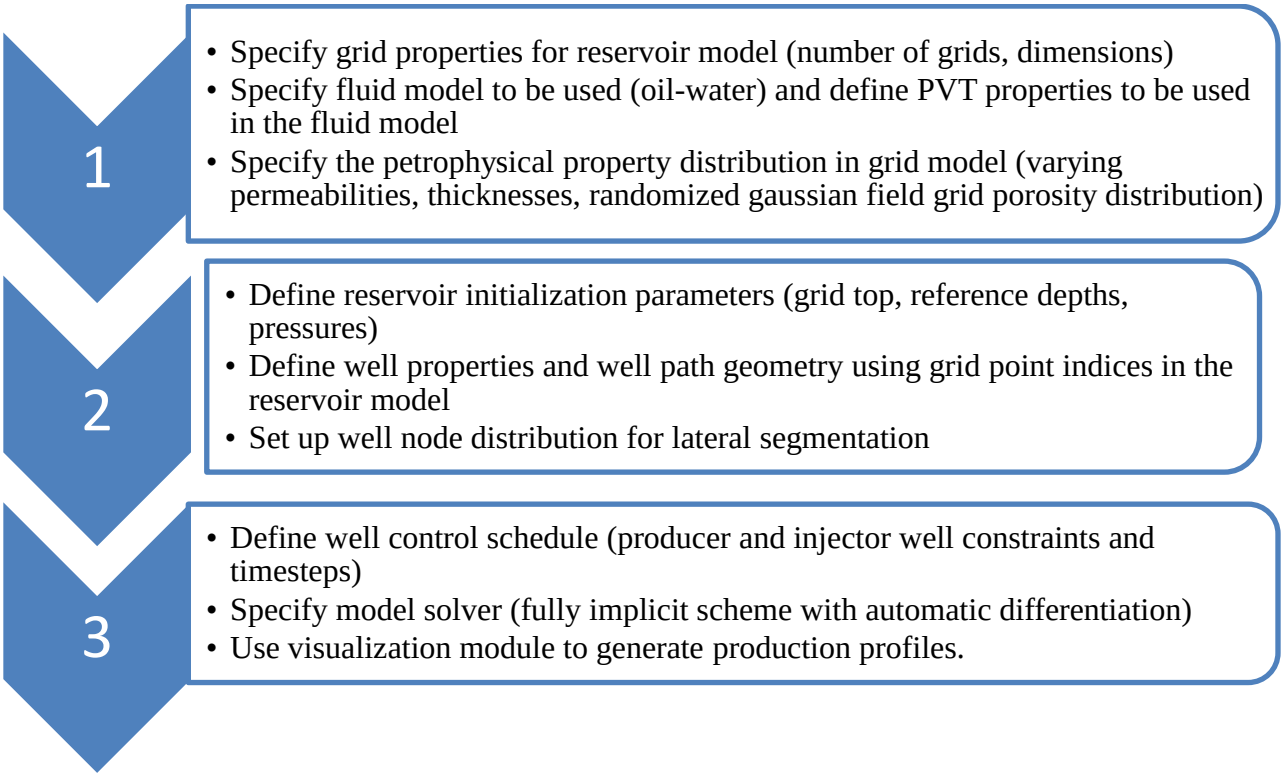

Figure 12 – Procedure for reservoir and well model set up in MRST

Commercial reservoir simulation packages like Eclipse® by Schlumberger, IMEX® by CMG (Computer Modeling Group) are widely used in industry. These simulation packages have different strengths and weaknesses depending on the purpose for which they are applied. These commercial software packages have one major limitation; they cannot be modified by the end-user. Consequently, studies that require an improvement or slight modification of the governing equations to suit specific purposes cannot be implemented in these softwares. However, MRST compensates for this lack of flexibility by aiding the development of new simulators for any reservoir type, fluid displacement type or well model for academic and research purposes provided they can be mathematically described by an appropriate set of equations.

3.2 CMG Governing Equations

The governing equations used in CMG is briefly presented below. Conservation of the water phase in a matrix sub-block *k* in the *x*-direction is written as:

$$T^{x}_{wm_{k-\frac{1}{2}}}\left(p^{n+1}_{wm_{k-1}} - p^{n+1}_{wm_k}\right) + T^{x}_{wm_{k+\frac{1}{2}}}\left(p^{n+1}_{w_v} - p^{n+1}_{wm_k}\right) - \frac{V_{b_k}}{\Delta t}\left[\left(\frac{\emptyset S_w}{B_w}\right)^{n+1}_{m_k} - \left(\frac{\emptyset S_w}{B_w}\right)^{n}_{m_k}\right] = 0 \quad (3.0a)$$

while the oil conservation equation for the matrix sub-block *k* is written as:

$$T^{x}_{om_{k-\frac{1}{2}}}\left(p^{n+1}_{om_{k-1}} - p^{n+1}_{om_k}\right) + T^{x}_{om_{k+\frac{1}{2}}}\left(p^{n+1}_{o_v} - p^{n+1}_{om_k}\right) - \frac{V_{b_k}}{\Delta t}\left[\left(\frac{\emptyset S_o}{B_o}\right)^{n+1}_{m_k} - \left(\frac{\emptyset S_o}{B_o}\right)^{n}_{m_k}\right] = 0 \quad (3.0b)$$

where T is the transmissibility index, p is the pressure in each grid block, t is the time, $\emptyset$ is the porosity, S is the phase saturation, B is the phase formation volume factor, and V_b is the volume of the grid block. Equations (3.0a) and (3.0b) are discretized into finite-difference form using first order backward differences in time, and central differences in space with upstream mobility (User's Guide IMEX, Version 2013.)

3.3 Matlab Reservoir Simulation Toolbox (MRST) Description

MRST was developed by SINTEF Applied Mathematics and is a result of their research and development effort on multiscale computational methodologies (Lie, 2016). The toolbox code is open source and can be downloaded under the terms of the GNU General Public License (GPL) (Lie et al., 2012). The toolbox contains routines for grid processing (based on finite volume discretization method), rock and fluid modeling, linear and nonlinear solvers, and results visualization (Lie, 2016). The basic structure of coding in MRST is shown in **Figure 13** below. The grid specification, fluid properties, and rock petrophysical data structures once fully defined are passed as inputs into the oil-water model function. The combination of the input data structures (grid, rock, and fluid properties) and the model function creates the base reservoir model we will modify and investigate for various compartmentalized scenarios. The well model property specification and boundary conditions are combined into a single data structure to make up the schedule. This makes up the parameters by which the system would be operated. The schedule contains the value of each time step, along with information about which driving forces that are active during each time step. The reservoir model is complete when the grid specification, fluid model, rock petrophysics, initial state, model class and well schedule have been fully specified.

The next step of the simulation is to pass it on to the fully implicit with automatic differentiation solver function. This function then passes back the results in the form of the well solution states struct.

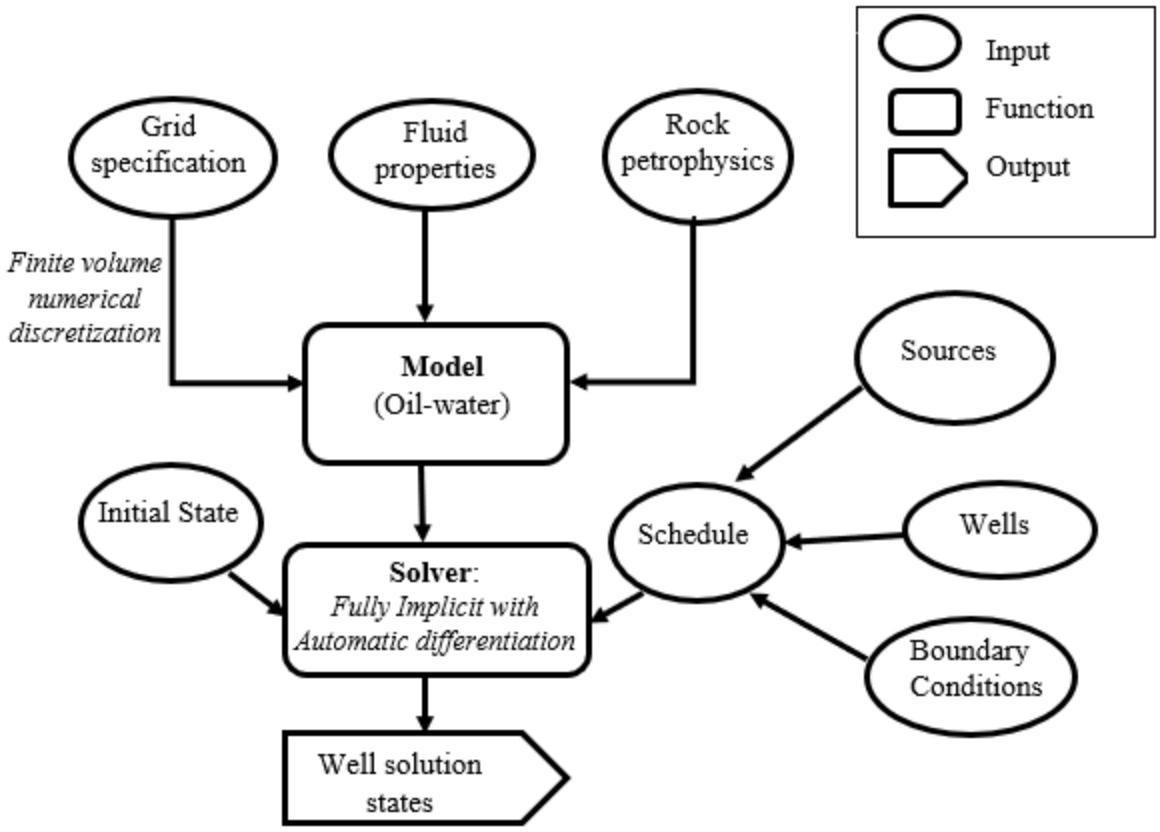

Figure 13 - Structure of the coding script in MRST (after Lie, 2016)

3.4 MRST Governing Equations (Oil - Water Mathematical Model)

The physical system to be modelled must first be expressed in terms of appropriate mathematical equations. The mass balance or continuity equation and the momentum equation provide the governing set of differential equations of fluid flow in the reservoir compartment. It is a generally accepted assumption that the reservoir fluid is in a local and instant thermodynamic equilibrium, therefore the number of mass conservation equations are identical to the number of fluid components (Aziz, 1979).

In this work, we assume strictly oil and water flow through the heterogenous reservoir medium. Also, the reservoir is horizontal and of constant thickness, with gravity and capillary forces neglected. Further, the reservoir considered to be in the secondary recovery phase (water injection)

where the pressures are kept above the bubble point pressure of the oil phase (i.e. no existing free gas cap or evolution out of the oil phase). Therefore, the case is that of two-phase immiscible flow, with no mass transfer between the two liquid phases. Further, the fluids and rocks are incompressible, isothermal conditions prevail, and there is no-flow at the outer boundaries of the reservoir model.

Due to no-flow at reservoir boundary conditions, the pressure differential between the reservoir and the specified well bottom hole pressure create the gradient / driving force in the model. The injector wells inject water while producer wells produce both oil and water. At the wells we can specify the rate (Neumann boundary condition) or the bottom-hole pressure (Dirichlet boundary condition). The Dirichlet boundary condition is used in the producer well while the Neumann condition is used for the injector well.

The Darcy momentum equation for porous media flow showing the relationship between fluid velocities and the pressure gradient is written as:

$$\boldsymbol{v}_{\propto} = -\frac{\boldsymbol{K}}{\mu_{\propto}} k_{r\propto}(\nabla P_{\propto} - \rho_{\propto} g \nabla z) \tag{3.1}$$

where subscript $\propto$ = oil, water phases, $k_{r\propto}$ is the fluid relative permeability, $\boldsymbol{K}$ is the absolute permeability tensor of the porous medium, μ is the fluid viscosity, g is the magnitude of the gravitational acceleration, z is the depth, and ∇ is the gradient operator:

$$\nabla p = \left(\frac{\partial p}{\partial x}, \frac{\partial p}{\partial y}, \frac{\partial p}{\partial z}\right) \tag{3.2a}$$

Introducing the saturation term (fraction of the pore space occupied by a fluid) to account for multiphase flow nature into the mass conservation equation, we have:

$$\frac{\partial}{\partial t}(\rho_{\alpha} \emptyset S_{\alpha}) + \nabla(\rho_{\alpha} \boldsymbol{v}_{\propto}) = \rho_{\alpha} q_{\alpha} \tag{3.2b}$$

Combining Eqs. (3.1)and (3.2b),

$$\frac{\partial}{\partial t}(\rho_\alpha \emptyset S_\alpha) = \nabla\left[\frac{\rho_\alpha}{\mu_\alpha} k_{r\alpha} \boldsymbol{K}(\nabla P_\alpha - \rho_\alpha g \nabla Z)\right] - \rho_\alpha q_\alpha \tag{3.3}$$

The permeability tensor ***K***, whose elements have units of surface area (square meter), represents how easily the fluids flow through the rock in different directions. Usually the orientation of the coordinate system can be aligned with the geological layering in the reservoir such that ***K*** is a diagonal matrix:

$$\boldsymbol{K} = diag\,(k_x, k_y, k_z) \tag{3.3b}$$

where k_x, k_y, k_z are directional permeabilities in the *x, y* and *z* coordinate directions. The dimensionless relative permeabilities, $k_{r\alpha}$ are functions of the water saturation, S_w, and are reduction factors that represent the increase in flow resistance caused by multiphase effects. The Corey relative permeability relationship (Aziz and Settari, 1979) used in the toolbox is stated as:

$$S_{N,\propto} = \frac{S - S_{\propto r}}{1 - S_{wr} - S_{or}} \tag{3.4}$$

$$k_{r\alpha} = {k_{r\alpha}}^0 \left(S_{N,\propto}\right)^{n_\propto} \tag{3.5}$$

where $S_{N,\propto}$ is the normalized water saturation, S_{wr} and S_{or} are the residual water, and oil saturations, ${k_{r\alpha}}^0$ is the end-point relative permeability for each phase $\propto$, and $n_\propto$ is the empirical coefficient (Corey's number) for phase $\propto$.

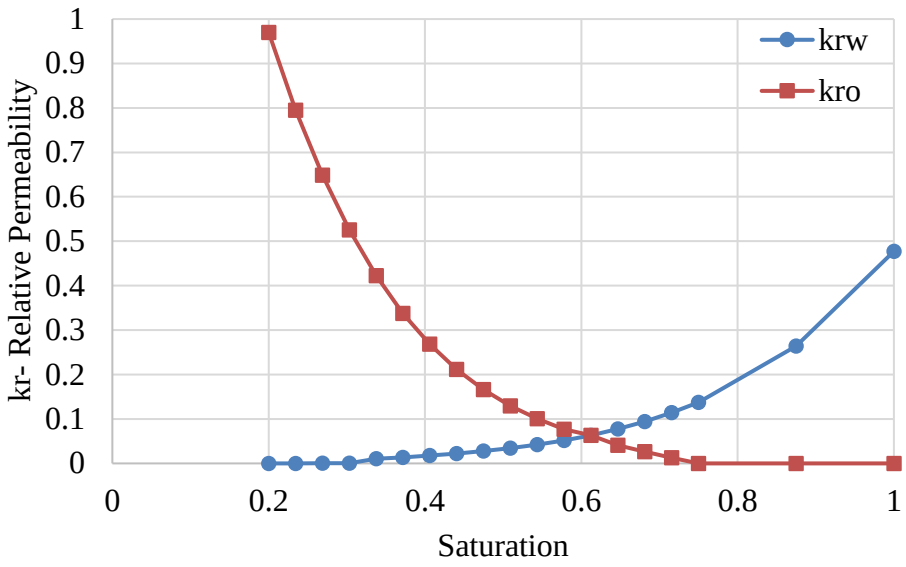

Figure 14 – The oil – water relative permeability curves

Figure 14 shows the relative permeability curves generated for the oil water system with a 20% connate water saturation (S_{wc}) and a 25% residual oil saturation (S_{or}).

Eq. (3.3) for each of the fluid phase results in four unknowns for pressure and saturation of each phase. Eq. (3.6) is an additional saturation relationship specified to reduce the number of unknowns in the equations.

$$S_o + S_w = 1.0 \tag{3.6}$$

Introducing mobility and fractional flow terms, and neglecting the effect of gravity, the pressure and saturation equations (3.1) and (3.3) become:

$$\boldsymbol{v} = -\lambda_t \boldsymbol{K} \nabla p \tag{3.7}$$

$$\phi \frac{\partial S}{\partial t} + \nabla . f_w\,(S)\boldsymbol{v} = q_w \tag{3.8}$$

In Eq. (3.7), the variable coefficient consists of the scalar total mobility λ_t, which depends on fluid distribution in the medium, and the absolute permeability ***K*.** Further details of the model used is presented in **Appendix A**.

3.4.1 The Finite Volume Discretization Scheme

The finite volume scheme implemented in MRST is based on the divergence theorem, i. e. for some continuously differentiable velocity field, $\vec{v}$, equations such as (3.7) can be transformed into a surface integral by

$$\int_{\Omega_i} (\nabla . \vec{v})\ dV = \int_{\partial\Omega_i} (\vec{v}.\vec{n})\ dA = \int_{\Omega_i} q\ dV \tag{3.9}$$

Figure 15 below shows the finite boundary of each control volume where the computational node is located at the centroid. Each computational node contains the properties of that control volume. The temporal and finite volume discretization for the pressure and saturation equation in the two-phase oil-water model applied in MRST is presented in **Appendix B**.

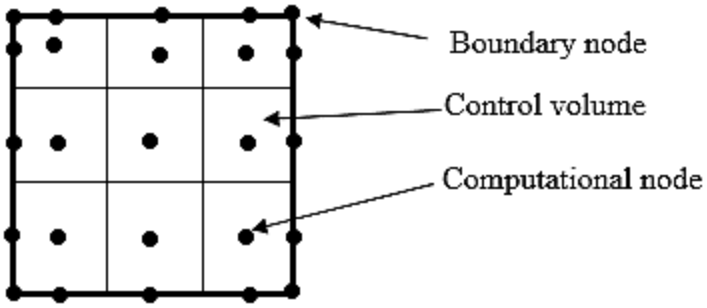

Figure 15 - Control volumes with nodes configuration (after Baker, 2002)

3.4.2 Method of Automatic Differentiation (A.D)

The standard approach for solving the nonlinear system of discrete equations arising from complex multiphase models is to compute the Jacobian matrix of first derivatives for the nonlinear system and use Newton's method to successively find a better approximation to the solution (Lie, 2016). Deriving and implementing the analytic expressions for Jacobian matrices is both error-prone and time-consuming, especially for flow equations of complex fluid and well model, thermodynamic influences, etc. The method of automatic differentiation implemented in the fully implicit

nonlinear and linear solver structures in MRST automatically constructs the Jacobian matrices as the gradient of the equations is computed. This allows for a simple way of coding simulators where the model equations are implemented in a residual form and we can specify the variables to be used in the linearization of the resulting nonlinear system (Lie, 2016). For instance, in conventional programming, a variable may contain one or more values. However, if the variable is of an automatic differentiable type, it will contain not only the values of the function at the current point, but also the derivatives of the function with respect to all the primary variables. i. e. for a variable *x*, initiated as an automatically differentiable variable, any calculations *f(x)* would automatically compute $\frac{d}{dx}f(x)$.

This technique aids the computational efficiency of computing the Jacobian matrix for several variables from the reservoir and well flow equations (Lie, 2016). Its implementation in MRST allows for simplified simulations and the ability to add and alter equations without worrying about the computation of the Jacobian.

3.4.3 Well Model

The well flow equation of Peaceman as implemented in MRST relates the reservoir volumetric flow rate, q_α of phase α, bottom hole pressure, p_{wf} and grid block pressure $p_{\alpha j}$. The advantage of Peaceman's well model is its ease of adaptation and extension to numerical solution for rectangular grids, anisotropic reservoirs, horizontal wells, multiphase flows. For a well producing from a single grid block *j*, the flow rate of a phase, $\propto$, (oil or water) into the well, this is represented by:

$$q_\alpha = WI_j \frac{k_{r\alpha}}{\mu_\alpha}\left(p_{wf} - p_{\alpha j}\right) \tag{3.10}$$

The well index, *WI* is described by Eq. (3.11). Its computation depends on the grid properties, permeabilities, and the well direction.

$$WI_j = 2\pi \frac{dz\sqrt[3]{k_x k_y k_z}}{V_{gb}(ln(r_o/r_w) + S)} \tag{3.11}$$

where dz is the well-segment length, V_{gb} is the volume of the well grid block, r_w is the wellbore radius, $k_{x,}k_{y,}k_z$ are permeabilities in the *x*, *y*, *z*- directions respectively, *S* is the skin factor, and r_o is the equivalent or effective well radius.

The sum of Eq. (3.10) over all the phases results in the well volumetric rate:

$$q_t = \sum_{\alpha=o,w} WI \frac{k_{r\alpha}}{\mu_\alpha}(p_{wf} - p_{\alpha j}) \tag{3.12}$$

Specifying the well constraints (rate for injector and bottom hole pressure for producer wells) introduces a new variable that will be solved per completion in the resulting nonlinear system.

3.4.3.1 Multi-Segment Well Approach

Holmes et al., (1998) introduced the multisegmented advanced well modeling concept in which the well is divided into several inflow segments with the assumption of radial influx into the segment. This same approach is used in MRST in the well model to determine the local (node) flow conditions in each lateral, most importantly, account for the flow-based pressure loss and pressure drop introduced by the flow control devices when we introduce flow control devices in the well for each lateral.

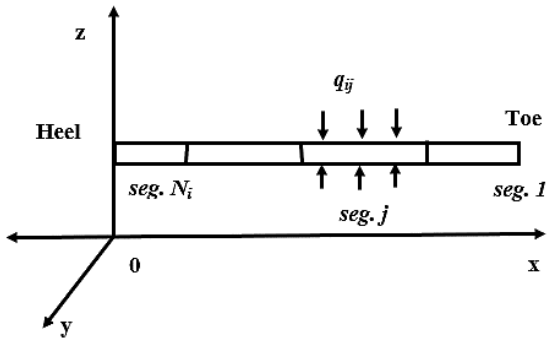

Figure 16 - Wellbore segmentation schematic (after Huanpeng et al., 2013)

For the *i*-th lateral divided into several segments, with each segment assigned with a number ranging from 1 at the toe to N_i at the heel, the relationship for the total number of segments, N_s for the multilateral well, i_w, with n_l laterals, and n_s segments is expressed as

$$N_s = \sum_{i_w=1}^{n_w} \sum_{i_w=1}^{n_l(i_w)} n_s\,(i_w, i_l) \tag{3.13}$$

In this study, each lateral is divided into six segments making the total number of segments, N_s in the trilateral well ($n_l = 3$) equal to eighteen segments.

3.4.3.2 Wellbore Hydraulics

The pipeline hydraulic model accounting for losses through the wellbore is expressed as

$$\frac{dP}{dL} = \left(\frac{dP}{dL}\right)_{hydrostatic} + \left(\frac{dP}{dL}\right)_{friction} + \left(\frac{dP}{dL}\right)_{acceleration} \tag{3.14}$$

In the toolbox, the pressure of each segment (P_n) is related to that of the preceding segment (P_{n-1}) through the pressure loss relationship expressed as**:**

$$P_n = P_{n-1} + \Delta P_f + \Delta P_a + \Delta P_h \tag{3.15}$$

where P_{n-1} is the pressure in the upstream well segment, P_n is the pressure in the current segment while the ΔP terms are the friction, acceleration and hydrostatic pressure loss components across the segment.

3.4.3.3 Multiphase Flow

The terms of pressure loss relationship expressed in the preceding section incorporates the multiphase nature of flow in the model. Average fluid properties are used in the pressure drop computation in the solver module of the toolbox:

$$dP = -2 * \frac{Lv}{D} * \frac{f_{TP}.\rho_{TP}}{v_{TP}^2} \tag{3.16}$$

where the subscript $_{TP}$ refers to the mixture average properties of velocity, density, and friction factor, $f(N_{Re})$. The value of the obtained Reynolds number is used to calculate the friction factor term in Eq. (3.16) and is given by:

$$f_{TP} = -\frac{3.6 * \log\left(\frac{6.9}{N_{Re}} + \frac{\varepsilon}{3.7D}\right)^{1.11}}{\log(10)^{-2}} \quad (3.17)$$

3.5 Reservoir and Well Properties

Table 1 & 2 outlines the synthetic data of the reservoir, well and fluid properties compiled from unpublished literature to represent the "base case" scenario in this study. The reservoir is characterized by a marked level of heterogeneity and anisotropy among the three sub-layers produced by each lateral of the trilateral well system. The top sub-layer (first two layers in the z-direction) have an average reservoir property specification, the middle sub-layer (grid layers 3 and 4) have the best reservoir quality of the three zones, while the bottom layer in the model is assigned the lowest permeability value. A Gaussian field random distribution function is used to generate porosity values for each of the grid cell in the reservoir model.

The sub-layers have a vertically transverse isotropic behavior ($Kv = 0.1*K_H$).

Table 1 - Fluid, well and reservoir properties

Reservoir Grid Properties		
Property	**Value**	**Unit**
n_x, n_y, n_z	25, 20, 5	--
Grid Dimension [D_x D_y D_z]	5, 4, 0.1	km
Fluid Properties		
Property	**Value**	**Unit**
Oil Viscosity, μ_o	5.00	cP
Water Viscosity, μ_w	1.00	cP
Oil Density, ρ_o	700	kg/m^3

Water Density, ρ_w	1000	kg/m^3
Oil Formation Volume Factor, B_o	1.0	-
Water Formation Volume Factor, B_w	1.0	-
Oil Saturation, S_o	0.7	%
Critical Water Saturation, S_{wc}	0.2	%
Residual Oil Saturation, $S_{or,}$	0.25	%
Residual Water Saturation, S_{rw}	0.3	%
Corey exponent, $n_{o,w}$	2, 2	--
Rock Properties		
Porosity distribution, ∅	18 - 24	%
Layer 1 Permeability $[K_{x1}, K_{y1}, K_{z1}]$	[300, 300, 30]	*mD*
Layer 2 Permeability $[K_{x2}, K_{y2}, K_{z2}]$	[500, 500, 50]	*mD*
Layer 3 Permeability $[K_{x3}, K_{y3}, K_{z3}]$	[200, 200, 20]	*mD*

Table 2 - Well Properties

Well Properties		
Property	**Value**	**Unit**
Diameter	5.0	inches
Roughness	$1.0*10^{-6}$	--
Lateral length [L1 L2 L3]	1800	meter
Segment length	300	meter
Initial Reservoir Pressure, P_i	5000	psia

Table 3 – Well schedule

Simulation Time	30 years
Producer BHP constraint	1000*psia
Injector well rate constraint	1 pore volume / simulation time

3.6 Case Modeling in MRST

An outline of the simulation procedure that MRST uses in setting up the reservoir and well model using the functions and structs implemented in the coding algorithm is outlined below:

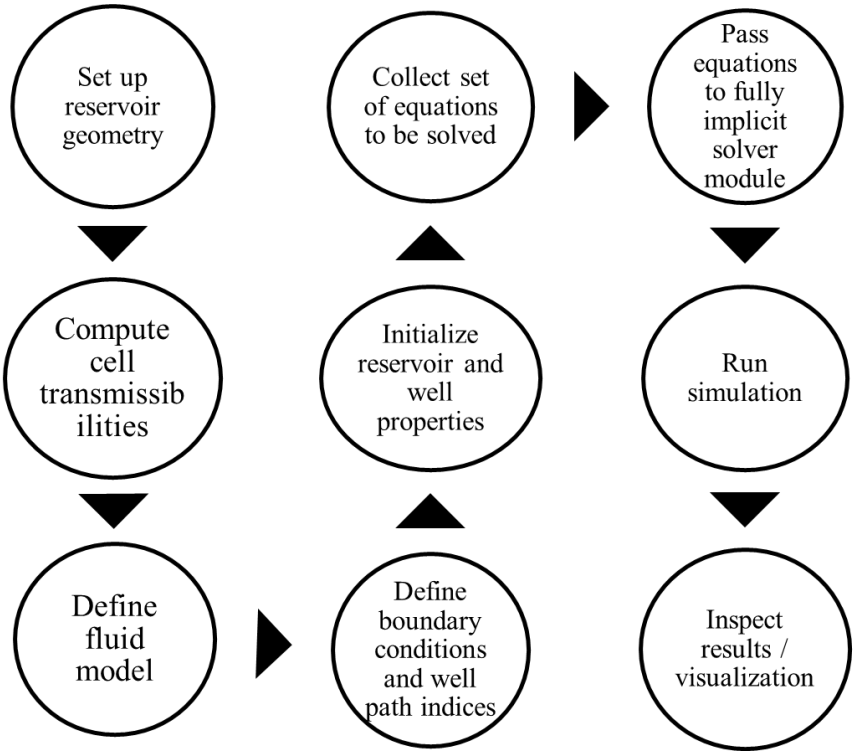

Figure 17 – Model set up procedure in MRST

3.6.1 Base Case Model Description

The reservoir model is a sub-layered type with macroscopic properties defined in **Table 1** above. The laterals are set to be of equal length in each of the reservoir sublayer. The permeability, porosity and sub-layer thickness are varied to incorporate a reasonable level of heterogeneity into the model as outlined above. A rate constrained vertical injector well is placed in the north-east corner of the model and completed throughout the thickness of the reservoir for pressure maintenance and increased sweep efficiency. Well properties, schedule and constraint parameters are outlined in **Tables 2** and **3** above.

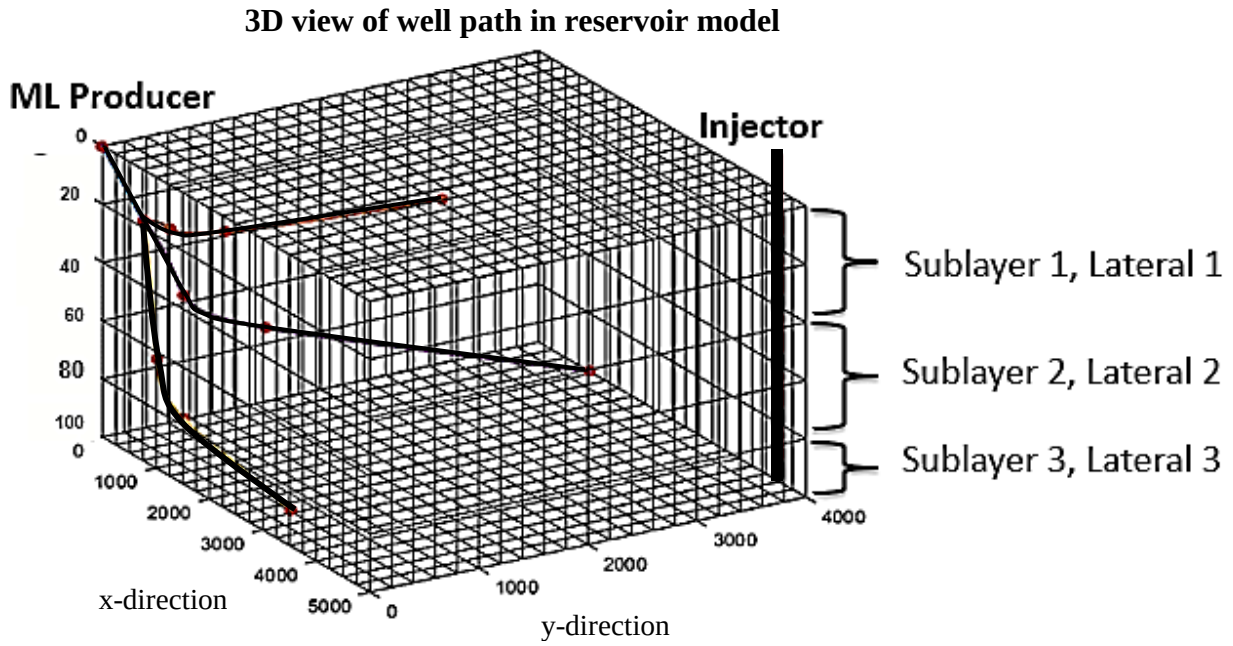

Figure 18 - Base case reservoir grid and well model

3.6.2 Pressure Drop Case Study

Three case studies are conducted in this section to investigate the well pressure drop behavior and influence on associated productivity using MRST. The base case reservoir model described above is used.

i. Pressure drop profile over time in the lateral to investigate the magnitude of pressure loss to be expected due to flow control valves which are used for controlling fluid influx and for production optimization purposes. This case uses one control valve per segment in the lateral. A nozzle valve model is implemented in the toolbox and is expressed as:

$$-\Delta p = \frac{\rho v^2}{2 * c_v^2} \tag{3.18}$$

where ρ represents the fluid density, v, fluid velocity, and c_v is the valve discharge coefficient.

ii. Sensitivity analysis to determine the heel-to-toe pressure drop profile with varying interval control valve (ICV) strength over simulation time is conducted.

iii. Analyze the productivity for the case of the lateral with flow control device (smart / intelligent completion) to the case of the lateral with no downhole lateral flow control devices (simple / conventional completion). For this scenario, flow through lateral 2 in sublayer 2 of the base case reservoir model is considered while laterals 1 and 3 are shut in. This was done to eliminate any effect of potential cross flow occurrence between the laterals thereby giving us a more accurate forecast of the productivity index per lateral in the well. Downhole flow control valve properties used is outlined in **Table 4** below. The results are presented in Section 4.2.

Table 4 - Valve properties

Property	**Value**
Roughness	$1*10^{-6}$
Diameter, d	3.50 in.
Valve discharge coefficient (C_v)	0.65

3.6.3 Compartmentalized Case Studies: Vertical, Horizontal and Combined

The influence of barriers demarcating the reservoir can have a major impact on recovery index, hence, we also investigate the influence of these barriers using MRST. The property (porosity) of the grid block coinciding with the fault plane in the reservoir is altered to partially allow or completely impede fluid flow.

3.6.4 Fault Modeling

We earlier established in the introduction and literature review sections, the ability of faults to compartmentalize a reservoir thereby reducing expected petroleum recovery. It is therefore

essential to account for the presence of both sealing and non-sealing faults in production simulation models to allow for a well-informed short term and long-term field development planning. In most reservoir simulation studies, the communicative property of a fault or barrier may be represented by altering the transmissibility property of the grid blocks around / surrounding the fault zone for history matching purposes (Fisher, 2005). A similar property used in CMG is the transmissibility multiplier term. A multiplier of zero is assigned for a fully sealing fault and a value of one is assigned for fully communicating faults. However, the transmissibility multiplier property is strongly grid dependent and refers to the connection between two neighboring / adjacent grid cells, rather than to the fault itself in the geological model being considered. In the simulation toolbox, we specify the porosity of the faults directly in the function class for the grid model code. This way, the property is dependent on the fault itself. For the partially communicating and fully sealing cases, we use very low porosity values of 10^{-2} and 10^{-4} respectively for the grid blocks coinciding with the fault plane in the reservoir.

Case 1: Vertical Reservoir Compartmentalization (Partially Sealing)

The first case we examine is that of a vertical fault which is partially sealing. The slightly shaded plane strip in **Figure 19** below depicts the low porosity fault region vertically separating the reservoir model. To implement this, the grid blocks coinciding with the location of the fault plane is assigned a porosity value of 10^{-2} in the grid definition input data struct of the code. All the other parameters (for the remaining grid blocks) earlier defined are kept constant as stated in the reservoir, well and fluid properties table in Section 3.5.

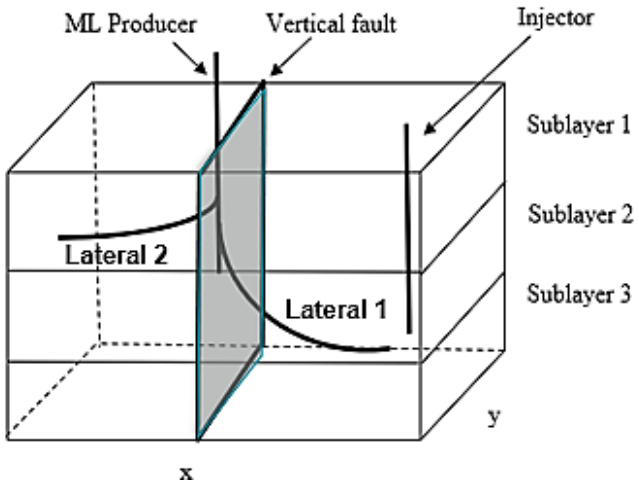

Figure 19 - Compartmentalized reservoir separated by partially sealing vertical fault

Case 2: Vertical Reservoir Compartmentalization (Sealing)

In this case, the grid blocks coinciding with the fault plane are adjusted to disallow communication between the compartments. Instead of using a zero-porosity value, we specify a value of 10^{-4} as the zero value throws an error in the code compilation process. The reservoir, well geometry and other parameters outlined in **Table 1** remains the same as with the partially sealing case above.

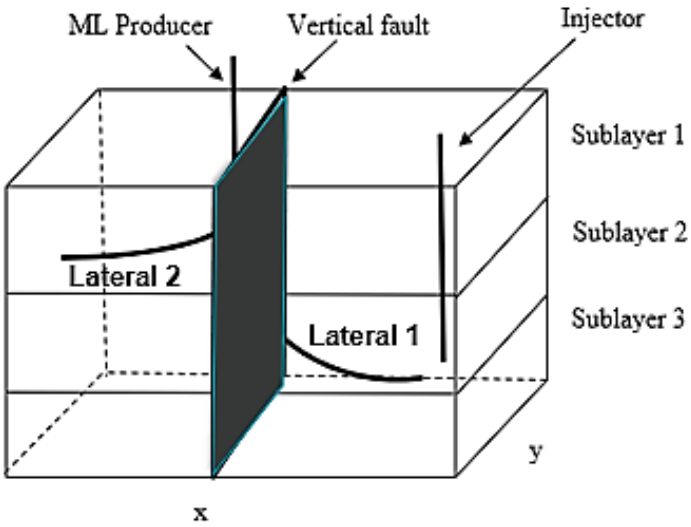

Figure 20 - Compartmentalized reservoir separated by fully sealing vertical fault

Case 3: Horizontal Reservoir Compartmentalization

In this case, the reservoir model is modified into two horizontal sub-layers. The first two grid layers in the vertical direction make up the top sub-layer and assigned a permeability of 200 mD produced by lateral 1 while the lower two sub-layers is assigned permeability of 300 mD and produced by lateral 2. The middle layer (layer 3) in the grid model represents the horizontal fault plane schematically represented in **Figure 21** below. We used the same method used in the vertical case, where the partially sealing fault is represented by assigning porosity value of 10^{-2} and a value of 10^{-4} for the fully sealing case. We use this assignment of low porosity values for the grid blocks coinciding with the fault plane in the reservoir model as an alternative method of representing resistance to fluid flow within the porous media. Recent literature has pointed out certain deficiencies of using the currently adopted single phase transmissibility values to represent fault blocks during reservoir simulation history matching activity to validate real field production outturn. A schematic representation for the partially and fully sealing fault case is presented below:

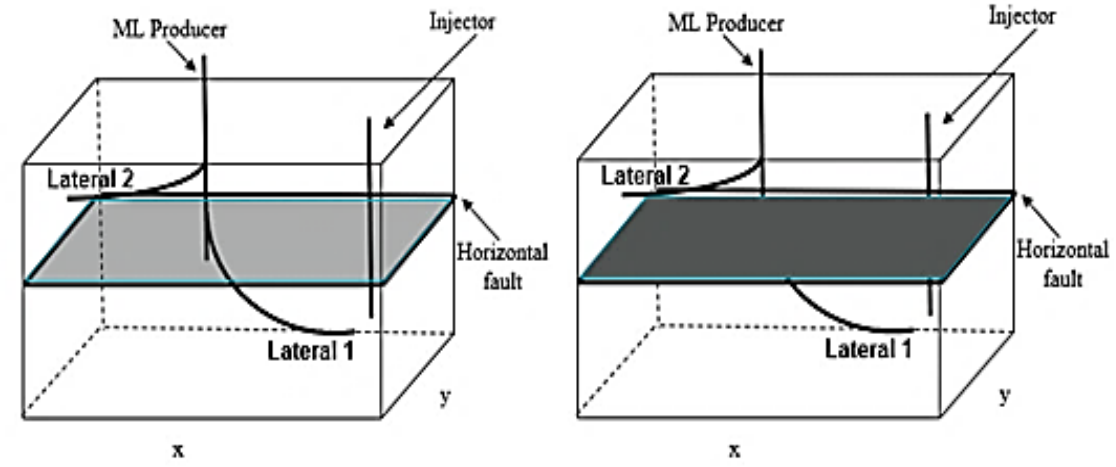

Figure 21 – (a) Partially sealing case (b) Fully sealing case

Case 4: Combined Partially and Fully Sealing Faults

Figure 22 below shows a schematic of the compartmentalized reservoir with both fully sealing (fault 1) and partially sealing (fault 2) fault. For the fully sealing fault, the same methodology as that of the fully sealing fault in case 1 above is used. However, for the partially sealing fault 2, a sub-layer juxtaposition is implemented where one half of the grid model is shifted upwards relative to the other half of the grid so that the top and bottom low permeability sublayers as defined in case 3 above are in contact with each other (partially sealing fault 2 region in **Figure 22** below). Vertical fault (2) is non-sealing while vertical fault (1) which divides compartment 1 and 2 is fully sealing. Compartments 1 and 2 are in communication with compartment 3 through the partially sealing fault 2.

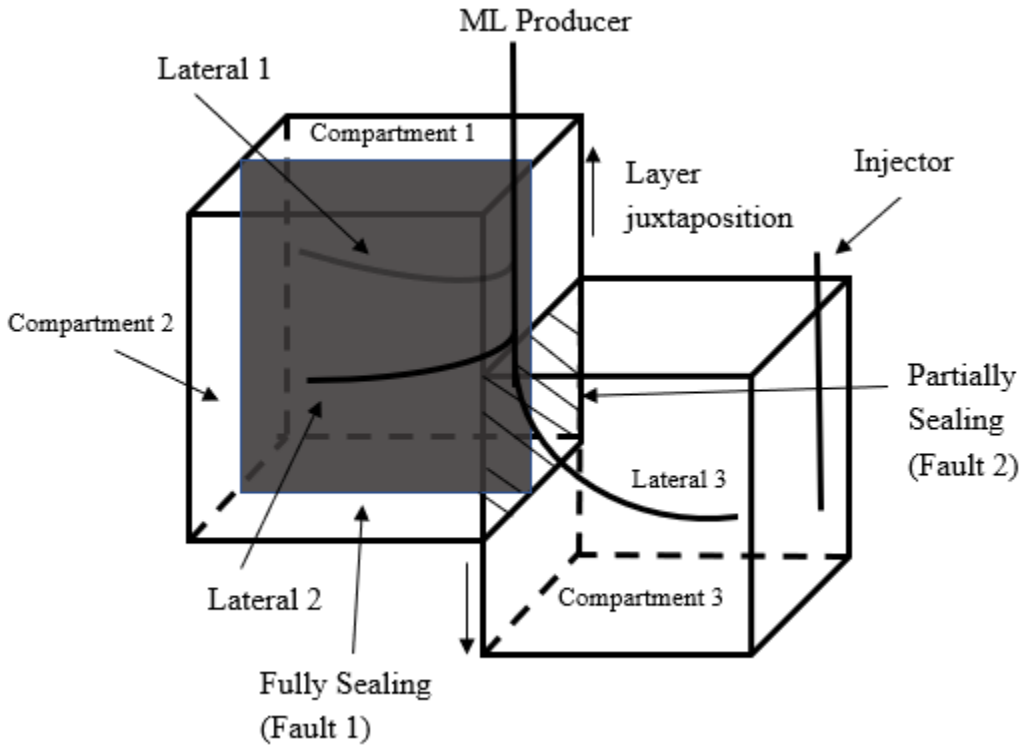

Figure 22- Combined partially and fully sealing fault case

3.7 Optimization

This part of the work investigates the optimization potential of the smart well. The adjoint module in MRST is used to determine the gradient of the objective function (net present value- NPV) with respect to the control settings listed in **Table 5**.

The *OptimizeObjective* function under the adjoint module in MRST uses an aggressive line search based on the given gradient. The algorithm handles the constraints by performing an iterative scheme and while applying the specified system constraints to the gradient until convergence is achieved (Bahadori, 2011).

The algorithm uses a gradient projection method which is the most efficient method to use when the constraints are simple in form, particularly when there are only bounds on the variables (i. e injection rate constraint, bottom hole pressure constraint). Each iteration of the gradient projection algorithm consists of two stages: the search along the steepest descent direction from the current point, and a search on the face of the feasible box region on which the local minimizer of the objective function exists (Bahadori, 2011).

Table 5 - Constraints and economic parameters for NPV optimization

	Constraints / Values	
Parameters	**Lower**	**Upper**
Injector well rate	0 m^3/d	400 m^3/d
Producer well pressure	100 bara	250 bara
Economic Parameters		
Property	**Value**	**Unit**
Yearly discount rate	0.05	%
Oil revenue	60	$/stb
Produced water handling cost	6	$/stb
Water injection cost	6	$/stb

Chapter Four Results and Discussion

4.1 Base Case Results

Figure 23 below shows the total oil and water cut fractions for the conventional well configuration. A sharp decline in the oil cut fraction commences in year five in which a corresponding increase in water cut is also observed i.e. the water flood front broke through around this time after simultaneous production and injection into the model commenced.

Figure 24 and **Figure 25** gives the breakdown of oil fraction cuts and production rate from each lateral respectively. The lateral production rate results obtained in **Figure 25** below is largely indicative of the macroscopic sub-layer reservoir properties produced by each lateral. Lateral 3 is seen to have the lowest production rate in this case due to highest flow resistance in the sub-layer among the three sub-layers.

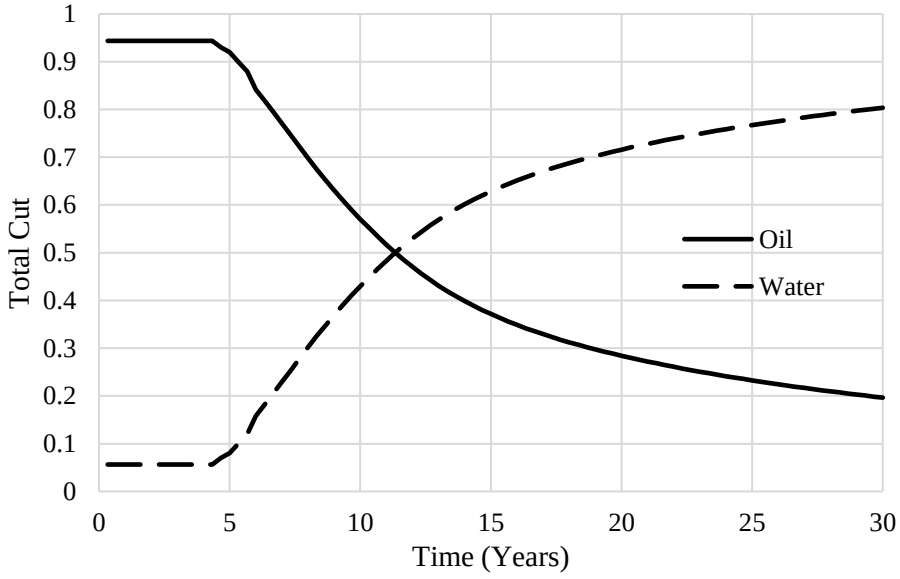

Figure 23 – Total well oil and water cut

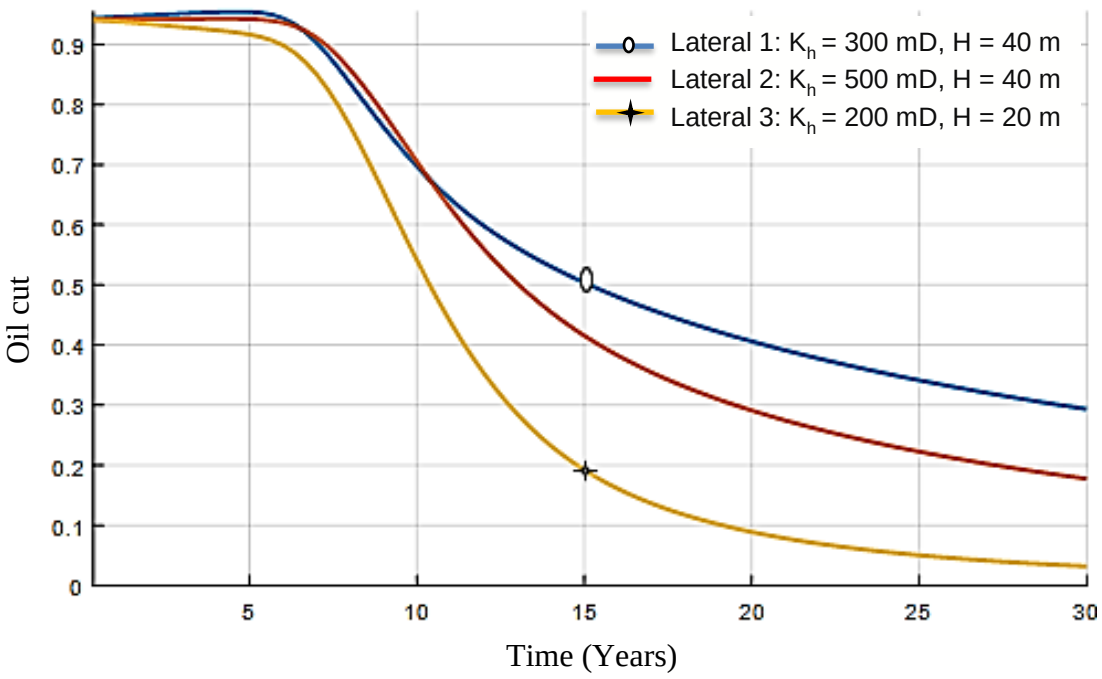

Figure 24 - Oil fraction by lateral

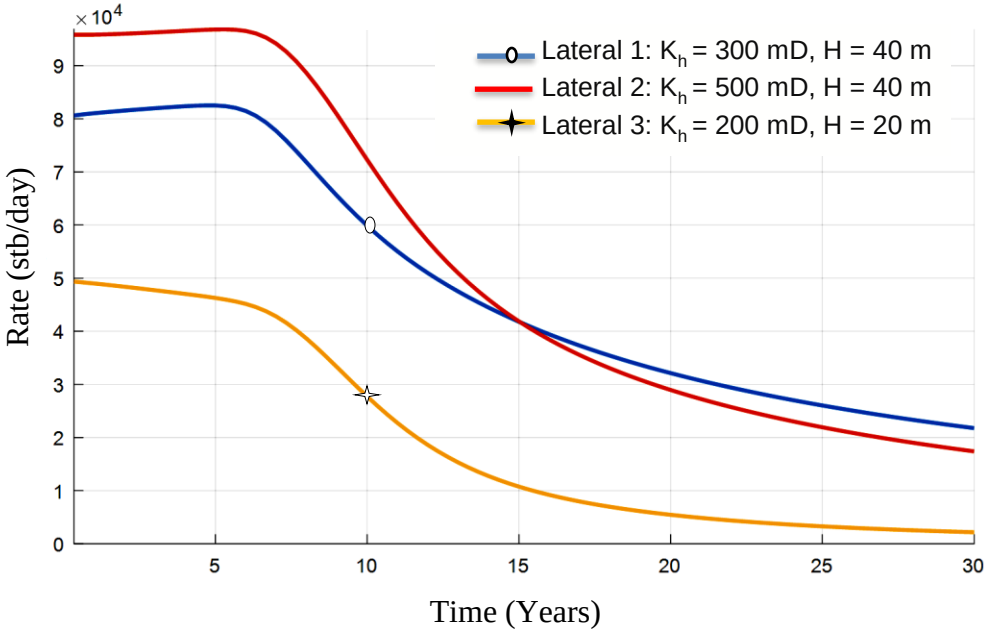

Figure 25 - Oil Production rate by lateral

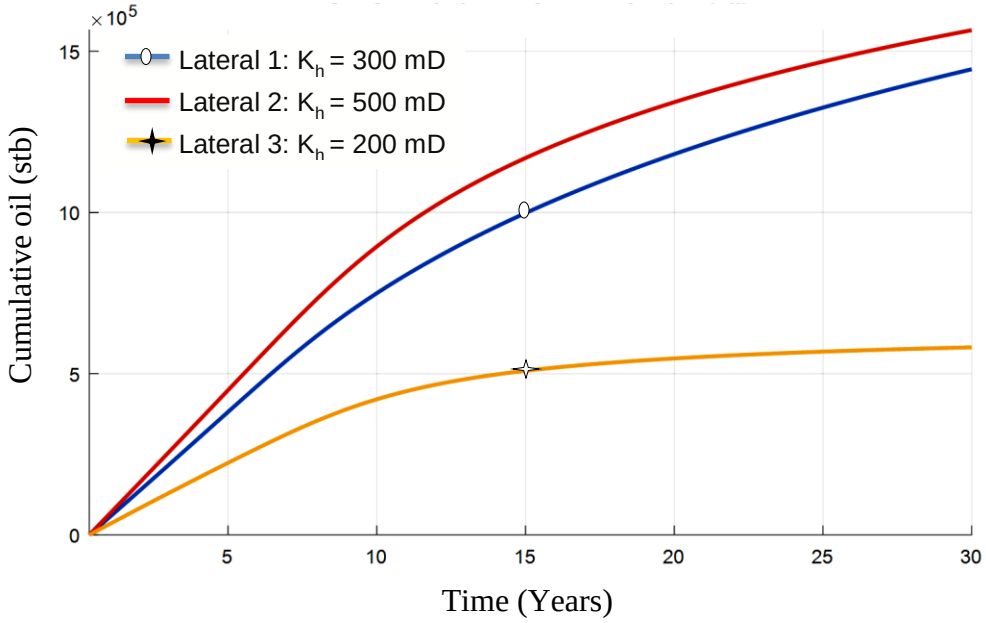

Figure 26 - Cumulative oil production

Figure 26 shows the cumulative oil produced from each of the lateral over the simulation period for this base reservoir setup. Lateral 2 produces the highest due to its high permeability property.

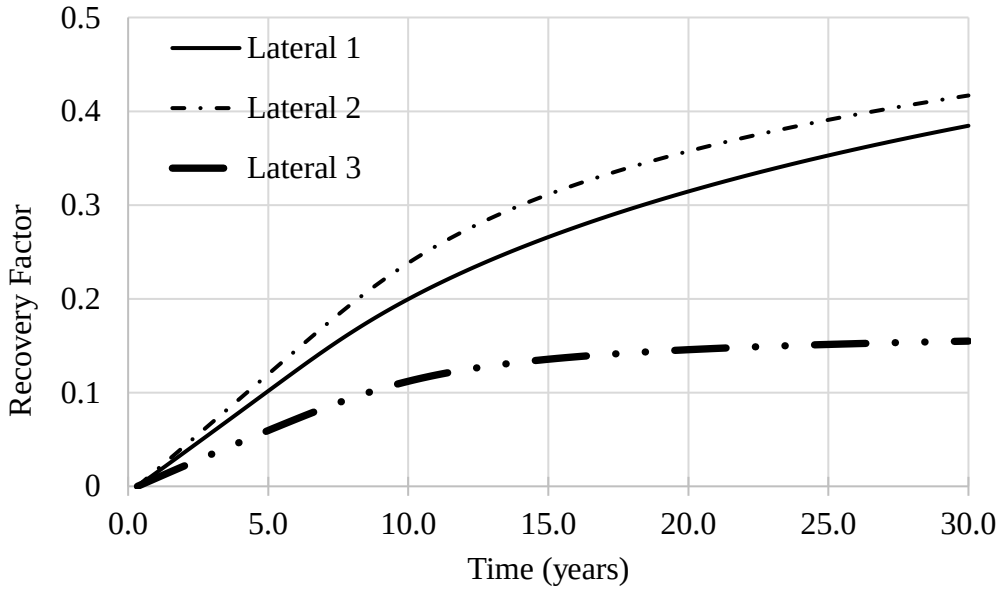

Figure 27 - Recovery factor profile for base case model

Figure 27 gives the breakdown of the recovery factor obtainable by lateral. A production optimization goal for this case may include extension of the initial oil fraction decline profile beyond five years (i. e. increase the time to water breakthrough at the laterals, especially in the high permeability sub-layer). To achieve this, optimum injection and production parameters for each sub-layer can be determined. For instance, reducing the injection rate through a high permeability streak may reduce fingering tendency through the layer thereby promoting a more steady / uniform displacement front in the sub-layer. Factors such as reservoir structure / orientation, and lateral placement optimization can also increase uniform fluid displacement and increased sweep efficiency through the reservoir to the well. Another optimization plan such as we considered in this work with the results presented in Section 4.2 is the application of downhole flow control devices to regulate flow along the length of the horizontal lateral so as to meet long term field development goals.

4.1.1 Results Comparison with CMG IMEX Simulator

Figure 28 below shows the results of total system output for the oil and water cut decline profile from the CMG IMEX simulator compared to the result from MRST earlier presented in **Figure 23** above. A significant level of similarity is observed between the results in the first half of the simulation period, after which there is a deviation in the fluid cut profiles. After 15 years, the oil cut trend from the CMG IMEX model had dropped to the oil residual saturation value while the oil cut profile in MRST maintained the depletion trend till the end of the simulation period.

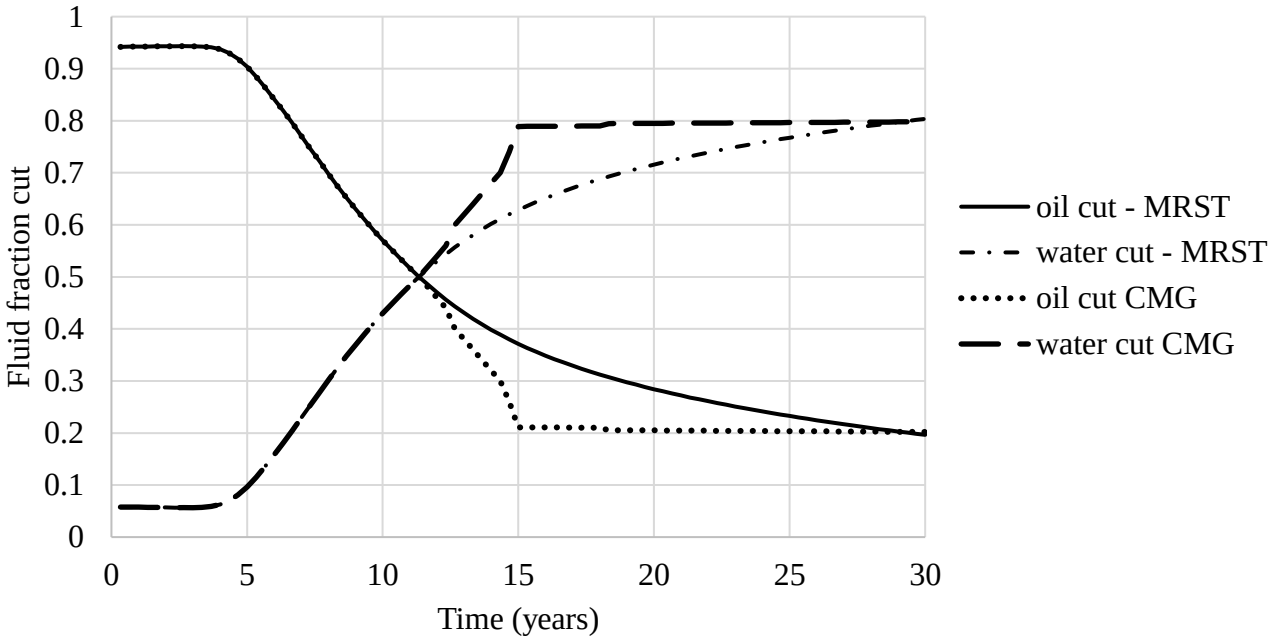

Figure 28 - Oil and water cut profile base case comparison

To further test the accuracy of these results, we perform a grid refinement operation. In reservoir simulation, carrying out a Local Grid Refinement (LGR) helps to capture flow behavior in greater detail by providing more resolution in the reservoir and near-well region (Aziz, 1979). This approach is widely used because of its simplicity. However, problems related to this method include reduced computational efficiency due to longer simulation run times, plus associated effects of numerical instability and time-step restrictions during computation. The goal of the grid refinement operation done here was to determine the grid resolution that would produce a similar depletion trend in both simulators. We first conducted a 2x and then a 4x grid refinement in the x - and y – directions and then did a simulation rerun in the IMEX simulator. All the other reservoir and well parameters as stated in **Tables 1 – 3** were kept the same.

Table 6 - Grid refinement case study runs

	Base case grid	Refined grid case 1 (2x)	Refined grid case 2 (4x)
MRST	25*20*5	25*20*5	25*20*5
CMG	25*20*5	50*40*5	100*50*5

In **Figure 29** below, it is observed that the grid refinement operation carried out in CMG continuously yielded closer results to the results from the finite volume numerical simulation in MRST. This comparison helps us to validate the level of accuracy we earlier expected from the finite volume grid discretization methodology implemented in MRST compared to the finite difference method implemented in the IMEX simulator and other FDM based simulation packages.

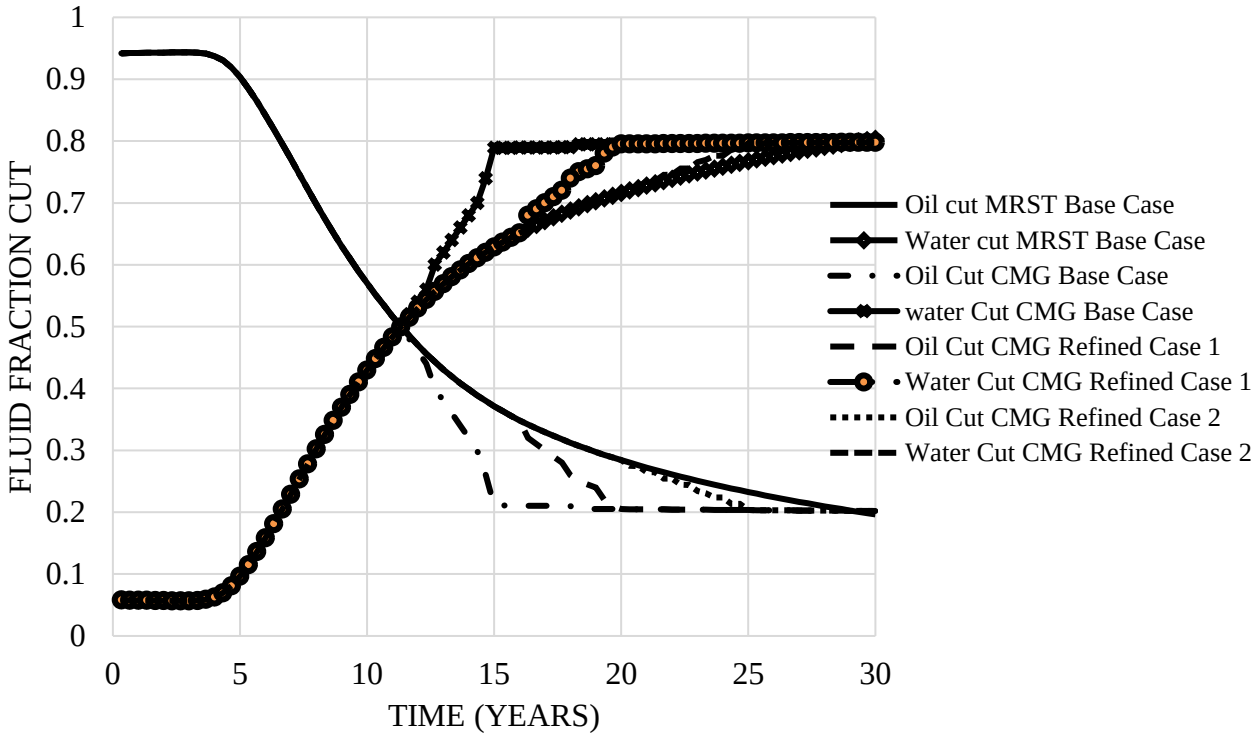

Figure 29 – Profile comparison for base and refined grid cases

4.2 Pressure Drop Case Study Results

Figure 30 shows the increasing pressure drop trend from the beginning of simulation time to the last time step. As the fluid velocity increases from the initial influx from the reservoir into the toe of the well and then to the heel, a corresponding increase in the node-to-node pressure drop profile is seen. This demonstrates the validity of pressure drop dependence on fluid velocity.

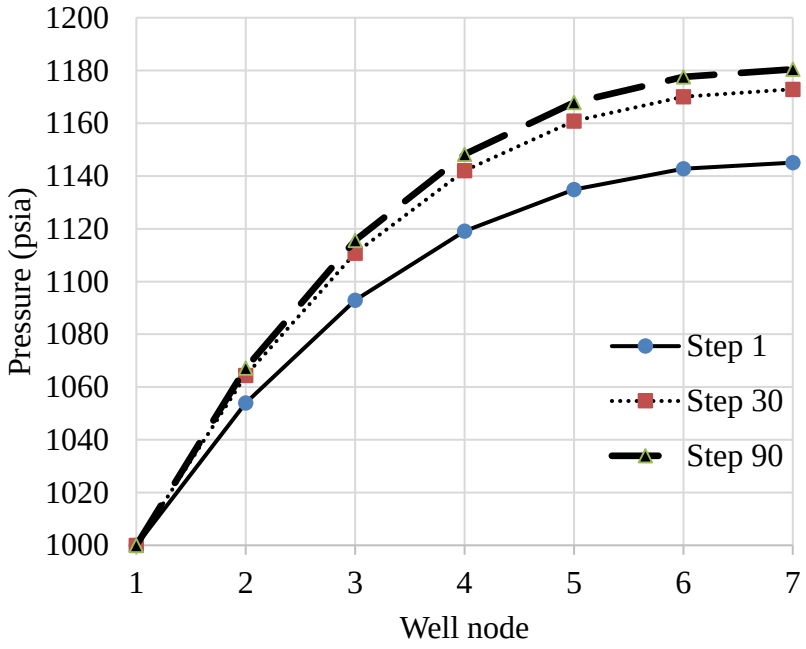

Figure 30 – Heel-to-toe pressure drop along lateral 2

Table 7 outlines the pressure drop in each of the lateral in the multilateral well system.

Table 7 - Pressure drop profile for each lateral

Node	Lateral 1 (Sublayer 1) Pressure, psia	Lateral 2 (Sublayer 2) Pressure, psia	Lateral 3 (Sublayer 3) Pressure, psia
1	1000	1000	1000
2	1067	1066	1066
3	1116	1114	1115
4	1150	1147	1147
5	1170	1166	1166
6	1180	1177	1175
7	1183	1180	1179

The results of the sensitivity analysis conducted to evaluate the effect of varying interval control valve strength on the lateral pressure drop profile is shown below. **Figure 31** shows an increasing pressure drop trend with increasing number of valves installed per segment in the lateral.

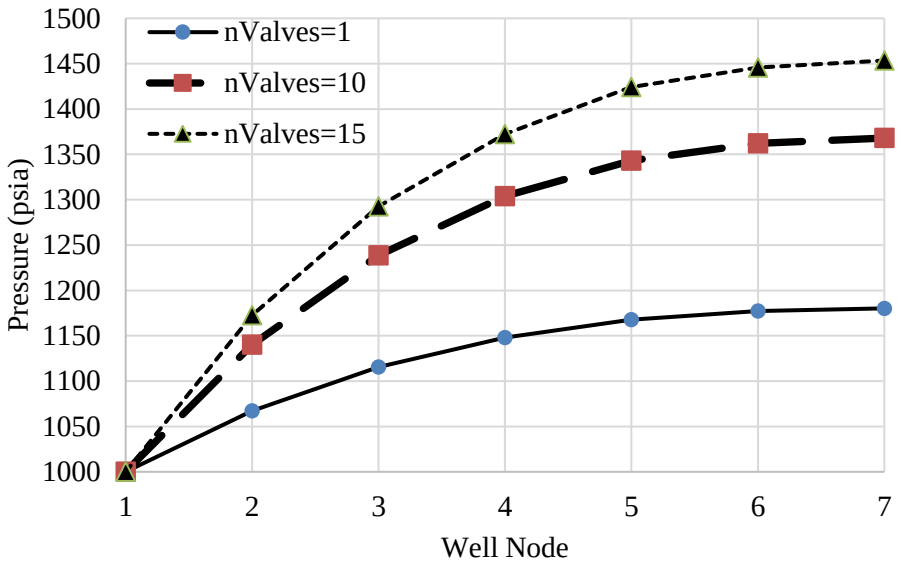

Figure 31 - Pressure drop variation increasing ICV strength

Figures 32-35 show the comparison of the smart / intelligent well (with downhole lateral flow control) to a simple well (without downhole lateral flow control) as a means of optimizing the oil production rate (revenue) and / or minimizing water production, treatment and reinjection costs (operating expenditure). Either one of the above or a combination of both strategies (increasing revenues and / or reducing operating expenditure) can significantly improve the project economic profitability criteria (expected cash flows and net present value). The production profile comparison of the smart and simple well completion in **Figure 32** below shows a decline in the oil fraction cut at about 15 years while the smart well had a sustained oil production plateau for an additional 10 years after oil production from the simple well completion started declining. **Figure 33** shows the corresponding water production profile cut from both completions.

The uncontrolled flow from the simple well completion may result in a coning situation in the reservoir and / or magnify an unstable waterflood front advancing through the reservoir, hence leading to the boom in produced water after 15 years.

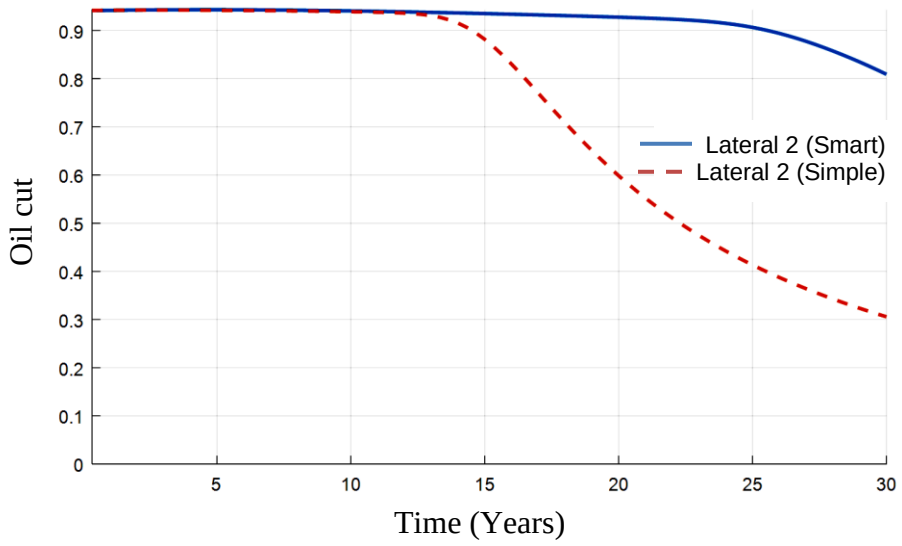

Figure 32 - Oil cut fraction comparison: smart vs. simple well completion

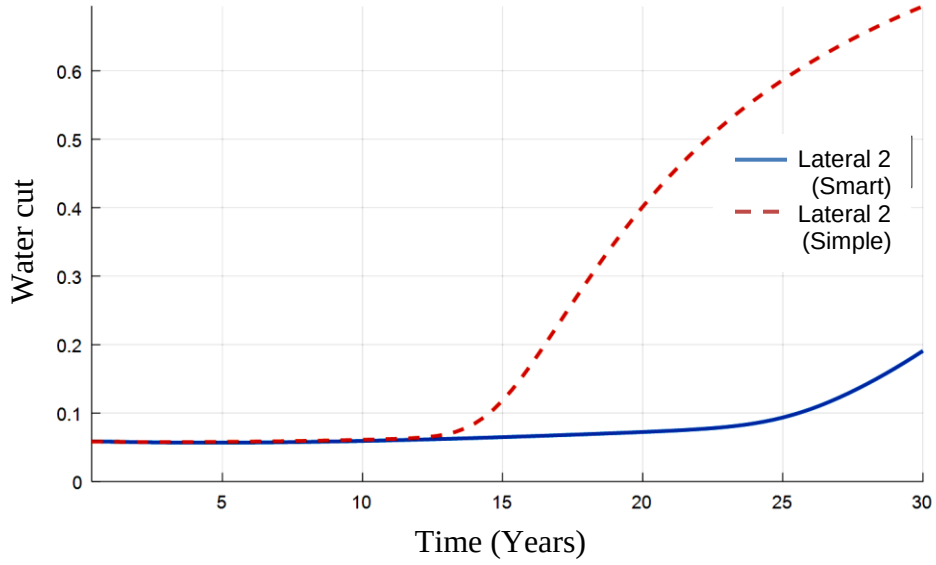

Figure 33 - Water cut fraction comparison: smart vs. simple well completion

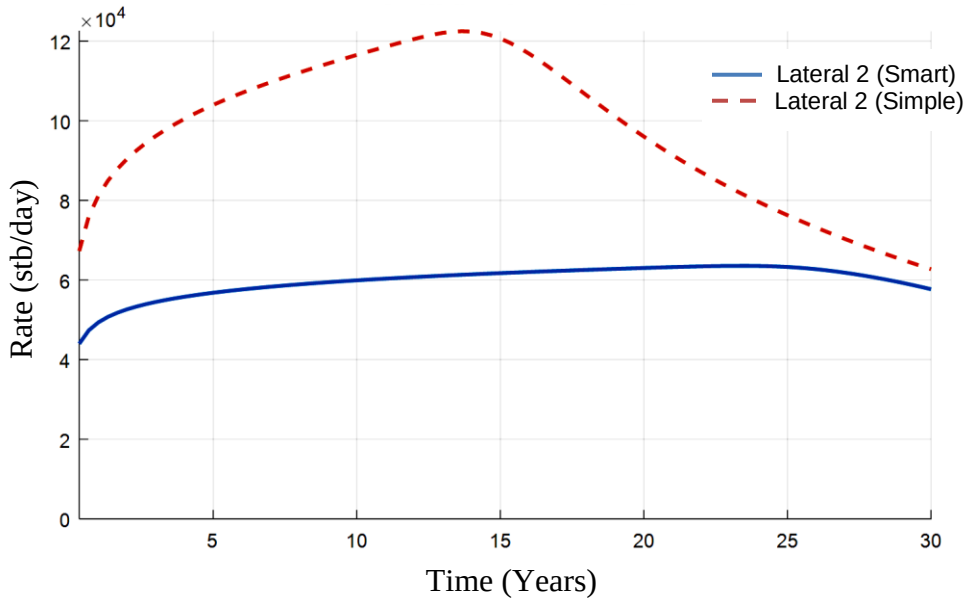

Figure 34 - Oil production rate comparison: smart vs. simple well completion

A drawback of the use of smart completion obtained in this simulation case is a lesser but steady production rate than the simple well as seen in **Figure 34** above. This ultimately results in a lesser cumulative fluid production from the smart well as seen in **Figure 35** below. However, an advantage of the smart well lies in the production rate peak of the simple well at about 10 years while the production rate from the smart well was stable and reached its peak around 25 years after initial production commenced.

As stated, the disadvantage of the smart completion in this case is that the extra oil produced in the early years by the conventional well is only obtained later in the life of the smart well. Alternatively, it is advisable to introduce the smart completion design later in the life of the well as opposed to starting out with it from the beginning of the well producing life. The advantage of the smart completions is the stable oil production profile, increased time to water breakthrough in the well, and reduced water production rate unlike in the simple well completion scenario.

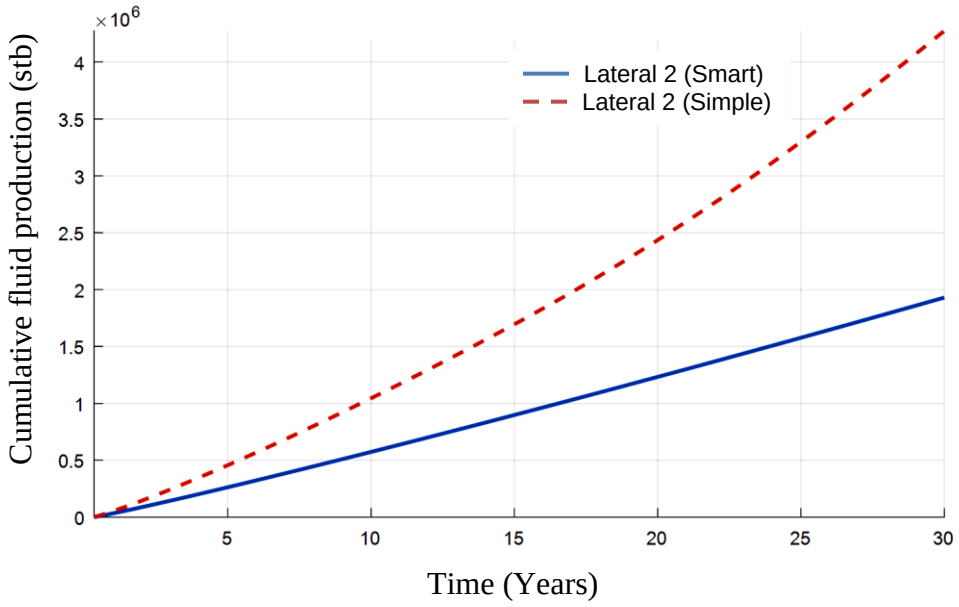

Figure 35 - Cumulative fluid production

4.3 Compartmentalized Reservoir Case Study Results

4.3.1 Case 1: Vertical Reservoir Compartmentalization (partially sealing)

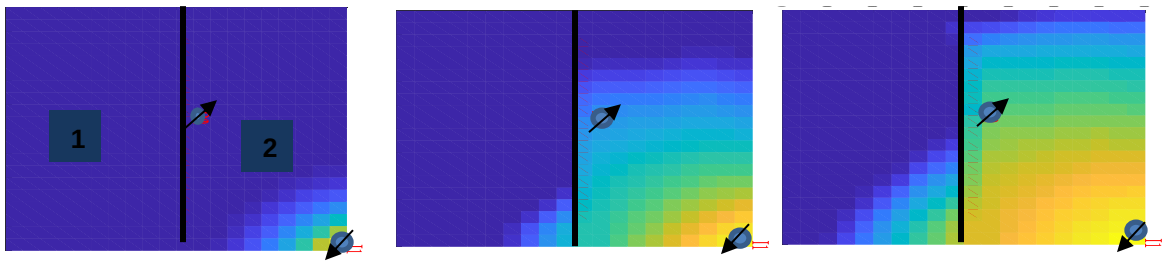

Figure 36 – Top view of water saturation advancement in reservoir model

Figure 37 below shows that lateral 2 initially starts out with a higher production rate as expected due to the presence of the injector in the compartment and its proximity to the injector. However, the high oil rate is not sustained as it dips below the production rate from lateral 1. A stable fluid displacement front from right side compartment through the non-sealing fault (low porosity grid blocks) into the adjoining compartment 1 leads to the sustained oil sweep towards lateral 1 whose displacement profile is shown in **Figure 36** above.

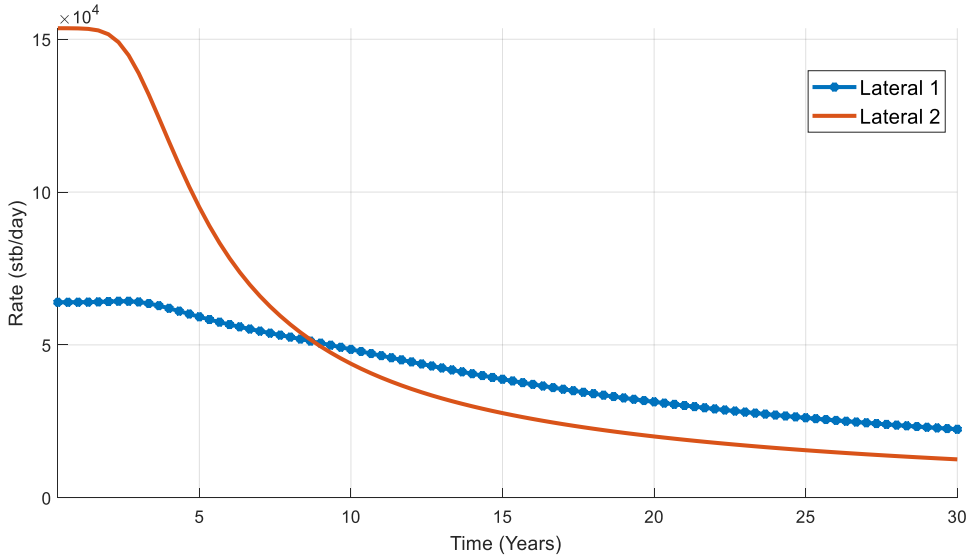

Figure 37 – Oil production rate from each lateral

Figure 38 below shows the water production rates from the laterals. As expected, lateral 2 in the compartment containing the injector well experiences an early boom in water production. An optimization plan in this case may involve installation of flow control devices to regulate the flow or shut off flow totally from the lateral later when it completely waters out while lateral 1 continues to produce oil.

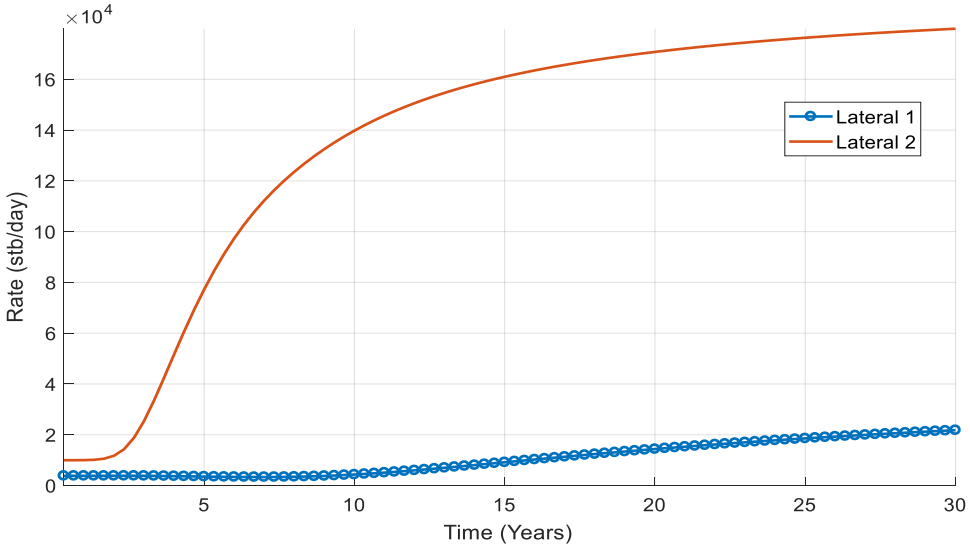

Figure 38 - Water Production rate

4.3.2 Case 2: Vertical Reservoir Compartmentalization (Sealing)

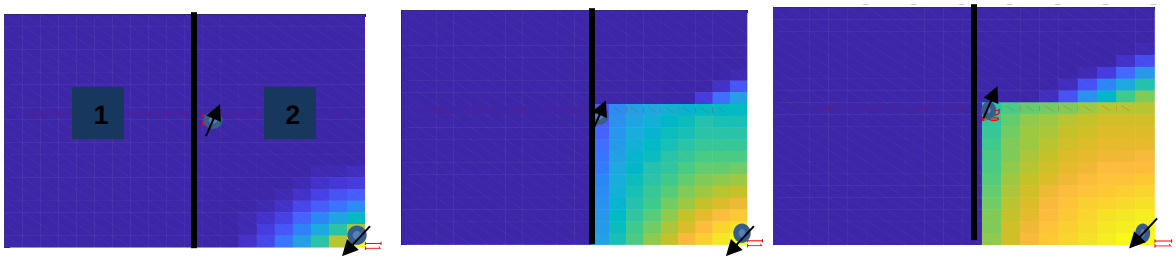

Figure 39 - Top view of the water saturation advancement in the reservoir model

The production rate plot below as illustrated in **Figure 40** below shows interference between the laterals where production is recorded from lateral 2 alone. Due to the injection in compartment 2, the flow rate from lateral 2 interferes with production from lateral 1 thereby hindering flow. This represents a reduced cumulative oil production potential from the field.

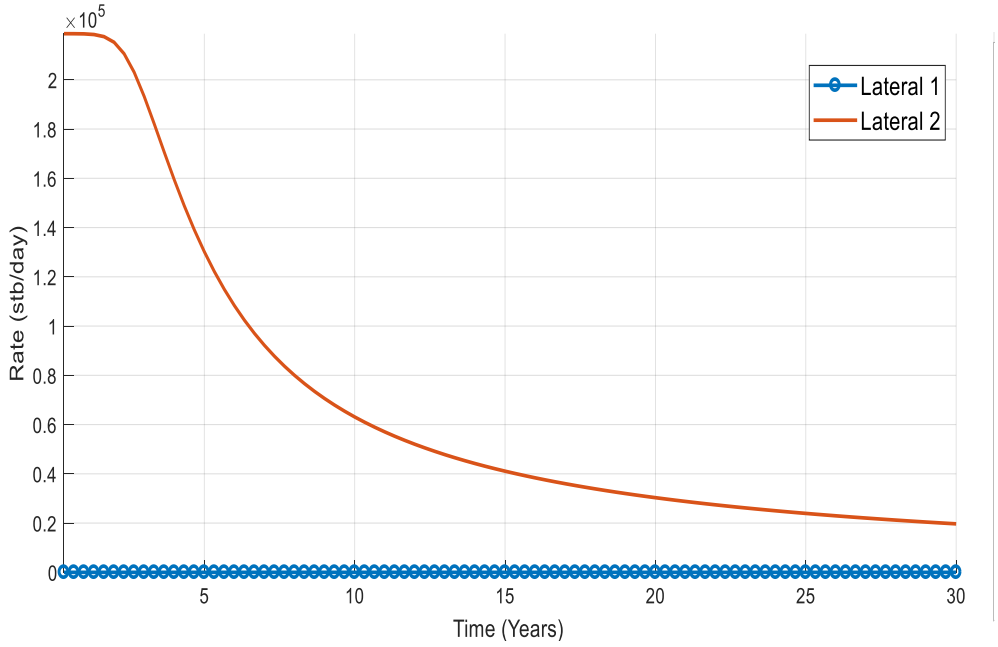

Figure 40 – Production profile showing interference between laterals 1 and 2

As suggested for case 1 above, the use of downhole control device in the domineering lateral can improve the oil production rate from lateral 1. Choking production from lateral 2 will prevent the complete shutdown and or reinjection of fluids produced from lateral 2 into lateral 1. **Figure 41**

below shows the corresponding water production profile from the same simulation case indicating negligible production from lateral 1 while production is recorded from lateral 2.

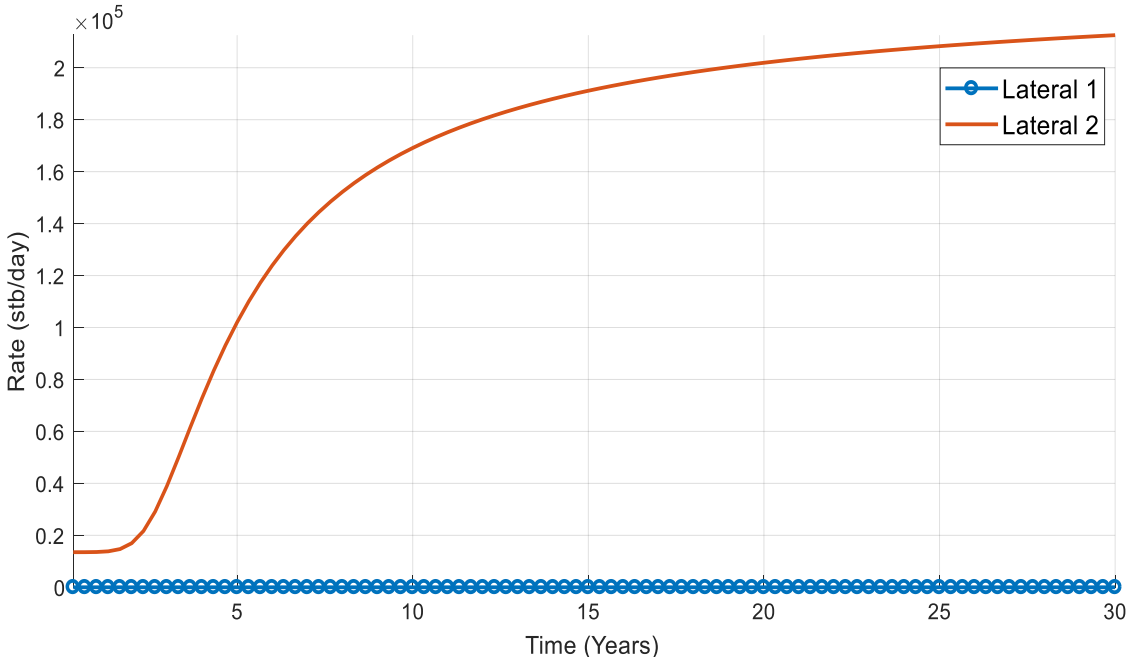

Figure 41 - Water production profile

4.3.3 Case 3: Horizontal Compartmentalization Partially Sealing

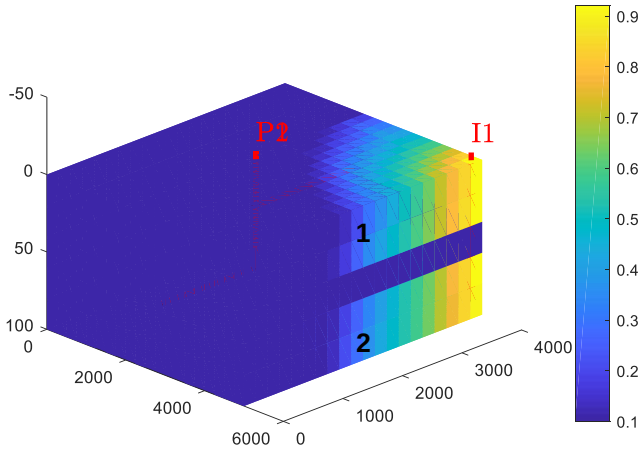

Figure 42 – Water saturation profile advancement through the reservoir sub-layers

Figure 42 shows the water saturation distribution profile in the reservoir for the horizontal compartmentalization case. **Figure 43** below shows similar production profile for the oil and water

rates from both compartments with lateral 2 producing slightly more than lateral 1 with the lesser sub-layer permeability (200 mD). No cross flow between the laterals is observed due to very low vertical permeability in the reservoir model.

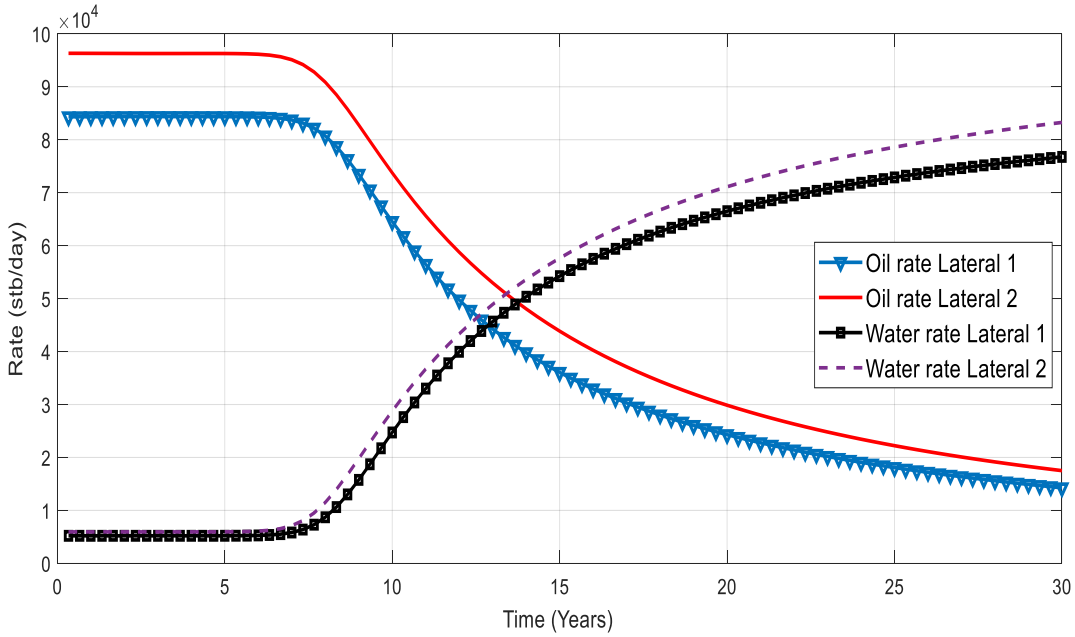

Figure 43 - Oil and water production rate over time for partially sealing case

4.3.4 Case 4: Horizontal Compartmentalization Fully Sealing

A similar trend to the partially sealing fault presented in **Figure 43** above is observed to be the case in the fully sealing case presented in **Figure 44** below.

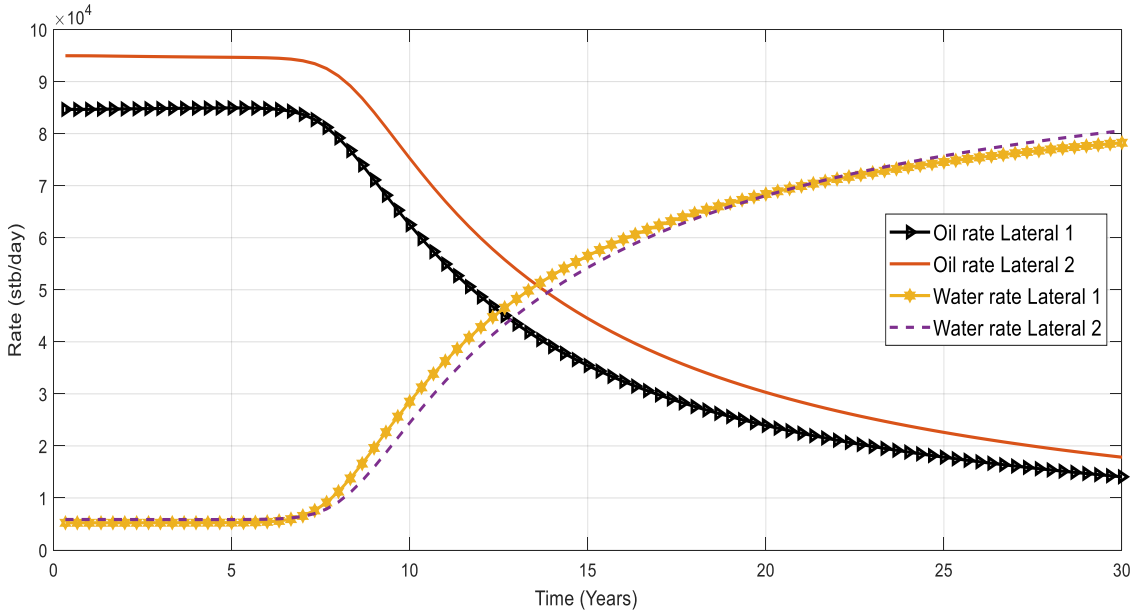

Figure 44 – Oil and water production rate for fully sealing case

4.3.4 Case 5: Combined Compartmentalization: Layer Juxtaposition and Faulting

We present the results for a combined compartmentalization case of both vertically sealing and non-sealing barriers in the reservoir model as depicted in the schematic earlier presented in **Figure 22**.

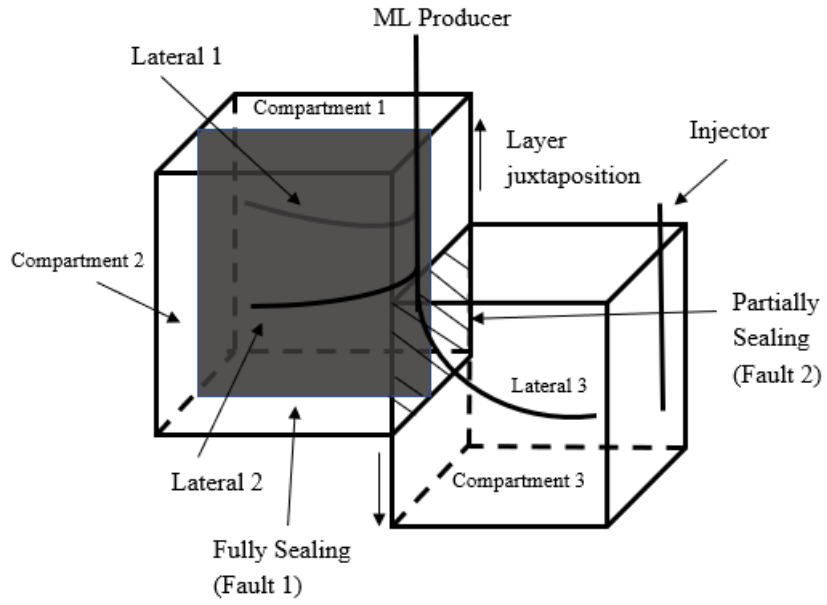

Figure 45 - Compartmentalized reservoir model with sealing and non-sealing faults

Vertical fault (2) is represented in the model as juxtaposed sub-layers and is non-sealing while vertical fault (1) is fully sealing and divides compartment 1 and 2.

Compartments 1 and 2 are in communication with compartment 3 through fault 2. However, compartments 1 and 2 are not in communication.

Figure 46 below shows the oil cut profile from each lateral in the system. We see the fastest decline trend in the oil cut profile through lateral 3 most especially due to its proximity to the injector well located in the same compartment 3, and a faster decline through lateral 1 in compartment 1 which is in partial communication with compartment 3 through the partially sealing fault 2.

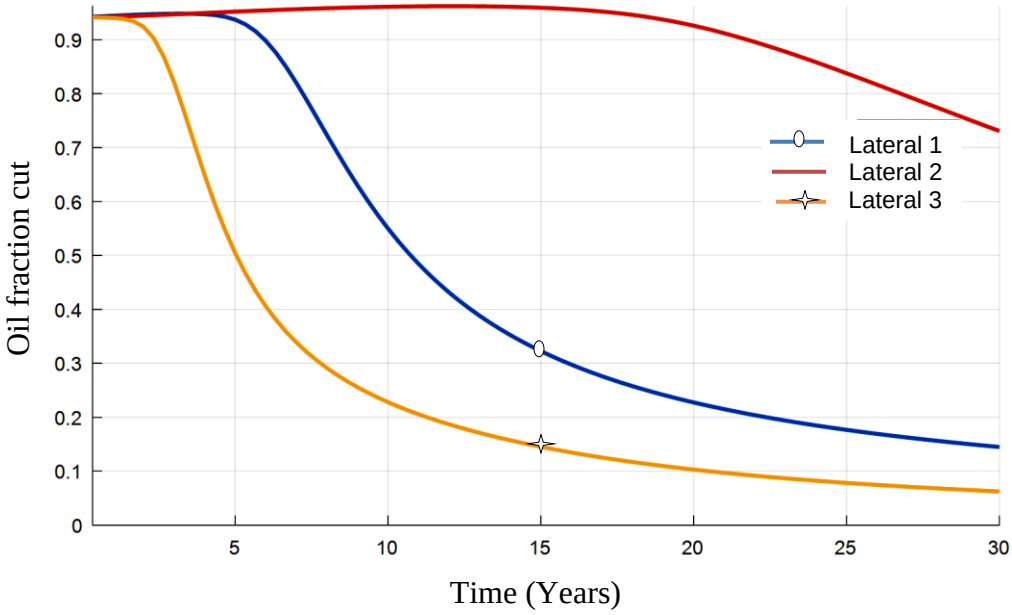

Figure 46 - Oil cut fraction profile

A corresponding behavior to the oil cut profile result presented above is observed in the water cut profile in **Figure 47** below where lateral 3 experiences the earliest breakthrough in water production and the highest water cut fraction among the three laterals, followed by lateral 1 which is in communication with compartment 3 through the partially sealing layer juxtaposition fault, and then the least water cut is produced from lateral 2 due to its location and distance (farthest)

from the injector well. The recommendation of installing lateral downhole control devices for the underperforming laterals (high water cut) such as was provided in the vertical compartmentalization case (case 2) presented earlier can also be implemented in a compartmentalized reservoir set up such as in this case to optimize oil production.

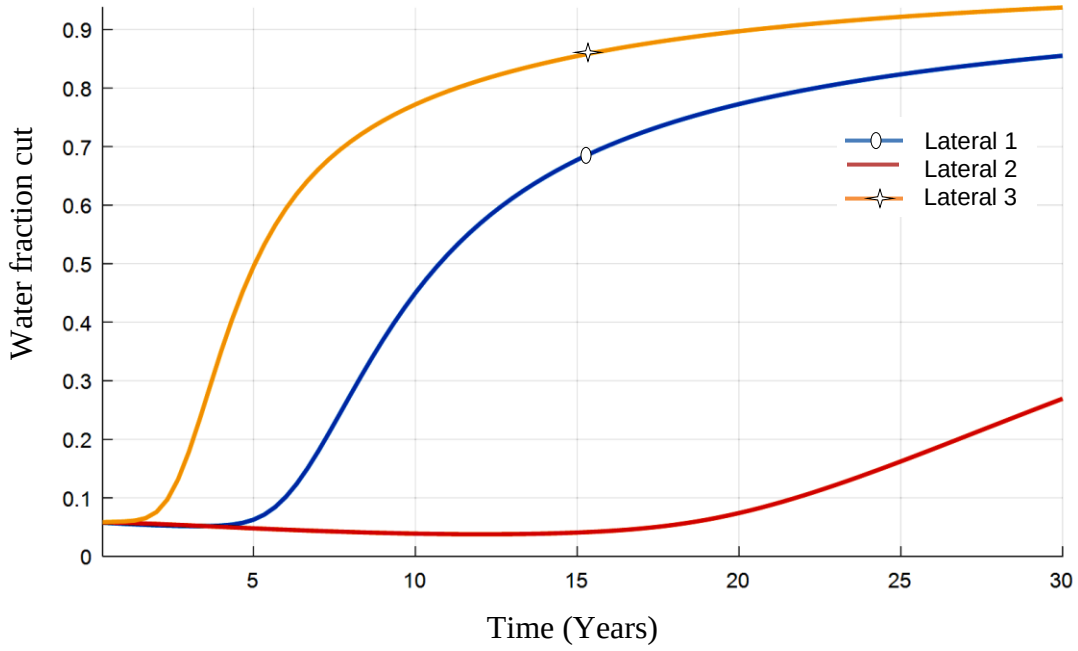

Figure 47 - Water cut fraction profile

Figure 48 below shows the corresponding oil and water production rate profile from each of the laterals. Lateral 3 starts out with a high oil production rate but experiences a steep decline as it experiences the earliest water breakthrough out of the 3 laterals in the system while lateral 2 has the lowest and sustained oil production rate over the production period. However, at a later period (after 15 years), lateral 2 becomes the best performing lateral with a higher production rate than laterals 1 and 3 which have experienced decline in the oil production rate.

The water production rate from the laterals is also presented in **Figure 47** showed lateral 3 with the shortest time to water breakthrough and the highest water production rate, followed by lateral 1, and the least water production rate from lateral 2.

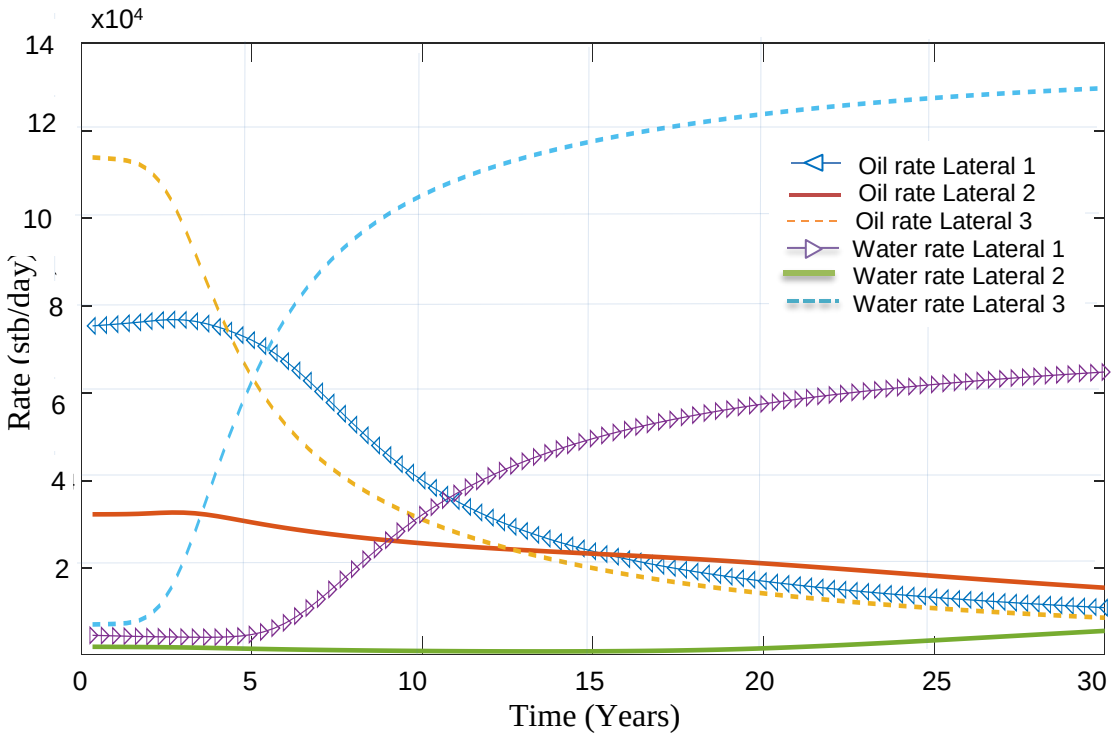

Figure 48 – Oil and water production rate

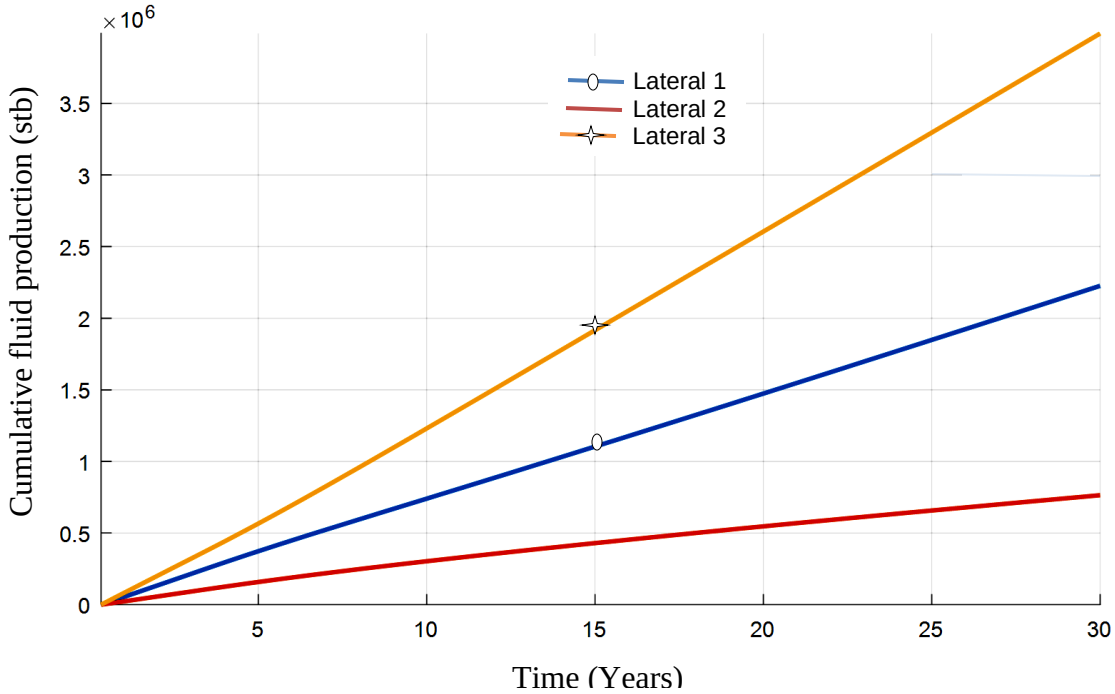

Figure 49 - Cumulative fluid production

Figure 49 shows the cumulative production profile from the compartmentalized reservoir system. This is majorly reflective of the proximity to the injection well, compartment size, and sealing character of the fault separating the compartments. Lateral 2 has the least cumulative total fluid (oil and water) produced as expected, due to the compartment location in the model, bounding faults, and distance to the injector well in the model. The cumulative effect of the faults results in a reduced fluid displacement and sweep efficiency in the model.

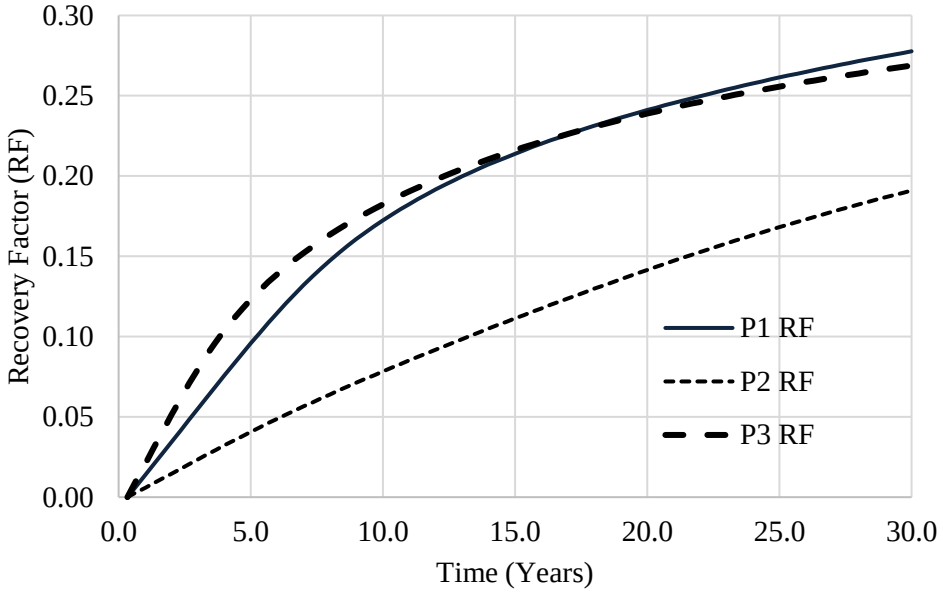

Figure 50 – Compartmentalized case recovery factor

Comparing this case to the base case scenario as in **Table 8** below, there is a significant reduction in the overall recovery factor potential due to flow impedance from the faults demarcating the reservoir.

Table 8 - Recovery Factor Comparison

Case	**Lateral 1 RF, %**	**Lateral 2 RF, %**	**Lateral 3 RF, %**	**Total % RF**
Base	38.4	41.7	15.5	**95.1**
Compartmentalized	28.0	19.1	27.2	**74.3**

4.4 Optimization Results

We present comparison results between the base case (simple or conventional completion well) net present value forecast and an optimal (smart well completion) simulation.

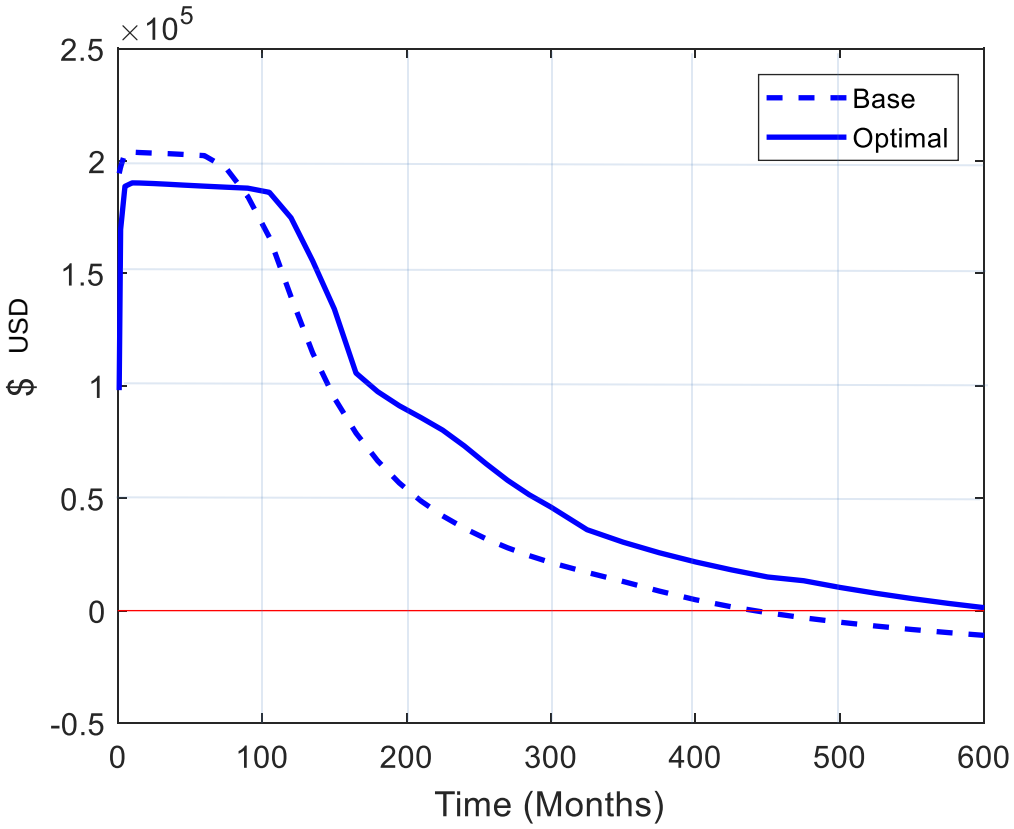

Figure 51 - Base case vs optimal case Net Cash flow profile

Figure 51 shows the net cash flow projection vs. time for the base case conventional well setup and the optimal case with smart well completions. In the early years of the field (up till 8.33 years), the conventional well set up yielded a more favorable net cash flow as expected due to the higher initial oil production rates. The economic benefit of the smart well completions kicked in after this time when the conventional well had reached the peak oil production and water production was on the rise. We then run the simulation until a time when both cases will yield a non positive net cash flow based on the economic indices as given in **Table 5.**

The net present value is then computed by calculating the sum (integral) of our discounted net cash flows. For the base case, the peak net present value as indicated in **Figure 52** is obtained at 450 months (37.3 years) while the optimal case still continued to show a marginal increase.

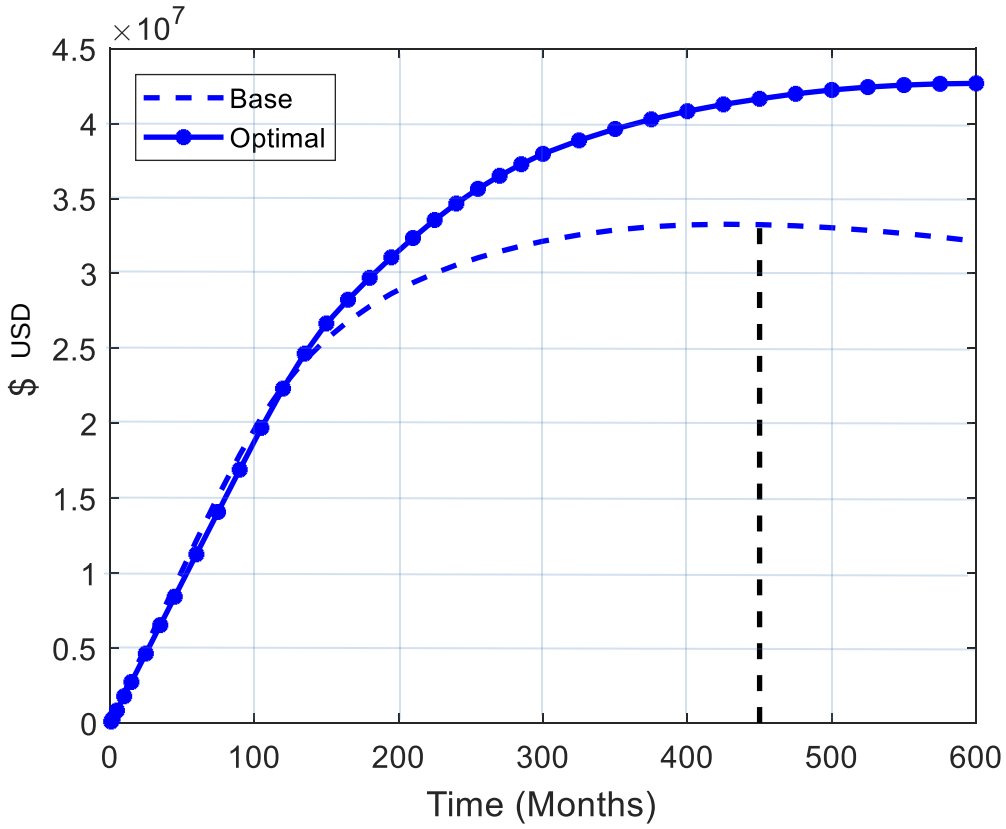

Figure 52 - Base case vs optimized case NPV forecast

Chapter Five Conclusions & Recommendations

5.1 Conclusions

The representation of reservoir structural complexities in numerical reservoir simulation is sometimes cumbersome, but better represented versus the over-simplified representation in analytical models. Using MRST, we developed and investigated different cases of compartmentalized reservoirs produced by a multilateral well system. Each lateral in the multilateral well structure is segmented, which enabled us to incorporate pressure drop effect from fluid flow and flow control devices for fluid and pressure control, the goal of which was to optimize commingled hydrocarbon production from the reservoir compartments.

The results we obtained showed the effect of the reservoir demarcations on potential production rates and recoveries in a bid to understand the dynamic behavior and have a more accurate forecast on future recovery indices. This will aid in advising field development plans for optimized recovery at future time intervals for the life of the well. From the results, we then examined the optimization potential of using smart completions in improving overall productivity, asset efficiency, and increased revenue stream (NPV).

We leveraged the versatility and accessibility of the simulation toolbox as an open source toolbox for engineers in industry as well as the academia to model and experiment with various complex reservoir and well structures, incorporate newly encountered or peculiar fluid flow relationships and mathematical equations to characterize unique properties or phenomena. This is an advantage, in contrast to most commercial simulators whose back-end development is a ‘black box’ (inaccessible coding). This presents difficulty in quality checking or verifying the integrity of

results obtained, especially for green fields with little to no dynamic history for matching the model. We demonstrate here that the fully implicit solvers developed in the toolbox framework can be applied to models that have the geometrical and petrophysical complexity seen in real reservoir models. The flexibility of the simulation toolbox also allowed us to incorporate the new trends of downhole flow control devices used in smart wells to control / optimize out turn hydrocarbon values. Simulation results show the capability of the simulation tool box in modeling reservoirs and simulating production especially from multiple reservoir compartments produced by a multilateral well.

The comparative level of accuracy of the productivity results obtained from both discretization methods investigated in our simulation presents further evidence that prequalify MRST as a dynamic and versatile modeling and simulation tool for conventional and intelligent multilateral well productivity studies from compartmentalized reservoirs. Further investigation in this regard will involve the application of both methods to investigate and compare results using established compartmentalized reservoir field cases.

5.2 Recommendations for future work

It is recommended that future work in this area include the following:

- Use of a more comprehensive wellbore multiphase model – e.g. Drift flux
- Investigate well placement and production optimization simultaneously.
- Consider compositional flow simulation for full fluid characterization from all the compartments.
- Incorporate geo-mechanical model to capture time-variant behavior of each reservoir compartment with production.

References

Ajayi, F and Konopczynski, A. (2003) – "A Dynamic Optimization Technique for Solution of Multi-zone Intelligent Well Systems in a Reservoir Development", Offshore Europe Conference, Aberdeen, UK.

Al-Umair, N. A. (2000) – "The First Multilateral/Dual lateral well completion in Saudi Arabia", paper IADC/SPE62271 presented at the 2000 IADC/SPE Asia Pacific Drilling Technology, Kuala Lumpur, Malaysia.

Aziz, K and Settari, A. (1979) – "Petroleum Reservoir Simulation", Applied Science Publishers Ltd., London

Aziz K. and Durolfsky L., (2004) – "Advanced Techniques for Reservoir Simulation and Modeling of Nonconventional Wells", Department of Energy Report, USA

Babu, D.K. and Odeh, A.S. (1989) - "Productivity of a Horizontal Well". SPE Reservoir Evaluation & Engineering; 4 (4): 417-421.SPE-18298-PA.

Babu, D.K., Odeh, A.S., Al-Khalifa, A.J., and McCann, R.C. (1991) - "The Relation between Well block and Wellbore Pressure in Numerical Simulation of Horizontal Wells –General Formulas for Arbitrary Well Locations in Grids," SPERE (February 1991) 324.

Borisov, J.P., - "Oil Production using Horizontal and Multiple Deviation Wells", Nedra, Moscow, 1964. Translated by J. Strauss, S.D. Josh, Phillips Petroleum Co., the R&D library translation, Bartlesville, Oklahoma, 1984.

Chen W., D. Zhu, and A.D. Hill (2000) – "A Comprehensive Model of Multilateral Well Deliverability", SPE 64751 SPE International Oil and Gas Conference and Exhibition in China held in Beijing, China, 7–10 November.

Cetkovic, I., Shammari, M., and Talal S. (2016) - "A Methodology for Multilateral-Well Optimization—Field Case Study,", paper SPE 183004 prepared for the 2016 Abu Dhabi International Petroleum Exhibition and Conference, Abu Dhabi, 7–10 November.

Collins, D.A. et al. (1991) - "Field-Scale Simulation of Horizontal Wells with Hybrid Grids," paper SPE 21218 presented at the SPE Symposium on Reservoir Simulation, Anaheim, California, 17–20 February.

Computer Modeling Group Manual - User's Guide IMEX, Version 2013, Calgary Canada

Dikken, B.J. (1990) - "Pressure Drop in Horizontal Wells and Its Effect on Production Performance," JPT 1426; Trans., AIME, 289.

Ebadi, F, Davies D. R., Gardiner A. R. and Corbett P. W. M. (2008) - Evaluation of added value in reservoir management by application of flow control with intelligent wells. Petroleum Geoscience, 14, 183-196, https://doi.org/10.1144/1354-079308-719

Economides, M.J., Deimbacher, F.X., Brand, C.W., and Heinemann, Z.E. (1991) – "Comprehensive Simulation of Horizontal-Well Performance". SPE Form Eval. 6 (4):418-426. SPE-20717-PA. doi: 10.2118/20717-PA.

Fisher, Q. J (2005) - Recent Advances in Fault Seal Analysis as an Aid to Reservoir Characterization and Production Simulation Modelling. SPE 94460 Society of Petroleum Engineers.

Fraija, J., Holmes, J, and Ahmed T., (2003) - "New Aspects of Multilateral Well Construction," Oilfield Review

Guidry, C. W., Pleasants, C., & Sheehan, J. (2011) - Merging Multilateral & Casing Exit Technologies to Increase Wellbore Junction Reliability by Reducing Rig & Openhole Exposure Times. Society of Petroleum Engineers. doi:10.2118/140274-MS

Folefac, A.N., Archer, J.S., Issa, R.I., and Arshad, A.M. (1991) – "Effect of Pressure Drop Along Horizontal Wellbores on Well Performance". Paper SPE 23094 presented at the SPE Offshore Europe Conference, Aberdeen

Furui, K., Zhu, D., and Hill, A.D. (2003) – "A Rigorous Formation Damage Skin Factor and Reservoir Inflow Model for a Horizontal Well". SPE Prod &Facilities 18 (3): 151-157. SPE-84964-PA.

Go. J, Smalley C., and Muggeridge, A. (2014) - "Characterizing Compartmentalization in Structurally Heterogeneous Reservoirs Using Fluid Mixing Time-scales"

Glaser, M, Butler, B, and Liland G. (2017) - "Reducing Well Costs and Extending Field Life with Intelligently Completed Trilateral and Quadrilateral TAML Level-5 Multilaterals", SPE paper 184608-MS presented at the SPE/IADC Drilling conference and Exhibition, The Hague, Netherlands.

Guo, B., Zhou, J., Liu, Y., and Ghalambor, A. (2007) – "A Rigorous Analytical Model for fluid flow in Drain Holes of Finite Conductivity Applied to Horizontal and Multilateral Wells". Paper SPE 106947 presented at the SPE Production Operations Symposium, Oklahoma.

Heinemann, Z.E., (1991) - "Modeling Reservoir Geometry with Irregular Grids." SPE Journal.

Helmy, M.W. and Wattenbarger, R.A. (1998) – "Simplified Productivity Equations for Horizontal Wells Producing at Constant Rate and Constant Pressure". Paper SPE 49090 presented at the SPE Annual Technical Conference and Exhibition.

Holmes, J. A., Barkve, T., & Lund, O. (1998) – "Application of a Multisegmented Well Model to Simulate Flow in Advanced Wells". Society of Petroleum Engineers.

Islam, M.R., and Chakma, A. (1990) – "Comprehensive Physical and Numerical Modeling of a Horizontal Well". Paper SPE 20627 presented at the SPE Annual Technical Conference and Exhibition, New Orleans, 23-26 September. doi:10.2118/20627-MS.

Jalali, Y. (2005) - Lessons Learnt from Reservoir Studies on Application of Multilateral Wells. Society of Petroleum Engineers. doi:10.2118/106322-MS

Jansen J.D, Okko H. B, & Paul M.J, Van den Hof (2008) – "Model-based control of multiphase flow in subsurface oil reservoirs". Journal of Process Control, March 2008

Kabir, K and Izgec, J. (2009) – "Diagnosis of Reservoir Compartmentalization from Measured Pressure / Rate Data During Primary Depletion"- Journal of Petroleum Science and Engineering.

Nolen, J.S. (1990) – "Treatment of wells in reservoir simulation". Technical report, July 1990

Oberkircher, J., Smith, R. and Thackwray, I. (2003) - “Boon or Bane? A Survey of the First 10 Years of Modern Multilateral Wells,” paper SPE 84025 presented at the SPE Annual Technical Conference and Exhibition, Denver, Colorado, 5 – 8 October.

Ouyang, L., Arbabi, S., and Aziz, K. (1996) – “General Wellbore Flow Model for Horizontal, Vertical, and Slanted Well Completions”, SPE 36608. SPE Annual Technical Conference and Exhibition, Denver, 6–9 October 1996.

Ouyang, L.-B., Arbabi, S., and Aziz, K. (1997) - “General Single-Phase Wellbore Flow Model,” topical report for U.S. DOE, Stanford University, California.

Ouyang, L.-B, Aziz, K. (1997) - “Simple but Accurate Equations for Wellbore Pressure Drawdown Calculation,” paper SPE 38314 presented at the SPE Western Regional Meeting, Long Beach, California, 25–27 June.

Ozkan, E., Sarica, C., Haciislamoglu, M., and Raghavan, R. (1995) – “Effect of Conductivity on Horizontal Well Pressure Behavior”. SPE Advanced Technology Series 3 (1): 85-94. SPE-24683-PA. doi: 10.2118/24683-PA.

Peaceman, D. W. (1977) – “Interpretation of well block pressures in numerical reservoir simulation”, SPE 6893, 52nd Annual Fall Technical Conference, and Exhibition, Denver.

Peaceman D. W. (1983) – “Interpretation of well-block pressures in numerical reservoir simulation with non-square grid blocks and anisotropic permeability”, Society of Petroleum Engineers Journal, 531–543.

Peaceman, D.W. (1987) - “Interpretation of Well-Block Pressures in Numerical Reservoir Simulation” – Part 3: Some Additional Well Geometries,” paper SPE 16976, presented at the 62nd SPE Annual Fall Technical Conference and Exhibition, Dallas, Texas.

Peaceman, D.W. (1991) - “Representation of a Horizontal Well in Numerical Reservoir Simulation,” paper SPE 21217, presented at the 11th SPE Symposium on Reservoir Simulation, Anaheim, California.

Peaceman, D.W. (1995) - “A New Method for Representing Multiple Wells with Arbitrary Rates in Numerical Reservoir Simulation,” paper SPE 29120, presented at the13th SPE Symposium on Reservoir Simulation, San Antonio, Texas.

Rivera, N, Spivey, J. P, and Sehbi, S. B (2003) – “Multilateral, intelligent well completion benefits explored” – Assessed at http://www.ogj.com/articles/print/volume-101/issue-15/drilling-production/multilateral-intelligent-well-completion-benefits-explored.html (Date assessed: July, 2016)

Rivera, N., Kumar, A., Kumar, A., & Jalali, Y. (2002) - Application of Multilateral Wells in Solution Gas-Drive Reservoirs. Society of Petroleum Engineers. doi:10.2118/74377-MS

Rahman, R and A. Ambastha (1997) – “Transient Pressure Behavior of Compartmentalized Reservoirs”, SPE Annual Conference Paper presentation

Schlumberger GeoQuest (2005) – “Multi-Segment Wells”, Eclipse Technical Description

Shadizadeh, S.R, Kargarpour, M.A, Ali, M., Zoveidavianpoor, M (2011) – "Modeling of Inflow Well Performance of Multilateral Wells: Employing the concept of Well Interference and the Joshi Expression". Iranian Journal of Chemical Engineering, Vol. 30, No 1, 2011.

Smalley P., and England W., (1994) – "Reservoir Compartmentalization Assessed with Fluid Compositional Data", SPE Reservoir Engineering, pp. 175- 180

Smith, D.A. (1966) - "Theoretical Considerations of Sealing and Non-Sealing Faults," AAPG Bull 50, No.2, 363-374.

Stone, T.W., Edmunds, N.R., and Kristo, B.J. (1989) – "A comprehensive wellbore-reservoir simulator". SPE, 141-153.

Stewart G., And Whaballa A., (1989) - "Pressure Behavior of Compartmentalized Reservoirs"- SPE Paper 19779 presented at the 1989 ATCE of SPE of AIME, San Antonio, Texas

Yildiz, T (2002) - "Long-Term Performance of Multilaterals in Commingled Reservoirs," paper SPE 78985 presented at the SPE International Thermal Operations and Heavy Oil Symposium and International Horizontal Well Technology Conference, Calgary, Alberta, Canada, 4 – 7 November.

Penmatcha, V.R. and Aziz, K. (1998) - "A Comprehensive Reservoir/Wellbore Model for Horizontal Wells," paper SPE 39521 presented at the SPE India Oil and Gas Conference and Exhibition, New Delhi, India, 17–19 February.

Salas, J.R., Jenkins, D. P., Clifford J. P. (1996) - "Multilateral Well Performance Prediction," Paper No. SPE 35711, SPE Western Regional Meeting, Anchorage, Alaska, May 22-24.

Vermeulen P.T.M. and A.W. Heemink (2006) - “Model-reduced variational data assimilation”. Mon. Weather Rev., 134 (10):2888–2899, 2006.

Yildiz, T. (2005) - Multilateral horizontal well productivity. Paper presented at the SPE Europe /EAGE Annual Conference.

Zhu, D., Hill, A. D., & Landrum, W. R. (2002) – “Evaluation of Crossflow Effects in Multilateral Wells”. Society of Petroleum Engineers. doi:10.2118/75250-MS

Appendices

Appendix A - Reservoir Flow Model Formulation

Consider a reservoir compartment of volume Ω with boundary $\partial\Omega$, and an outward pointing unit, **n** on the boundary as illustrated below (**Figure 53**) with a quantity *c* conserved over a period.

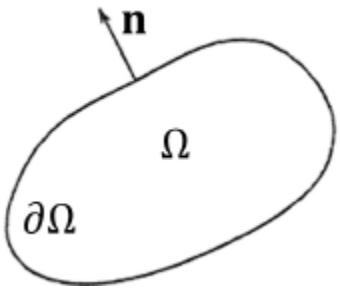

Figure 53 - Porous medium Ω in two-dimensional space

This can be expressed as

$$\frac{\partial}{\partial t}\int_{\Omega} c\, dV + \oint_{\partial\Omega} \mathbf{F}\,.\,\mathbf{n}\, ds = \int_{\Omega} q\, dV \qquad (A1)$$

F is the mass flux and q is the source/sink term. Eq. (A1) implies that the rate of change inside Ω is equal to the rate of mass entering or leaving through the boundary $\partial\Omega$ and the rate of mass contributed by sources or sinks. Using Gauss's divergence theorem, we get

$$\int_{\Omega} \left(\frac{\partial c}{\partial t} + \nabla.\mathbf{F}\right) dV = \int_{\Omega} q\, dV \qquad (A2)$$

from which we obtain the continuity equation:

$$\frac{\partial c}{\partial t} + \nabla.\mathbf{F} = q \qquad (A3)$$

We now write the continuity equation (A3) for the conserved quantity c which is the mass of each phase flowing in the compartment ($\rho_\alpha \emptyset S_\alpha$). ρ is the fluid density, ∅ is the porosity, and S is the fluid saturation of the pore space ($0 \leq S \leq 1$), and the subscript $\propto \in \{o, w\}$ indicates the oil and water phases respectively.

The density and the porosity are independent of pressure. We assume rock and fluid incompressibility. Substituting for mass flux $\mathbf{F}_\alpha = \rho_\alpha \mathbf{v}_\alpha$ in (A3), where **v** is the superficial fluid velocity results in

$$\frac{\partial}{\partial t}(\rho_\alpha \emptyset S_\alpha) + \nabla.(\rho_\alpha \boldsymbol{v}_\propto) = \breve{q}_\alpha \tag{A4}$$

Darcy's law, relating the fluid velocity to the pressure gradient in the medium is expressed as

$$\boldsymbol{v}_\propto = -\frac{k_{r\propto}}{\mu_\propto}\boldsymbol{K}(\nabla P_\propto - \rho_\propto g \nabla d) \tag{A5}$$

where **K** is the permeability tensor, μ fluid viscosity, k_r relative permeability, p, pressure, g, acceleration of gravity, and d, depth. The ratio $\left.\frac{k_{r\propto}}{\mu_\propto}\right/$ is called the phase mobility, λ_α. Employing the no gravity and capillary assumption, Darcy's law will simplify to

$$\boldsymbol{v}_\propto = -\lambda_\alpha \boldsymbol{K}(\nabla P_\propto) \tag{A6}$$

Substituting (A6) into (A4) and noting that porosity and density are independent of pressure, we get

$$\emptyset \frac{\partial S_\alpha}{\partial t} + \nabla.\boldsymbol{v}_\propto = \frac{\breve{q}_\alpha}{\rho_\alpha} \tag{A7}$$

Writing equation (A7) for each phase, we have 4 unknowns: $p_w,\ p_o,\ S_w,\ S_o$, two of which can be eliminated with additional relationships of saturation and capillary pressure.

$$S_o + S_w = 1.0 \tag{A8}$$

$$P_c(S_w) = P_o - P_w \tag{A9}$$

where $P_c(S_w)$ is the oil-water capillary pressure which is another source of nonlinearity in the flow equations. However, since we employ the no capillary pressure condition, Eq. (A9) to $p_o = p_w = p$. It is common to choose the water saturation S_w as the primary unknown variable and define it simply as variable S. Now, the primary variables are the pressure, p and water saturation S.

Defining the total velocity as $\boldsymbol{v} = \boldsymbol{v_o} + \boldsymbol{v_w}$ and applying it to (A6) and (A7) results in

$$\boldsymbol{v} = -\lambda_t \boldsymbol{K} \nabla p, \qquad within\ \Omega \tag{A10}$$

$$\nabla . \boldsymbol{v} = q, \qquad within\ \Omega \tag{A11}$$

$$\boldsymbol{v} . \boldsymbol{n} = 0, \quad on\ \ \partial\Omega \tag{A12}$$

where q in (A11) is the total volumetric rate and λ_t is the total mobility.

$$q = q_o + q_w = \frac{\breve{q}_o}{\rho_o} + \frac{\breve{q}_w}{\rho_w} \tag{A13}$$

$$\lambda_t(S) = \lambda_{t_o} + \lambda_{t_w} = \frac{k_{ro}}{\mu_o} + \frac{k_{rw}}{\mu_w} \tag{A14}$$

The combination of (A10) and (A11) with the no-flow boundary condition in (A12) are the pressure equations, which are elliptic in nature. Now, we obtain water velocity from (A10) as follows

$$\boldsymbol{v}_{\propto} = -\lambda_w \boldsymbol{K}\nabla p = -\frac{\lambda_w}{\lambda_t}\boldsymbol{v} = \frac{\lambda_w}{\lambda_w + \lambda_o}\boldsymbol{v} \tag{A15}$$

Referring to $\frac{\lambda_w}{\lambda_w+\lambda_o}$ as the water fractional flow, denoting it by $f_w(S)$, and substituting (A15) for the water phase of (A7), we obtain

$$\phi\frac{\partial S}{\partial t} + \nabla . f_w(S)\boldsymbol{v} = q_w \tag{A16}$$

Equation (A16) is the saturation equation.

Appendix B.1 - The Finite Volume Discretization Scheme

In this method, information is typically cell-centered or node-centered, and the calculation of fluid movement from one finite volume cell to another is carried out through the calculation of "fluxes" at the cell "faces". We then "assemble" the governing equations by adding the contributions from all the cells involved by using the additive property of integrals.

Consider a single control-volume Ω_i as seen in **Figure 53**, discrete equivalents of the model equation can be gotten by the finite volume method. Considering the elliptic pressure equation (3.7), we can transform the continuously differentiable velocity field, $\vec{v}$, into a surface integral by the divergence theorem using a single cell Ω_i, in the discrete grid as control volume.

$$\int_{\Omega_i} (\nabla . \vec{v})\ dV = \int_{\partial\Omega_i} (\vec{v}.\vec{n})\ ds = \int_{\Omega_i} q\ d\vec{x} \tag{A17}$$

$$\int_{\partial\Omega_i} \boldsymbol{K}\lambda\,(s_w^k)\nabla p^{k+1}\,.\ dV = \int_{\Omega_i} q\ d\vec{x} - \int_{\partial\Omega_i} \boldsymbol{K}\,\langle\lambda_w\,(s_w^k)\ + \lambda_o\,(s_w^k)\rangle\,.\vec{n}\quad dV \tag{A18}$$

where the superscript *k* denotes the current time step. The left hand side term, and the second integral term over the cell boundaries on the RHS are computed with the two point flux approximation (TPFA) scheme which is presented next in **Appendix B.2**

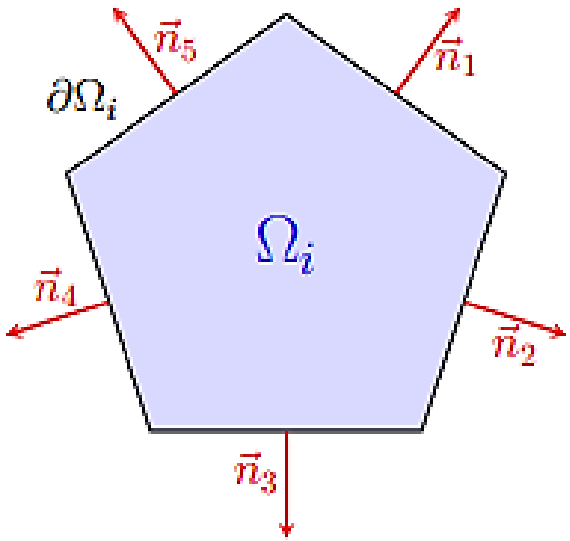

Figure 54 - Control-volume Ω_i, with boundary $\partial\Omega_i$ and normal vectors for each interface $\vec{n}_{ij}$

Appendix B.2 - Two Point Flux Approximation (TPFA) Scheme

The simplest and most widely used finite volume discretization scheme is the two-point stencil, referred to as the two-point flux-approximation (TPFA) scheme. In order to integrate the fluxes over the control volumes representing individual cells, we require an expression at the interface between two adjacent cells.

In figure A3 below, let Γ_{ij} represent the interface between Ω_i and Ω_j, and denoted by $\Gamma_{ij} = \partial\Omega_i \cap \partial\Omega_j$ and x_f be the face centroid, A_f, the area of the face and n_f be the unit normal to the interface. The flux through the interface can be approximated by

$$\int_{\Gamma_{ij}} \vec{v}.\vec{n}\ ds = \approx A_f \vec{v}(x_f).\vec{n} \tag{A19}$$

The flux at the interface can be approximated by a two-point difference approximation using Darcy's law for the pressure at the face centroid p (x_f) and the cell centroid pressure in the left cell $p\ (x_i)$,

$$\vec{v}(x_f) = -\boldsymbol{K_i}\nabla p \approx -\boldsymbol{K_i}\ \frac{\vec{c}_i}{|\vec{c}_i|^2}\left(p(x_f) - (x_i)\right) = -T_{\boldsymbol{if}}\left(p(x_f) - (x_i)\right) \tag{A20}$$

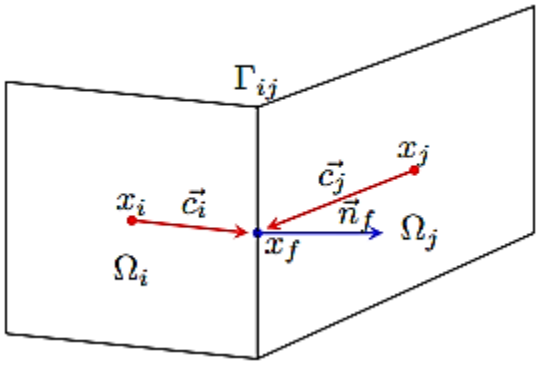

Figure 55 - Two control-volumes Ω_i and Ω_j, along with their centroids x_i and x_j.

The face centroid $\boldsymbol{x_f}$ is used to define the cell-face centroid vectors $\vec{c}_i$ and $\vec{c}_j$ that are required to derive the two-point flux approximation.

where $\vec{c}_i$ is defined as the vector from cell-centroid to face-centroid, as well as the half-face transmissibility, $T_{\boldsymbol{if}}$**.** There exists an analogous expression for the same velocity from the other side of the interface. Here, the only difference is a change in sign,

$$\vec{v}(x_f) = \boldsymbol{K_j}\nabla p \approx -\boldsymbol{K_i}\ \frac{\vec{c}_j}{|\vec{c}_j|^2}\left(p(x_f) - (x_i)\right) = T_{jf}\left(p(x_f) - (x_i)\right) \tag{A21}$$

If we assume that the pressure is continuous at the interface, we can rearrange Eq. (A20) and (A21) to eliminate the face pressure $p\ (\boldsymbol{x_f})$,

$$\vec{v}(x_f) = \frac{1}{T_{jf}^{-1} + T_{if}^{-1}} \left(p(x_i) - (x_j)\right) \tag{A22}$$

Eq. (A22) can be combined with Eq. (A19) to obtain the final expression for two-point flux,

$$\int_{\Gamma} \vec{v}.\vec{n}\ dA = \approx \frac{A_f}{T_{jf}^{-1} + T_{if}^{-1}} .\vec{n}\left(p(x_i) - (x_j)\right) = T_{ij}\left(p(x_i) - p(x_j)\right) \tag{A23}$$

Therefore, the resulting finite volume scheme for the pressure equation of (A10) is written as

$$\sum\nolimits_{j \in N_i} v_{ij} = \sum\nolimits_{j \in N_i} T_{ij}\left(p(x_i) - p(x_j)\right) = Q_i \tag{A24}$$

where v_{ij} is the discrete flux between cells *i* and *j* and N_i is the set of all cell neighbors for the cell. i. e. Q_i is the volume integrated source term in the cell. Each cell will in the TPFA scheme only be connected to the neighbors it shares faces with.

Upwinding of Advected quantities

For water saturation advancement through the control volume, upwind solution scheme is adopted. The figure below displays the movement of the waterfront through the reservoir domain.

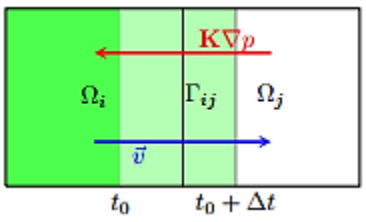

Figure 56 - Conceptual illustration for the first-order upwind scheme

The water phase, in green, sweeps through the domain as the time progresses. For the evaluation of saturation dependent functions at the cell interface, the inflow (upwind) cell is chosen to approximate the mobility value. The standard first order upwind scheme is expressed as:

$$(\lambda_{\propto})_{ij} \approx \begin{cases} (\lambda_{\propto})_i\,, & if\ \left(V_{ij}\right)_{\alpha} > 0 \\ (\lambda_{\propto})_j\,, & if\ \left(V_{ij}\right)_{\alpha} \leq 0 \end{cases} \tag{A25}$$

Appendix B.3 – Simulation Script Codes

```
%Base case no compartment
clear;clc;
mrstModule add ad-core ad-blackoil ad-props mrst-gui ad-fi

%% Set up grid and rock structure
nx=25; ny=20; nz=5; %Dx,Dy= [200], Dz=[20]
grdecl = simpleGrdecl([nx, ny,
nz],0.2,'flat',true,'undisturbed',true,'physDims',[5000, 4000, 100]*meter);
G = processGRDECL(grdecl, 'Verbose', true, 'checkgrid', true);
G.nodes.coords(:,3)= 2000+ G.nodes.coords(:,3);
G = computeGeometry(G);
plotGrid(G, 'FaceAlpha', 0.625); view(3); axis tight;

%% Create layer in model grid
[I, J, K] = gridLogicalIndices(G);
top = K < G.cartDims(3)/3;
lower = K > 2*G.cartDims(3)/3;
middle = ~(lower | top);

px = ones(G.cells.num, 1);
px(lower) = 300*milli*darcy;
px(middle) = 500*milli*darcy;
px(top) = 200*milli*darcy;
% Introduce anisotropy by setting K_x = 10*K_z.
perm = [px, px, 0.1*px];
poro = gaussianField((G.cells.num), [0.18 0.24], [11 3], 2.5)';
rock= makeRock(G, perm, poro);

%% Set up wells and schedule
pv = poreVolume(G, rock);
time = 30*year;
irate = sum(pv)/(time); %inject one pore volume over simulation period
c1 = nx*ny + (2:12)';  c2= 1002:nx:1275; c3 = 3*(nx*ny) + (2:12)';

W = struct([]);
W = addWell(W, G, rock, (500:nx*ny:2500),'Name', 'I1', 'radius', 5*inch,...
    'Type', 'bhp', 'Val', 10000*psia, 'comp_i', [1, 0], 'Sign', 1);
W = addWell(W, G, rock, c1, 'Name', 'P1', 'radius', 5*inch, ...
    'Type', 'bhp', 'Val', 1000*psia, 'comp_i', [0, 1], 'Sign', -1);
W = addWell(W, G, rock, c2, 'Name', 'P2', 'radius', 5*inch, ...
    'Type', 'bhp', 'Val', 1000*psia, 'comp_i', [0, 1],'Sign', -1);
W = addWell(W, G, rock, c3, 'Name', 'P3', 'radius', 5*inch, ...
    'Type', 'bhp', 'Val', 1000*psia, 'comp_i', [0, 1], 'Sign', -1);

figure(); plotGrid(G, 'facec', 'none', 'edgea', .1);
plotWell(G, W); view(40, 56); axis tight;
```

```
%% Prod schedule
n = 90; % number of time steps
dt = time/n;
timesteps = repmat(dt, n, 1);

% Set up the schedule containing both the wells and the timesteps
schedule = simpleSchedule(timesteps, 'W', W);

%% Set up fluid and simulation model
fluid = initSimpleADIFluid('phases',    'WO', ...
                           'rho',       [1000, 700], ...
                           'n',         [2, 2], ...
                           'mu',        [1, 5]*centi*poise ...
                           );
% Set up twophase, immiscible model with fully implicit discretization
model = TwoPhaseOilWaterModel(G, rock, fluid);

% Set up initial reservoir at 5000 psi pressure and 90% oil saturation.
State0 = initResSol(G, 5000*psia, [0.1, 0.9]);
Time = cumsum(schedule.step.val);
[wellSols, state, report]= simulateScheduleAD(State0, model, schedule);
plotWellSols(wellSols, Time);
%%
figure();
plotToolbar(G, state); plotWell(G, W), view(3);

================================================================================

%% Vertical faulting/ compartmentalization case
clc;clear;
mrstModule add ad-core ad-blackoil ad-props mrst-gui ad-fi blackoil-
sequential incomp

%% Set up the geomodel and specify wells
[nx,ny] = deal(20);
G = cartGrid([nx,ny,1],[5000,4000,100]);
G = computeGeometry(G);
p = gaussianField(G.cartDims(1:2), [0.2 0.26], [11 3], 2.5);
%%
p(1:end,11)=1e-3;
%%
K = p.^3.*(1.5e-5)^2./(0.81*72*(1-p).^2);
%%
rock = makeRock(G, K(:) , p(:));
%% Set up and solve flow problem, compute diagnostics
pv = poreVolume(G, rock);
time = 30*year;
irate = sum(pv)/(time); %inject pore volume over simulation period
c1 = (209:20:369)';  c2= (209:-20:29)';
W = struct([]);
W = addWell(W, G, rock, (400),'Name', 'I1', 'radius', 6*inch,'Type', 'bhp',
'Val', 10000*psia, 'comp_i', [1, 0], 'Sign', 1);
W = addWell(W, G, rock, c1, 'Name', 'P1', 'radius', 6*inch, ...
    'Type', 'bhp', 'Val', 1000*psia, 'comp_i', [0, 1],'Sign', -1);
```

```
W = addWell(W, G, rock, c2, 'Name', 'P2', 'radius', 6*inch, ...
    'Type', 'bhp', 'Val', 1000*psia, 'comp_i', [0, 1],'Sign', -1);
% W = addWell(W, G, rock, c3, 'Name', 'P3', 'radius', 5*inch, ...
%     'Type', 'bhp', 'Val', 100*barsa, 'comp_i', [0, 1], 'refDepth',
10,'Sign', -1);

figure(); plotGrid(G, 'facec', 'none', 'edgea', .1);
plotWell(G, W); view(40, 56);

%%
close all;
mrstModule add diagnostics
interactiveDiagnostics(G, rock, W, 'showGrid', true);
axis normal tight; view(0,90);

%%
n = 90;
dt = time/n;
timesteps = repmat(dt, n, 1);

% Set up the schedule containing both the wells and the timesteps
schedule = simpleSchedule(timesteps, 'W', W);

%% Set up fluid and simulation model
fluid = initSimpleADIFluid('phases',    'WO', ...
                           'rho',       [1000, 700], ...
                           'n',         [2, 2], ...
                           'mu',        [1, 5]*centi*poise ...
                           );
% Set up twophase, immiscible model with fully implicit discretization
model = TwoPhaseOilWaterModel(G, rock, fluid);

% Set up initial reservoir at 5000 psia pressure and completely oil filled.
State0 = initResSol(G, 5000*psia, [0.1, 0.9]);
Time = cumsum(schedule.step.val);
[wellSols, state, report]= simulateScheduleAD(State0, model, schedule);
plotWellSols(wellSols, Time);

figure();
plotToolbar(G, state); plotWell(G, W)
=====================================================================
%% For horizontal compartmentalization
clc;clear;
mrstModule add ad-core ad-blackoil ad-props mrst-gui ad-fi blackoil-
sequential incomp

%% Set up the geomodel and specify wells
[nx,ny] = deal(20);
G = cartGrid([nx,ny,5],[5000,4000,100]);
G = computeGeometry(G);
%%
p = gaussianField((G.cells.num), [0.18 0.24], [11 3], 2.5)';
%%
```

```
[I, J, K] = gridLogicalIndices(G);
p(K==3)=1e-3;

%%
top = K < 3;
lower = K > 3;

%%
perm = p.^3.*(1.5e-5)^2./(0.81*72*(1-p).^2);
%%
rock = makeRock(G, perm(:) , p(:));
%% Set up and solve flow problem, compute diagnostics
pv = poreVolume(G, rock);
time = 30*year;
irate = sum(pv)/(time); %inject pore volume over simulation period
c1 = (609:20:769)';  c2= (1409:-20:1249)';
W = struct([]);
W = addWell(W, G, rock, (400:400:2000),'Name', 'I1', 'radius', 6*inch,'Type',
'bhp', 'Val', 9000*psia, 'comp_i', [1, 0], 'Sign', 1);
W = addWell(W, G, rock, c1, 'Name', 'P1', 'radius', 5*inch, ...
    'Type', 'bhp', 'Val', 100*barsa, 'comp_i', [0, 1],'refDepth', 10, 'Sign',
-1);
W = addWell(W, G, rock, c2, 'Name', 'P2', 'radius', 5*inch, ...
    'Type', 'bhp', 'Val', 100*barsa, 'comp_i', [0, 1], 'refDepth', 10,'Sign',
-1);
% W = addWell(W, G, rock, c3, 'Name', 'P3', 'radius', 5*inch, ...
%     'Type', 'bhp', 'Val', 100*barsa, 'comp_i', [0, 1], 'refDepth',
10,'Sign', -1);

% close 3rd layer completion
W(1).cstatus = [1;1;0;1;1];
figure(); plotGrid(G, 'facec', 'none', 'edgea', .1);
plotWell(G, W); view(40, 56);

%%
close all;
mrstModule add diagnostics
interactiveDiagnostics(G, rock, W, 'showGrid', true);
axis normal tight; view(0,90);

%%
n = 90;
dt = time/n;
timesteps = repmat(dt, n, 1);

% Set up the schedule containing both the wells and the timesteps
schedule = simpleSchedule(timesteps, 'W', W);

%% Set up fluid and simulation model
fluid = initSimpleADIFluid('phases',    'WO', ...
                           'rho',       [1000, 700], ...
                           'n',         [2, 2], ...
                           'mu',        [1, 5]*centi*poise ...
                           );
```

```
% Set up twophase, immiscible model with fully implicit discretization
model = TwoPhaseOilWaterModel(G, rock, fluid);

% Set up initial reservoir at 5000 psia pressure and completely oil filled.
State0 = initResSol(G, 5000*psia, [0.1, 0.9]);
Time = cumsum(schedule.step.val);
[wellSols, state, report]= simulateScheduleAD(State0, model, schedule);
plotWellSols(wellSols, Time);

figure();
plotToolbar(G, state); plotWell(G, W)

%% plot ocut and wcut - create variables
figure();
h=plot(Time/year, horzcomptocut, '-o', Time/year, horzcomptwcut, '-x');
xlabel('Time [Years]'), ylabel('Fraction'), title ('% fluid production from
each lateral');
legend('OilcutP1', 'OilcutP2', 'WatercutP1', 'WatercutP2', 'Location',
'east');

================================================================
% Multisegmented well (with DCV) pressure profile development
clear;clc;
%for equal sat distribution [0.1 0.9] and segregated distrr. and varying
nvalves
mrstModule add ad-core ad-blackoil ad-props mrst-gui incomp ad-fi blackoil-
sequential

%% Set up grid and rock structure
nx=25; ny=20; nz = 5; %Dx,Dy= [200], Dz=[20]
km=1000;
pdims = [5, 4, 0.1]'*km;
dims = [25, 20, 5];
G = cartGrid(dims, pdims);

G = computeGeometry(G);
plotGrid(G, 'FaceAlpha', 0.625); view(3); axis tight;

[I, J, K] = gridLogicalIndices(G);

top = K < G.cartDims(3)/3;
lower = K > 2*G.cartDims(3)/3;
middle = ~(lower | top);

px = ones(G.cells.num, 1);
px(lower) = 300*milli*darcy;
px(middle) = 500*milli*darcy;
px(top) = 200*milli*darcy;

% Introduce anisotropy by setting K_x = 10*K_z.
perm = [px, px, 0.1*px];
poro = gaussianField((G.cells.num), [0.18 0.24], [11 3], 2.5)';
rock = makeRock(G, perm, poro);
```

```
%% Set up wells and schedule
pv = poreVolume(G, rock);
time = 30*year;
irate = sum(pv)/(time); %inject one pore volume over simulation period
c3 = (2*(nx*ny) + (2:7))';
W = struct([]);
%Simple Producer
W = addWell(W, G, rock, c3, 'Name', 'P1', 'radius', 6*inch, ...
    'Type', 'bhp', 'Val', 1000*psia, 'comp_i', [0, 1, 0],'Dir', 'x', 'Sign',
-1);

Wms = W;
%% Define MS Well Properties
topo = [1 2 3 4 5 6 2 3  4  5  6  7
        2 3 4 5 6 7 8 9 10 11 12 13]';
% Create sparse cell-to-node mapping
cell2node = sparse((8:13)', (1:6)', 1, 13, 6);
lengths = [200*ones(6,1); nan(6,1)];
diam    = [.1*ones(6,1); nan(6,1)]; %3.94 inches
depths  = G.cells.centroids(c3(1), 3)*ones(13,1);
vols    = ones(13,1);

% Convert to ms-well
Wms = convert2MSWell(Wms,'cell2node', cell2node, 'topo', topo, 'G', G, 'vol',
vols, ...
                     'nodeDepth', depths, 'segLength', lengths, 'segDiam',
diam);

%define wellbore nodes and reservoir nodes
[wbix, vix]  = deal(1:6, 7:12);
% valve properties
roughness = 1e-4; nozzleD   = .0025; discharge = 0.7;
nValves   = 30; % number of valves per connection
% Set up flow model as a function of velocity, density and viscosity
Wms.segments.flowModel = @(v, rho, mu)...
    [wellBoreFriction(v(wbix), rho(wbix), mu(wbix), Wms.segments.diam(wbix),
...
                      Wms.segments.length(wbix), roughness, 'massRate'); ...
     nozzleValve(v(vix)/nValves, rho(vix), nozzleD, discharge, 'massRate')];

figure();
plotGrid(G, 'facec', 'none', 'edgea', .1); hold on; plotWell(G, W);
%% Set up fluid and simulation model
fluid = initSimpleADIFluid('phases',    'WOG', ...
                           'rho',       [1000, 700 1], ...
                           'n',         [2, 2, 1], ...
                           'mu',        [1, 5, 1]*centi*poise ...
                           );
% Set up twophase, immiscible model with fully implicit discretization
model = ThreePhaseBlackOilModel(G, rock, fluid);
%%
sW = 0.9*ones(G.cells.num, 1);
sW(G.cells.centroids(:, 3) < 2090) = 0.1;
```

```
sWg = zeros(G.cells.num,1);
sat = [sW, 1 - sW, sWg];
sat(2001:2500,2)=0;
sat(2001:2500,1)=1;
sat(1500:2000)= 0.7;
sat(1500:2000,2)= 0.3;
sat(1000:1500)= 0.3;
sat(1000:1500,2)= 0.7;
sat(500:1000)= 0.15;
sat(500:1000,2)= 0.85;

% sat= [0.1 0.9];% 90% Oil Sat and 10% Sw

g = model.gravity(3);

% Compute initial pressure
p_ref= 5000*psia;
p_res = p_ref + g*G.cells.centroids(:, 3).*(sW.*model.fluid.rhoWS + (1 -
sW).*model.fluid.rhoOS);

%% Initial state
% state0 = initResSol(G, p_res, sat);
state0 = initResSol(G, p_res, sat);
figure();
plotCellData(G, state0.s(:,1)); plotWell(G,W); view(50, 50), axis tight %sw
figure();
plotCellData(G, state0.s(:,2)); plotWell(G,W); view(50, 50), axis tight % so
 %% Define Injection well
inj = addWell([], G, rock, (500:nx*ny:2500),'Name', 'I1', 'radius',
5*inch,'Type', 'bhp', 'Val', 10000*psia, 'comp_i', [1, 0, 0], 'refDepth',
0*meter, 'Sign', 1);

W_simple = [inj W]; % combine injector and simple well

n = 90; dt = time/n; timesteps = repmat(dt, n, 1);
% Set up the schedule containing both the wells and the timesteps
schedule1 = simpleSchedule(timesteps, 'W', W_simple);
Time = cumsum(schedule1.step.val);
%% Run Simple schedule
[wellSolsSimple, statesSimple] = simulateScheduleAD(state0, model,
schedule1);

%% Combine Injector and MS Well
W_comp = combineMSwithRegularWells(inj, Wms);

%% Run MS Well Schedule
schedule2 = simpleSchedule(timesteps, 'W', W_comp);

[wellSols, states, report] = simulateScheduleAD(state0, model, schedule2,
'verbose', true);

%% Plot the well-bore pressure in the multisegment well
% Plot pressure along wellbore for step 1 and step 90 (final step)
```

```
figure(), hold on
for k =  [1 45 90]
    plot([wellSols{k}(2).bhp; wellSols{k}(2).nodePressure(1:6)]/psia, ...
         '-o', 'LineWidth', 2);
end
legend('Step 1','Step 45','Step 90', 'Location', 'northwest');
title('Pressure drop along well bore');
set(gca, 'Fontsize', 14), xlabel('Well node'), ylabel('Pressure [psia]')

%% Launch Interractive plotting
plotWellSols({wellSols, wellSolsSimple}, report.ReservoirTime, ...
            'datasetnames', {'Ms Well', 'Simple well'});
```

```
=====================================================================
clear;clc; % combined compartmentalization (horz & vert)
mrstModule add ad-core ad-blackoil ad-props mrst-gui incomp ad-fi blackoil-
sequential

%% Set up grid and rock structure
nx=25; ny=20; nz = 5; %Dx,Dy= [200], Dz=[20]
km = kilo*meter;
pdims = [5, 4, 0.10]'*km; %x by y by z dimension of cartesian model
dims = [nx, ny, nz]; % no of grid cells in cartesian direction
%Create Grid
G = cartGrid(dims, pdims);
G = computeGeometry(G);
G.nodes.coords(:,3)= 2000+ G.nodes.coords(:,3);

plotGrid(G, 'FaceAlpha', 0.9, 'FaceColor', 'none'); view(3); axis tight;

%% Create layer in model grid

poro = gaussianField((G.cells.num), [0.18 0.24])';
poro(201:210)=1e-3;
poro(601:610)=1e-3;
poro(1001:1010)=1e-3;
poro(1401:1410)=1e-3;
poro(1801:1810)=1e-3;
perm = poro.^3.*(1.5e-5)^2./(0.81*72*(1-poro).^2);
rock= makeRock(G, perm, poro);

perm(1:200) = 300*milli*darcy;
perm(211:400)= 300*milli*darcy;
perm(401:600) = 500 * milli*darcy;
perm (611:800)= 500 * milli*darcy;
perm(800:1000) = 500 * milli*darcy;
perm(1011:1200)= 500 * milli*darcy;
perm(1201:1400)= 200 * milli*darcy;
perm(1411:1600)= 200 * milli*darcy;
perm(1601:1800)= 200 * milli*darcy;
perm(1811:2000)= 200 * milli*darcy;

% Introduce anisotropy by setting K_x = 10*K_z.
```

```
perm = [perm, perm, 0.1*perm];
plotCellData(G,log10(rock.poro(:,1)),'EdgeColor','k','EdgeAlpha',0.1);
%% Set up wells and schedule
pv = poreVolume(G, rock);
time = 30*year;
irate = sum(pv)/(time); %inject one pore volume over simulation period
c1 = nx*ny + (185:nx:385)';  c2= (985:-nx:805)'; c3 = 3*(nx*ny) + (185:195)';

W = struct([]);
W = addWell(W, G, rock, (400:nx*ny:2000),'Name', 'I1', 'radius',
5*inch,'Type', 'rate', 'Val', irate, 'comp_i', [1, 0], 'Sign', 1);
W = addWell(W, G, rock, c1, 'Name', 'P1', 'radius', 5*inch, ...
    'Type', 'bhp', 'Val', 1000*psia, 'comp_i', [0, 1],'Sign', -1);
W = addWell(W, G, rock, c2, 'Name', 'P2', 'radius', 5*inch, ...
    'Type', 'bhp', 'Val', 1000*psia, 'comp_i', [0, 1], 'Sign', -1);
W = addWell(W, G, rock, c3, 'Name', 'P3', 'radius', 5*inch, ...
    'Type', 'bhp', 'Val', 1000*psia, 'comp_i', [0, 1], 'Sign', -1);

figure(); plotGrid(G, 'facec', 'none', 'edgea', .1);
plotWell(G, W); view(40, 56);
%%
time = 30*year;
n = 90;
dt = time/n;
timesteps = repmat(dt, n, 1);

% Set up the schedule containing both the wells and the timesteps
schedule = simpleSchedule(timesteps, 'W', W);

%% Set up fluid and simulation model
fluid = initSimpleADIFluid('phases',    'WO', ...
                           'rho',       [1000, 700], ...
                           'n',         [2, 2], ...
                           'mu',        [1, 5]*centi*poise ...
                           );
srw = 0.20; sro = 0.25;

% Fluid relative permeabilities (use name convention from SWOF keyword)
fluid.krW  = coreyPhaseRelpermAD(2, srw, 0.55, srw + sro);
fluid.krO = coreyPhaseRelpermAD(2, sro, 0.8, srw + sro);
fluid.krOW = coreyPhaseRelpermAD(4, sro, 1, srw + sro);

% Set up twophase, immiscible model with fully implicit discretization
model = TwoPhaseOilWaterModel(G, rock, fluid);

% Set up initial reservoir at 5000*psia pressure
State0 = initResSol(G, 5000*psia, [0.3, 0.7]);
Time = cumsum(schedule.step.val);
[wellSols, state, report]= simulateScheduleAD(State0, model, schedule);
plotWellSols(wellSols, Time);

figure();
plotToolbar(G, state); plotWell(G, W)
 %% Get well rates and plot
```

```
qOs = abs(getWellOutput(wellSols, 'qOs', 2:4));
qWs = abs(getWellOutput(wellSols, 'qWs', 2:4));
rates = [qOs, qWs];
figure;
Time = cumsum(schedule.step.val);
plot(convertTo(Time, year), convertTo(rates, stb/day));
legend('Oil rateP1', 'Oil rateP2','Oil rateP3','Water rateP1',  'Water
rateP2','Water rateP3')

%% plot oi prod rate and oil cut
plotyy(Time/year, oprodrate,Time/year, ocut);
legend('Oil rateP1', 'Oil rateP2','Oil rateP3','Oil cut P1', 'Oil cut P2',
'Oil Cut P3');
xlabel('Time (years)'); ylabel('rate (Stb/day)');
```